THE UNIVERSITY OF HULL

Identifying substructure in LoCuSS Abell clusters

being a Thesis submitted for the Degree of Master of Physics

in the University of Hull

by

Joshua Marsh, BSc Physics with Astrophysics

September 2020

"What we face may look insurmountable, but what I learned is we are always stronger than we know"

– Arnold Schwarzenegger, *38th Govenor of California*

Acknowledgements

I would like to express my gratitude to my primary supervisor, Dr Kevin Pimbblet, my secondary supervisor Dr Chris Haines and my friends and family who supported me throughout this thesis and without whom it would not have been possible to complete.

Declaration of Originality

This thesis is submitted in partial fulfilment of the degree of Master of Physics from the University of Hull. I declare that the work undertaken in this thesis is original and my own and was carried out under the supervision of Dr Kevin Pimbblet and Dr Chris Haines. Where work, results, or ideas have been taken from other sources, those sources are explicitly referenced.

The work that has been published from this thesis was the principle responsibility of myself in terms of driving the science case, analysis, and writing up. The observations used were conducted by others as part of large scale surveys, and the data products from these observations are explicitly referenced.

Candidates signature: Joshua Marsh

Date: 15/08/2021

Contents

List of Figures

1. Theoretical Background

1.1 Aims of this thesis

This thesis aims to provide an analysis of galaxy evolution and evaluation of dynamical state in a suite of 5 Abell clusters: A1763, A963, A1758, A1835 and A1689. This will be achieved by processing spectra collected by the Local Cluster Substructure Survey (LoCuSS) and using equivalent width values for spectral lines of Hα, Hδ and [OII]. Using these values to determine the star formation rate and indicate whether a starburst has occurred thus helping to understand the history of these clusters. Determining the strength of the D4000 break is going to act as an indicator of galaxy metalicity and plotting it as a function of phase space will reveal substructure in the clusters.

In this first section I will detail the evolution of galaxies in terms of their morphology and colour. The creation of large scale structures in the Universe formed from these galaxies, such as clusters and filaments. Lastly I will discuss the importance of being able to identify morphological change and how it can show the history of large scale structure in the Universe.

1.2 Galaxy evolution

Galaxies by their nature come in many different morphological types, as shown by the earliest of observations by Edwin Hubble. His invention of the Hubble sequence in 1926 (Figure 1.1) displays an early theory of galaxy classification. Galaxies however have existed since the early Universe and their evolution has been thoroughly studied in an attempt to understand the processes that cause morphological changes. Understanding galaxy evolution is key to being able to map both interaction events that have happened in the past and the implications of future events that could happen. By establishing what to look for helps drive telescope design and allows for advancements in observational techniques and therefore our understanding of the Universe.

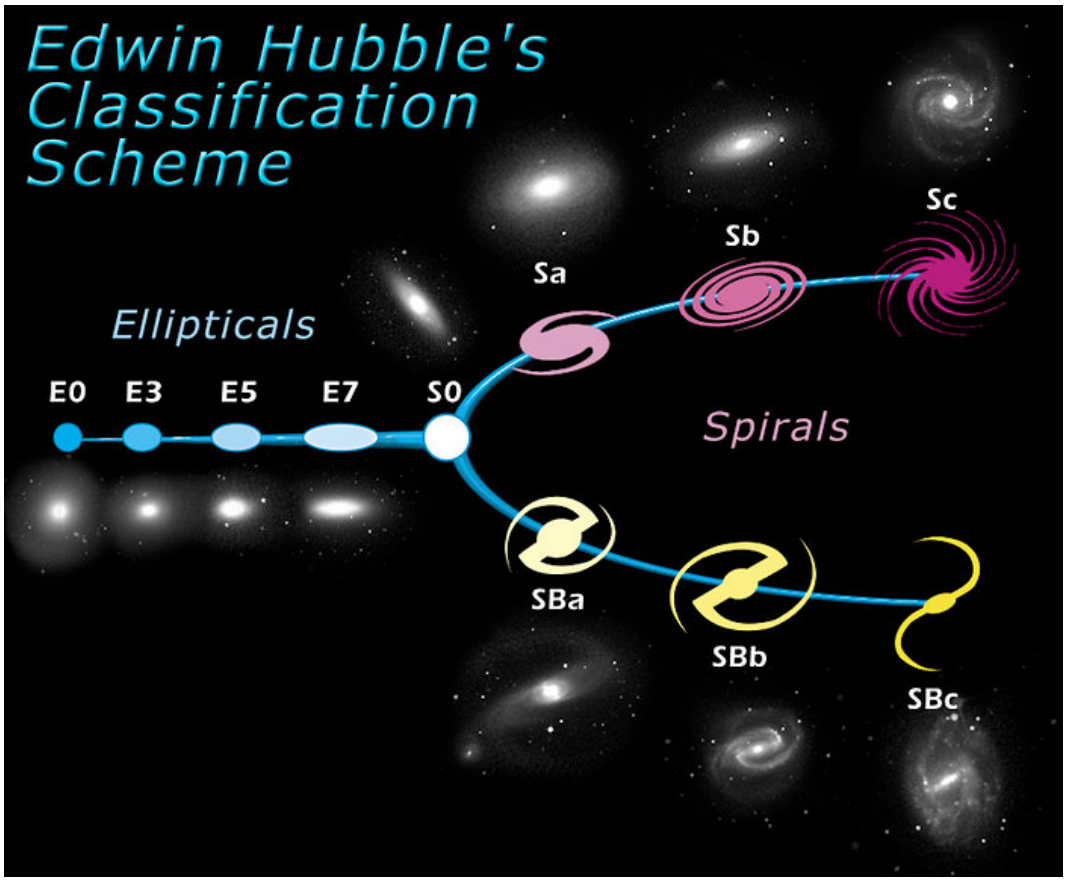

Figure 1.1: Hubble Sequence showing a range of classification types for galaxies, depending on their displayed morphology. This ranges from barred (SB types) and unbarred (S types) spirals to ellipitcal (E types) Credit:ESA/Hubble.

To understand the evolution of galaxies, it is necessary to know the process of their creation. In the early stages of the Universe the distribution of matter was not perfectly uniform. Regions of slightly higher density accreted more matter than lower density regions. Upon the expansion of the Universe these minor density fluctuations over time become large regions of increased density (Nilsson et al., 2006). These more dense regions cause neutral atomic hydrogen gas (H1) to pool and form molecular clouds, providing the mass-to-flux ratio of the cloud is super critical (Heiles & Troland, 2005). Regions of the molecular cloud experience collapse due to gravitational forces, causing the cloud to fragment into smaller clouds of dense gas. Further gravitational collapse causes dense cores to be formed, these cores then collapse to form a hydrostatic protostar. These groups of gravitationally bound protostars, gas and dust form a protogalaxy. The way galaxies evolve is influenced by internal

factors such as: mass, supernova feedback and active galactic nucleus (AGN) feedback and external factors include: Galaxy harassment, local density, mergers with other galaxies and ram pressure stripping. In this introductory section of this work, I discuss how galaxy properties such as: colour, morphology or star formation rate (SFR) change considering both internal and external factors, and the importance of post starburst galaxies in determining recent interaction.

Colour is one of the easiest observables and the colour of a galaxy reflects its stellar population, each star in the Universe exists on a spectrum of blue to red, therefore galaxies also exist on this spectrum. When comparing two extreme stars on the Hertzsprung–Russell diagram (Figure 1.2), one from the O class (β-Centauri) and the other from the M class (DX Cancri), we can see a multitude of differences between them. Firstly the O class star has a temperature that is a factor of 10 higher than the M class and a solar radius a factor of 100 larger, knowing that the luminosity relation states L= σ $T^4 4$ πR^2 (Sholukhova et al., 2015) we can infer its solar luminosity is a factor of 10^9 greater. This knowledge is critical in understanding why some galaxies appear more blue than others. The presence of O, B, even A class stars that have the ability to outshine up to billions of K,M class (redder) stars. These stars have large orders of size, mass and luminosity, so they must have an extremely high rate of fusion in the core to maintain hydrostatic equilibrium which causes them to be short lived (10^7 years). Compare this to the life expectancy of an M class star of mass 0.2 solar masses (10^{12} years) and it can be seen that red stars far outlive blue ones. Therefore, it is natural to assume that galaxies over time will shift from having a large fraction of blue stars to having a smaller fraction of blue stars and thus the evolutionary path for any given galaxy is to move from blue to red, assuming no new star formation (Hashimoto et al., 2019). Galaxy colour can be used instead of morphology to describe the galaxies population, this is beneficial because galaxy colour is accurately quantifiable and models can be used to determine an accurate star formation history (SFH) (Bruzual & Charlot, 2003).

Star formation rate (SFR) is the total mass of stars formed per year, it is a parameter derived mainly from spectra but can also be derived from colour. Star formation rate is important when referring to galaxy evolution, as it is an indicator in telling whether a galaxy

has recently interacted with other galaxies. It is closely tied to both colour and local density, the density of a locally defined region, it can also be used to determine time from the last star formation event. If SFR is high, galaxies will appear blue, this is seen in the spiral arms of our own galaxy the Milky Way which has an SFR of $1.6 M_{\odot}$/year (Licquia & Newman, 2015). The reason galaxies with high SFR appear blue is due to blue stars having a much greater luminosity than red ones. This doesn't mean red stars aren't also being created, although it differs depending on galaxy environment, the red stars are just contributing less luminosity than the bluer stars. Blue stars need a large amount of fuel to maintain fusion, and so they go supernova first and ongoing star formation leads to steady colour after a few million years after star formation occurs we are left with only redder stars and the luminosity of the galaxy returns back to how it originally was before the star formation phase, notably more red (Hashimoto et al., 2019). SFR also has an effect on the morphology in early galaxy creation, (Yamasawa et al., 2011) determined that SFR is linked to the amount H2 present in the gas component of the galaxy and that higher SFR (high H2) leads to an elliptical type being formed, whereas lower SFR (low H2) leads to the formation of spiral type galaxy. SFR however, can be shut down. One way this can happen is via a starburst event where SFR will increase dramatically (Schneider, 2010) before the galaxy uses all its gas and dust to form new stars, becoming a post starburst galaxy. It is also important to note at higher redshifts star formation is found to be more efficient than at local redshifts (Sobral et al., 2010) and SFR is also affected by mass of the dark matter halo. (Sobral et al., 2010) for example found that typical Hα emitters at z = 0.84, were typically located in dark matter halos of $\approx 10^{12}\ M_{\odot}$ but those with the highest SFR were located in dark matter halos of $\approx 10^{13}\ M_{\odot}$.

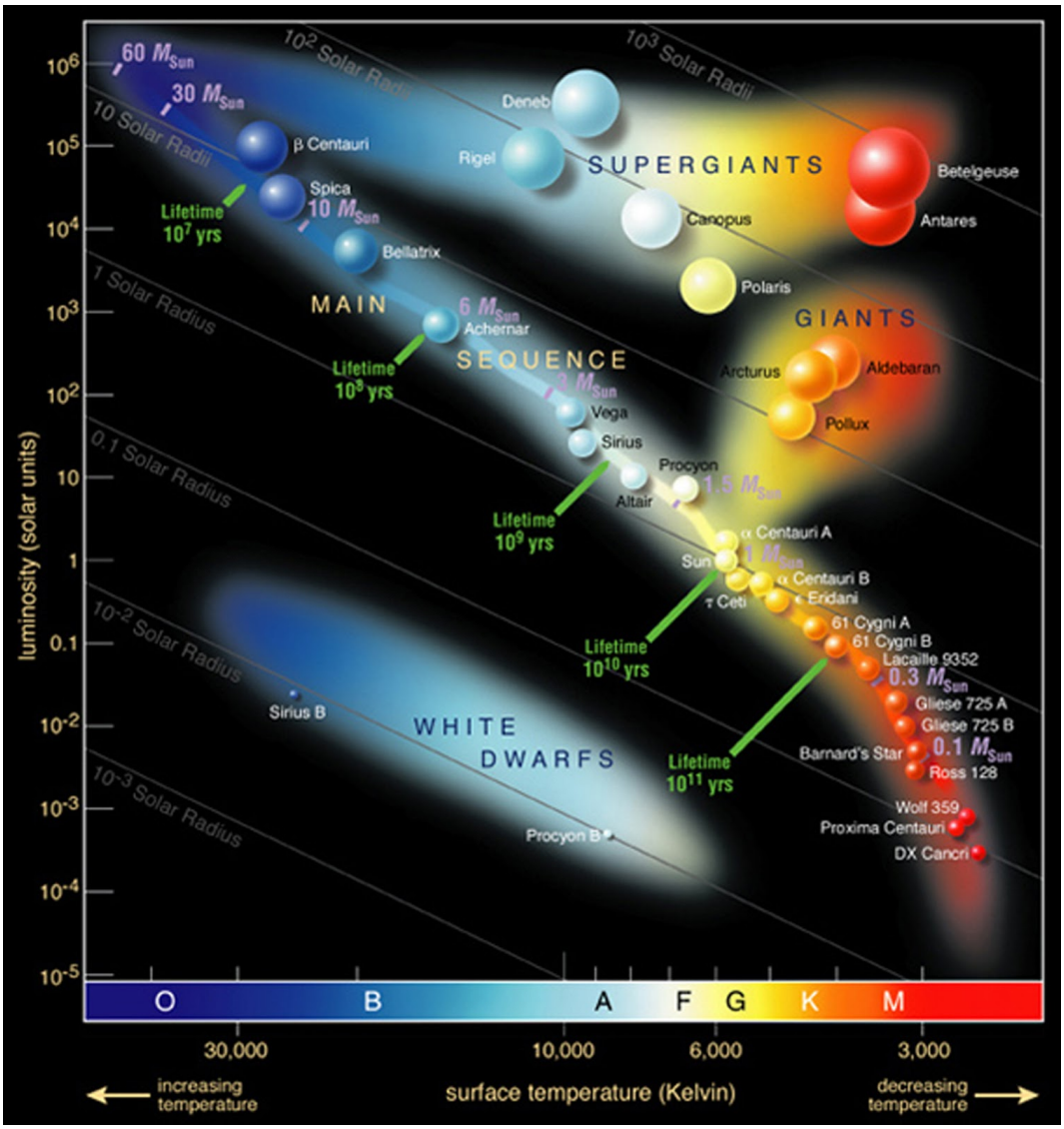

Figure 1.2: A Hertzsprung-Russel diagram showing the distribution of different classifications of stars, along with the expected temperature, luminosity and radius for stars of similar types. Credit:ESO/José Francisco (josefrancisco.org).

A galaxy can experience an extremely high star formation rate if it undergoes a starburst event, this event will last significantly shorter than the life span of the galaxy (Kennicutt, 1998). The event is normally triggered by interaction with other galaxies. They are primarily found in regions of higher galactic density as the chance for interaction increases (Moore et al., 1996). As two or more galaxies come in close proximity, the massive gravitational forces at play cause the gas and dust in each of the galaxies to be compacted igniting star formation via the activation of AGN (Sanders et al., 1988). The rate of star formation in our own galaxy

is approximately 1.6 $M_{\odot}$ per year (Licquia & Newman, 2015), but by contrast, starburst galaxies can exceed this rate by a factor of more than 100 times (Schneider, 2010). This huge rate of star formation requires a lot of gas from the galaxies' gas stores and consequently a post starburst galaxy is barren of most of its gas and dust. This phase of extremely fast star formation occurs on a timescale much shorter than the age of the galaxy, approximately 100 million years (Falgarone et al., 2017), and due to the formation of many new blue stars the luminosity profile of the galaxy will shift before returning back to a more steady colour (Hashimoto et al., 2019).

1.3 Large scale structure

Galaxies are not randomly scattered throughout the Universe, they exist distributed in a filament dominated web like structure (Bond et al., 1996). Galaxies can be found in clusters, groups or filaments. There isn't a clear divide between clusters and groups, however clusters are comprised of multiple galaxies bound gravitationally with an intracluster medium existing between them. Filaments are the largest systems in the Universe and feed clusters with an influx of galaxies and galaxy groups. Upon infalling from a filament environment to a cluster environment there can be an increase in star formation rate or the trigger of a starburst event. The cluster Abell 1763, for example, is fed by a star forming filament that links it to a nearby cluster Abell 1770, Edwards et al. (2010) used Spitzer MIPS data to determine that for galaxies in the filament there is an increased fraction of star formation relative to the cluster core. Complimentary to this Fadda et al. (2008) obtained redshift data for more than 500 infrared sources in the field, through the use of the wide field fiber spectrograph Hydra on the WIYN telescope and the multi-slit spectrograph Dolores on the Telescopio Nazionale Galileo (TNG telescope). They found over 100 cluster members bright in the infrared, mostly along a radial region hinting that these galaxies are entering the cluster environment for the first time, by analysing optical spectra they determined that this emission is mainly a result of obscured star formation.

Lewis et al. (2002) studied 17 clusters using redshift and Hα equivalent widths (EW) measured from the Two-degree-Field Galaxy Redshift Survey (2dFGRS). This was in order

to look at the relationship between SFR, radius from cluster core and local density (Figure 1.3). Lewis found that local galaxy density has the most affect on SFR, showing that galaxies in low density regions form stars better than at cluster centres. However galaxy evolution can be driven by processes other than ram pressure stripping similar to the conclusion by Dressler (1980). Correlations with density are found to be due to physical transformations that galaxies undergo in dense regions of space, and that the link between SFR and morphology with regards to density is not tenable. This is because the morphological change of a galaxy happens on a much greater timescale than star formation. Complementary to this is the work done by Gómez et al. (2003) in which they investigated 8598 galaxies within a redshift of $0.05 < z < 0.095$ using SDSS data. This showed a more detailed link between SFR, density and radius such that SFR decreases as density increases and radius decreases, in this case SFR dropped past 3-4 virial radii. Both Lewis et al. (2002) and Gómez et al. (2003) used different data methods and came to the same conclusion which gives the finding weight. Furthermore separate galaxies with the same morphology at very similar densities had different SFR indicating that there are other factors determining SFR other than density and environment.

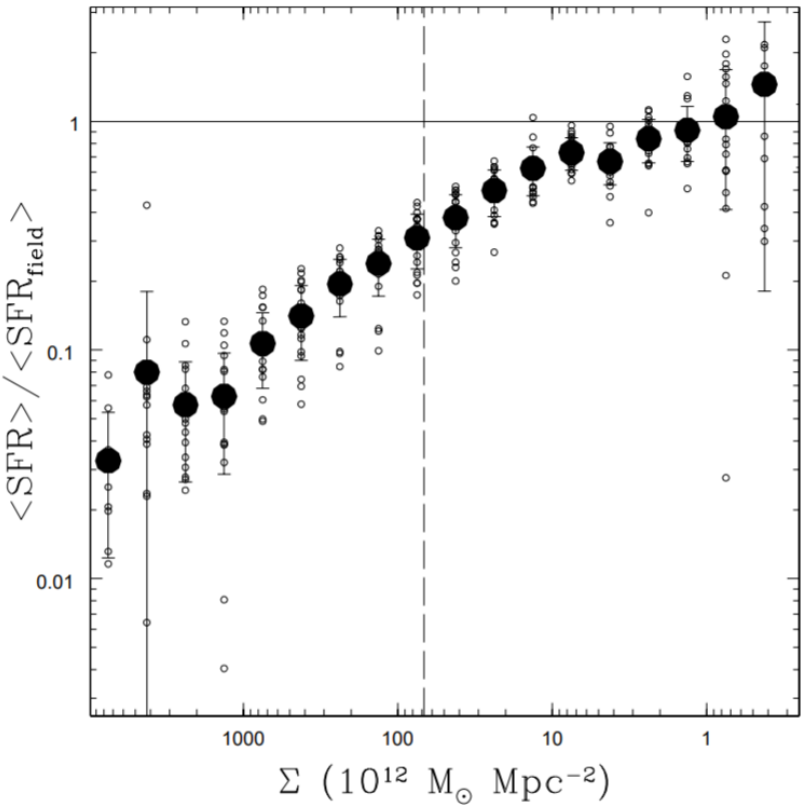

Figure 1.3: Star formation rate as a function of density, for groups, from Lewis et al. (2002). Where small, open points are results from a single projection of each of six model clusters; the large solid point is the mean, and the error bar is the standard deviation of the 18 realizations of the model. The dashed line shows the mean density of particles within the virial radius. The plot shows that as we increase the density in these groups the ratio of SFR to SFR of the field decreases.

Galaxies can evolve through a variety of processes, one of these is harassment. Harassment is a chain of interactions between two or more galaxies that come in close proximity but do not collide and merge, the massive gravitational forces can warp the morphology and composition of the galaxies more on each successive interaction. As the galaxies come close, the gas and dust in each of the galaxies can cause a starburst event and reignite star formation in those galaxies (Sanders et al., 1988). This newly started starburst dramatically affects the luminosity output of the galaxies as many new blue stars will be formed, this luminosity profile will remain shifted until the blue stars go supernova. However, these interactions can cause the loss of angular momentum in the galaxies and therefore, an inability to maintain the spiral arms, creating the barred spiral represented by SBx in the Hubble tuning fork (Figure 1.1).

Moore et al. (1996) analysed simulations of galaxy harassment and showed that harassment is a mechanism that can perturb a galaxies morphology, changing its shape, gas distribution and stellar content. Further, Moore gave examples of how interactions change galaxy morphology, such as low luminosity spirals becoming dwarf ellipticals after going through harassment.

Galaxies can often grow by merging with other galaxies in merger events. Originally it was thought that non primordial elliptical galaxies were the result of spiral galaxies being swept, producing a tightly wound round galaxy with little gas and dust. Dressler (1980) studied a sample of 55 rich clusters, using data gathered from these clusters Dressler compared the relationship between galaxy density and morphological type in regular/irregular, and high/low concentration galaxies. Dressler analysed this data to show that S0 galaxies aren't an evolution of spiral galaxies, having been swept via ram pressure stripping or evaporation. Dressler then introduces evidence showing that an increase in galaxy density leads to a decrease in disk growth and an increase in the luminosity of the spheroidal component of a galaxy, explaining why in high density regions spirals are less common. Furthermore, Dressler looked at the bulge/disk ratios of S0 and spiral galaxies in different density regimes, to find that they were not similar and thus providing evidence that spiral sweeping wasn't the driving force behind the creation of S0 type galaxies. In contrast, Dressler presented data showing alternative processes that were responsible for the relationship between galaxy morphology and density, such as: late galaxy formation, mergers and a density sensitive formation mechanism. These processes found showed a well defined relationship between local galaxy density and galaxy morphology, as well as less convincing argument for spiral sweeping being the creator of S0 types.

Spiral mergers seem to be a primary mechanism for the creation of elliptical type galaxies, there are three prongs of thought behind this. Elliptical galaxies do not contain as much dust and gas as a spiral counterpart. This implies that if two (or more) spiral galaxies merge a lot of the interstellar medium would have collided and brought about a starburst, a new wave of star formation. This is further compounded by a lot of elliptical galaxies showing signs that star formation has occurred recently (astronomically speaking). Alongside this ellipticals tend to exist in regions of high galactic density, where there is the highest probability of a

galaxy merger taking place. Finally it is important to note that in the early Universe mergers were more common because all galaxies were closer together, affected most were galaxies in clusters where the probability of a merger was already more likely.

(Carlberg, 1986) provided further evidence for collisions of disk systems creating elliptical type galaxies. He found that the phase space density in an elliptical galaxy is much higher than in a disk galaxy of similar mass, concluding that it would be fundamentally impossible for a disk system to become an elliptical without any collisions. This is further supported by (Merrifield, 2010) where he concludes that phase space density is a key behind galaxy evolution.

One way in which a galaxy can lose its gas content is through ram pressure stripping. Ram pressure is the force applied by the intracluster medium winds, causing any body falling towards a galaxy cluster to experience pressure due to the force. Ram pressure stripping (RPS) occurs when the force applied by ram pressure is greater than the gravitational forces binding the dust and gas to a galaxy. It is approximately equal to the product of the intracluster gas density (e) and the relative velocity (v) of the galaxy relative to the cluster and is given by the equation, $P_r \approx \rho_e v^2$ determined by Gunn & Gott (1972). A good example of RPS is the 'jellyfish galaxy' ESO 137-001 (Figure 1.4) which is having its gas stripped from the top left of the picture towards the bottom right. In this image ESO 137-001 leaves many bright tails indicating its stellar gas and dust is being forced out as the moves within its cluster, this shows the galaxy doesn't have the gravitational forces to contain the gas and dust. Ebeling et al. (2014) introduced three criteria to decide whether a galaxy is undergoing RPS: i) A morphology disturbance due to a force acting on one side of the galaxy, ii) bright colour gradients indicating bursts of star formation, iii) the presence of a tail of gas trailing behind the galaxy.

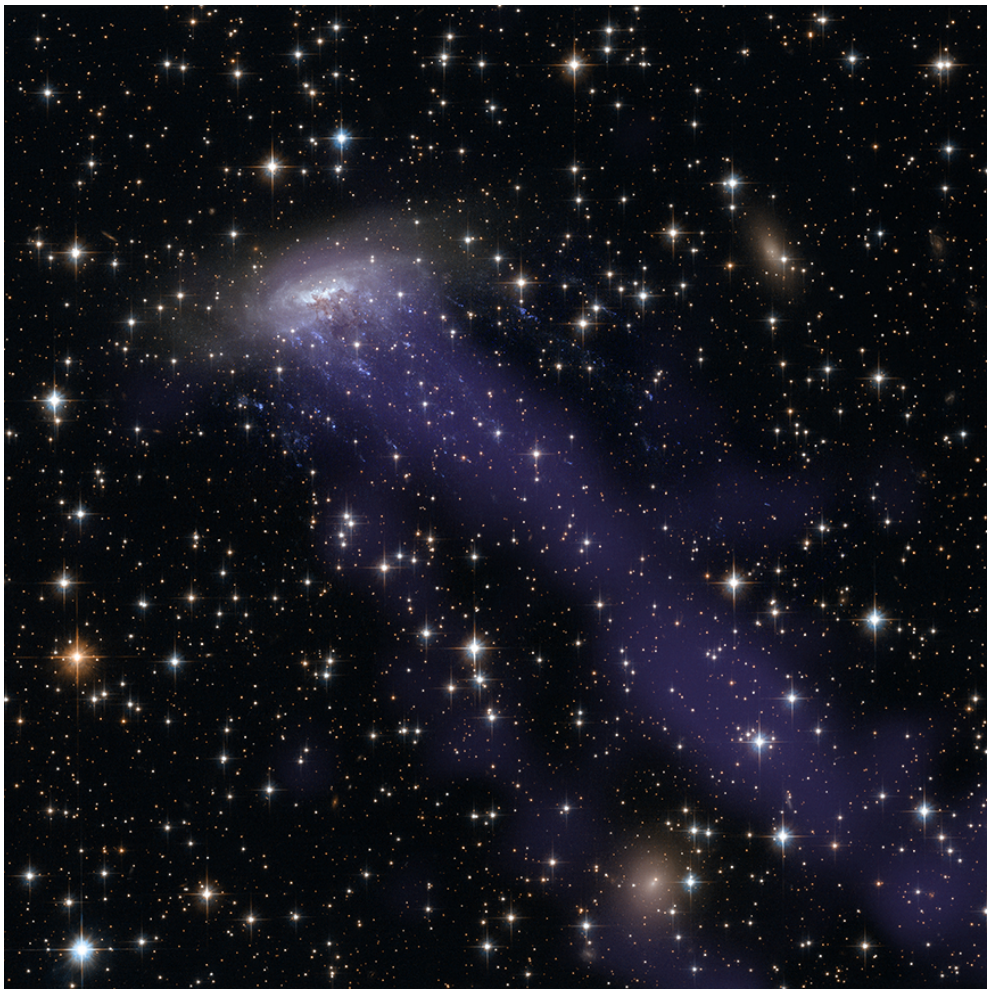

Figure 1.4: RAM pressure stripping occurring in ESO 137-001, the galaxy is being stripped in the direction of the bottom left, and the blue trail is the stripped gas. Credit:X-ray:NASA/CXC/UAH/M.Sun et al; Optical: NASA, ESA, the Hubble Heritage Team (STScI/AURA).

Merluzzi et al.(2016) studied two galaxies in the Shapley supercluster to examine the effects of both RPS and tidal forces on galaxies at the core of the cluster. This was to give another case study to look at with respect to RPS, as only a few tens of RPS events have been studied and researched in detail. They found that both SOS 61086 and SOS 90630, the two galaxies studied, exhibited the criteria set by Ebeling et al. (2014) such that they left tails behind them, the stellar and gas components had their kinematics decoupled and the disks were truncated. However, RPS simulations indicate that the tail left by SOS 90630 was not due to RPS but instead due to tidal interactions between this galaxy and another. This is important because it shows that there are other potential systems that can be mistaken for RPS and is somewhat subjective as it identified partly by visual inspection (McPartland et al.,

2016). Further evidence for this comes from Poggianti et al. (2016) who looked at local potential RPS cases, respective to our galaxy, and found that only 4/13 of the galaxies they observed experienced RPS.

1.4 Quenching

Quenching is the result of a galaxy using all its gas or not being able to use its gas to make new stars, as a result the star formation in a galaxy is quenched.

Clusters of galaxies exist at the intersections of filaments, due to the clusters being higher density regions there is a flow of galaxies from a filament environment to a cluster environment. Haines et al. (2013) suggests that a star forming galaxy upon transitioning to a cluster environment has its star formation rate slowly quenched. Haines et al. (2013) used a representative sample of 30 massive galaxy clusters between 0.15 <z< 0.30 from the Local Cluster Substructure Survey (LoCuSS) and found that star-forming cluster galaxies within r_{200} had a SFR 28% +/- 3% lower than galaxies in the field with a fixed mass and redshift, this is a significance of 8.7σ. This mechanism of SFR quenching was found to be consistent with the observed ram-pressure stripping that occurs when a spiral galaxy infalls into a cluster and interacts with the intracluster medium and occurs on scales 0.7Gyr-2Gyr. Haines et al. (2013) concluded that 1/3 of quenching occurs due to the galaxy being in a cluster environment and the other 2/3 occurs during infall.

This is supported by follow up work done by Haines et al. (2015) during an analysis of the kinematics of the same sample. They found that the fraction of star forming galaxies rises steadily with cluster centric radius, increasing five fold at $2r_{200}$. This drop in SFR is consistent with these galaxies being pre-processed in galaxy groups, despite this the surface density of star forming galaxies actually declines with radius falling $\approx 15x$ between the core and $2r_{200}$. This means star formation must survive withing the recently accreted spirals for 2-3Gyr to account for the observed quantity of star forming galaxies within clusters. This work puts forward a model that states SFR declines exponentially on quenching timescales 1.73+/-0.25Gyr upon accretion.

As a galaxy enters the more dense regions of a cluster the time scale on which quenching occurs changes. Maier et al. (2019) studied 7 clusters from LoCuSS at 0.15<z<0.26, combining this with spectroscopic data from the Arizona cluster redshift survey (ACRES) they measured the fluxes of O[II]3727, Hβ, O[III]5007, Hα and N[II]6584 emission lines. Using Hα to measure star formation rates and O[II], O[III] and Hβ to calculate the O/H metalicities, from the Lilly et al. (2013) model, they combined this to a field sample of 705 galaxies at a similar redshift. They found that although the median SFR of the cluster and the field were similar, the non-field sample have a higher O/H metalicity in a lower mass bin, within the radius of $R < r_{200}$. This is evidence for a slow quenching model, as quenching occurs with in fall into the cluster, SFR is fed by disk gas and metalicity is increased on a scale of 1-2Gyr, in agreement with Haines et al. (2015). As the galaxy travels to the denser regions, RAM pressure increases and quenching occurs at a much faster rate (Figure 1.5) , stripping all the gas from the galaxy and shutting down star formation.

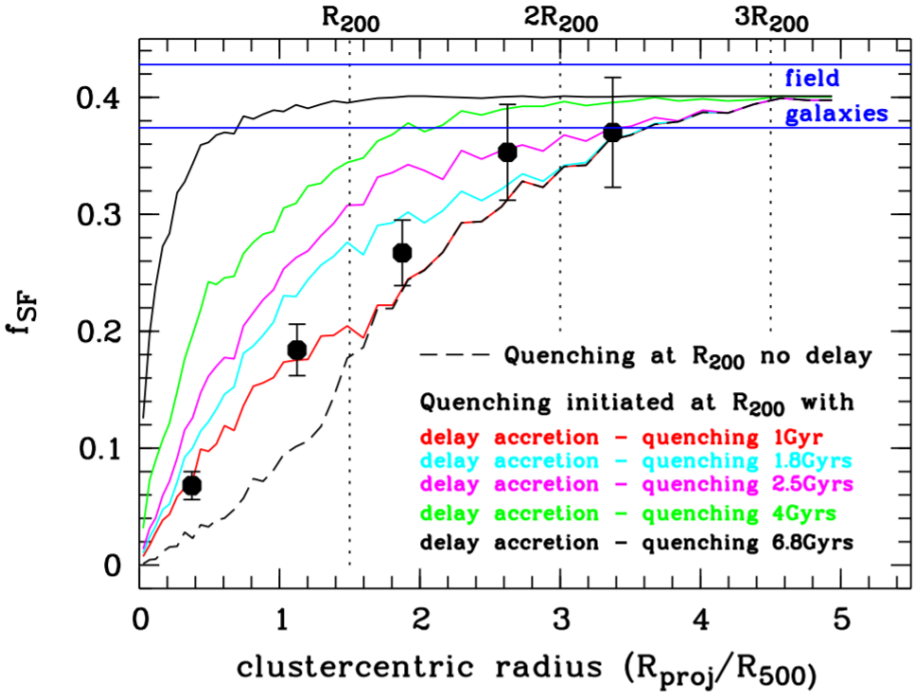

Figure 1.5: Star formation rate as a function of cluster centric radius for varying accretion delays from (Maier et al., 2019). The filled black circles are representative of star forming cluster galaxies in the mass complete sample. The longer the delay on accretion the higher fraction of star formers as a the cluster centric radius is decreased.

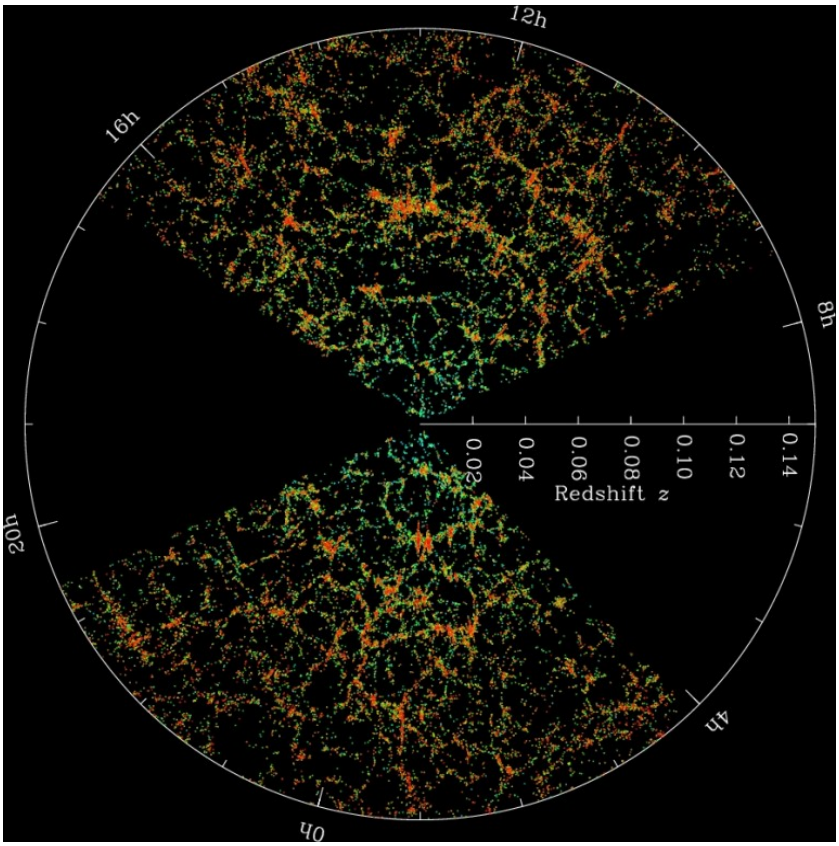

Figure 1.6: A map of large scale structure in the universe between redshift 0 and 0.15, red points are galaxies with more red light. The filament structure can be seen linking dense cluster regions. Credit: M. Blanton and SDSS

Looking at cluster environments, galaxies can be found infalling into the cluster or there is a second population of galaxies that have already been inside the cluster and are making their way back out, these are coined backsplashing galaxies. Gill et al. (2005) used eight high resolution N-body simulations with a standard cold dark matter cosmology to analyse galaxy dynamics in clusters. They found that approximately half of the galaxies within the 1-2 virial radii range are backsplash galaxies, and 90 percent of these entered to within 50 percent of the virial radius. They also found that these backsplashed galaxies have a different mass function than galaxies infalling for the first time, due to tidal disruptions from moving through the cluster environment, backsplashed galaxies have on average 40 percent less mass. Supplementary to this is the work done by Pimbblet (2011) where they looked at a sample of 14 redshift-isolated galaxy clusters from the Sloan digital sky survey, cleaned the sample to eliminate cluster on cluster mergers to leave just backsplashing galaxies.

Using mixture modelling they were able to differentiate between infalling galaxies and backsplashing galaxies. They found a fraction $f = 0.052R/R_{virial} + 0.612 \pm 0.06$ which they interpret as the backsplashing population fraction at $1 < R/R_{virial} < 2$.

Galaxies evolve in lots of interesting ways and exist in many different environments. In this thesis, I will specifically look at the equivalent widths of Hα, Hδ, [OII] and the value of the D4000 break. I will also look into galaxy colour and the blue fraction for each cluster, this relates to the science presented in this first chapter. I have made the assumptions that $H_0 = 69.6$ and $\Omega_\lambda = 0.714$ throughout. The plan for this thesis is to overview the data and current literature background for the clusters in Chapter 2. Chapter 3 will detail the data processing and measurements taken in this thesis. Chapter 4 will detail the analysis of A1763, the main cluster of this study. Chapter 5 will detail the analysis of the other 4 clusters. Chapter 6 will finalise the analysis for all of the clusters and conclude the thesis.

2. Data

2.1 Local cluster substructure survey

In this chapter we will introduce the data that was used in this thesis. This covers optical, Infrared (IR) and redshift measurements collected in the local cluster substructure survey (LoCuSS), which was proposed by (Smith, 2006). I will then detail the analysis of the data of the five clusters looked at for my thesis.

LoCuSS is a multi-wavelength survey that aims to link the structure of a morphologically unbiased population of clusters with their dark matter and non baryonic components. I have used data collected from this survey to probe five galaxy clusters, detailed below.

2.2 Data Capture

LoCuSS takes spectroscopic data from the Arizona cluster redshift survery (ACReS) Haines et al. (2012). The data was collected by the MMT/Hectospec, which is a 300 fiber multi-object spectrograph with a circular field of view of 1^o of diameter on the 6.5m MMT telescope at Mount Hopkins Arizona. The 270 line grating was used giving a wavelength range 3650-9200Å with a 6.2Å resolution and in total ACReS produced $\approx 30,000$ spectra, $\approx 10,000$ of which are cluster members and 100-500 redshift values for cluster members.

LoCuSS takes optical data from Suprime-Cam on the 8.2m Subaru telescope (Miyazaki et al., 2002). The Suprime-Cam is a 80-mega pixels (10240×8192) mosaic CCD camera with a 34'×27' field of view and a resolution of 0."202 per pixel. The Suprime-Cam uses two filters, a V band filter (more blue) and an i band filter (more red) both have photometric calibration to 10% precision through the use of Landolt standard stars (Landolt, 1992) and stellar photometry data from the Sloan Digital Sky Survey (SDSS) data release 8 (Eisenstein et al., 2011).

LoCuSS takes X-ray luminous clusters from the ROSAT all sky survey cluster catalogues (Ebeling et al., 1998) at a redshift of $0.15 \leq z \leq 0.30$, this equates to a lookback time of

1.9Gyr to 3.448Gyr. Using both far ultraviolet (UV) through to far infrared (IR) observations as well as gravitational lensing analysis and X-ray data LoCuSS measures variables such as: X-ray temperature, star formation rate and far-infrared galaxy luminosity function with minimal cluster to cluster scatter up to a flux limit of $5x10^{-13}$erg cm^{-2} s^{-1} (Voges et al., 1999). Each cluster was observed with a field of view of 25'x25' at 24 μm with multiband imaging photometer for Spitzer (MIPS) (Rieke et al., 2004) on the Spitzer Space telescope (Werner et al., 2004) consisting of a 5x5 grid of MIPS pointings in fixed cluster, to a sensitivity of 400μJy. Small-field photometry observations were taken in two cycles at each grid point within a time frame of 3s, making the total exposure time per pixel 90s (Haines et al., 2009). Using clusters that had been imaged already by the Guaranteed Time Observations Program 83 to a much greater depth (3000s per pixel) combined with the 24 m data, Haines et al. (2009) was able to give complete coverage of the entire field centred on each cluster in the sample.

The completeness of LoCuSS is detailed in Haines et al. (2013) and shown in Table 2.1 (below). By using three targeting aims for sources detected in our Spitzer 24μm, they wanted to provide a complete census. Firstly, they selected all galaxies $f_{24} > 1mJy$ (f_{24} is the fraction of galaxies detected in Spitzer) in the galaxy catalog, irrespective of colour, to give complete redshift coverage. Secondly, they target probable cluster members, based on their J − K color, with $0.4 < f_{24} < 1.0mJy$. Their aim was to complete the census of obscured star formation within cluster galaxies down to SFRs of 1 to $3M_{sun}/yr$. Lastly, they target probable cluster galaxies with $M_K < M*_K$ +2.0, prioritizing first those galaxies within the cluster core and those brighter than the k-band luminosity $L*_K$. The depth of K and J colour is ≈ 19 and ≈ 21 respectively.

Cluster name	Spectroscopic completeness of possible cluster members with ($f24 > 0.4mJy$)
A1763	505/510
A1689	149/150
A1758	323/325
A1835	199/203
A963	420/470

Table 2.1: The completeness of LoCuSS detailed in Haines et al. (2013).

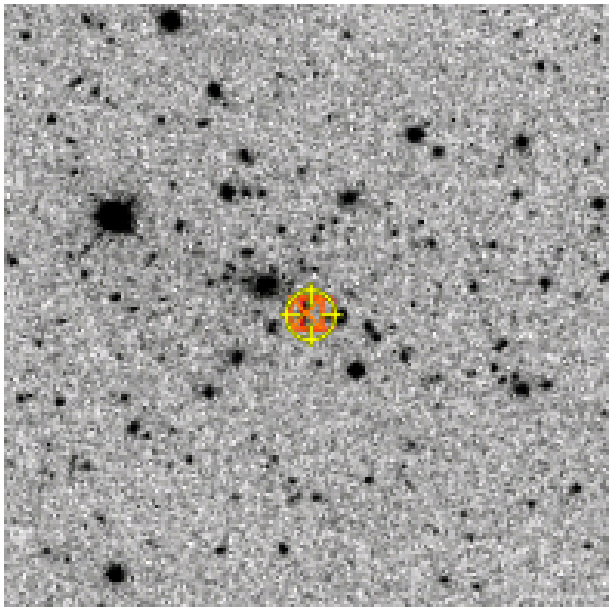

Figure 2.1: An image showing A1763 in r band, from SDSS. This shows the distribution of the galaxies in the cluster in the r band.

The cluster A1763 has a well defined centre which is dominated by a super giant elliptical (cD type) galaxy (Figure 2.1). There is a mass distribution peak located at the same position as the cD type galaxy indicating that this is the central cluster component (Dahle et al., 2002). The mass, light, and number density distributions all point towards A1763 being a relaxed system (Dahle et al., 2002). Using cosmic shear surveys we can obtain direct measurements of the mass distribution indicating the sub structure of the cluster and also detail of the distribution of its dark matter. Weak lensing measures the mass of objects and can be compared precisely

to theoretical models of formation of structure and substructure in clusters via the detection of shear signal.((Refregier, 2003), (Hirata et al., 2007)). Smith et al. (2005) found that when fitting a model that uses the single cluster-scale mass component as the sole free parameter, the model fails to reproduce the shear signal to the west of the cD type galaxy at the centre of the cluster. This residual signal is interpreted by Smith et al. (2005) as an indication of substructure in the cluster.

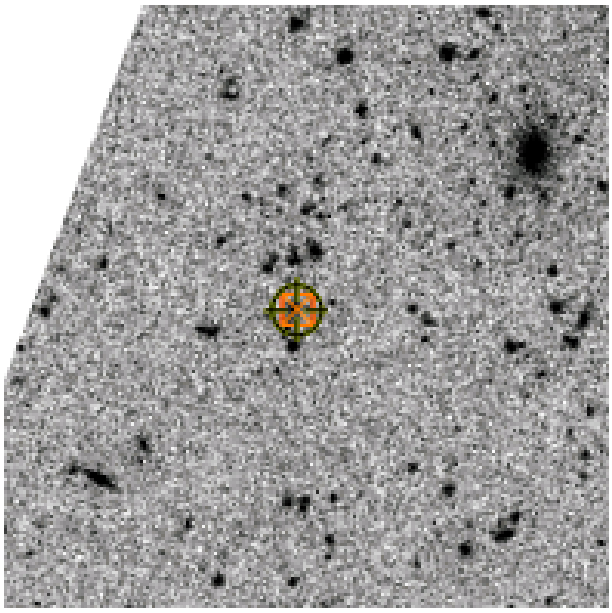

Figure 2.2: An image showing A963 in r band, from SDSS. Centered on the yellow circle. This shows the distribution of the galaxies in the cluster in the r band.

The cluster A963 was described by Jeltema et al. (2005) as elliptical in nature and relaxed, with small-scale structure at the core, the distribution of galaxies can be seen in Figure 2.2. Lavery & Henry (1988) discovered blue cluster members that show signs of recent star formation, had a much higher chance of having neighbours within 5 arc seconds was significantly higher than in red cluster members. They discovered through the use of x-ray analysis, that it has a centrally dominant elliptical galaxy with a north-south elongation and is a candidate for cluster cooling flow. Cluster cooling flow occurs when a cluster centre cools rapidly and as a response hydro static equilibrium attracts material to the centre of the cluster (McDonald et al., 2018).

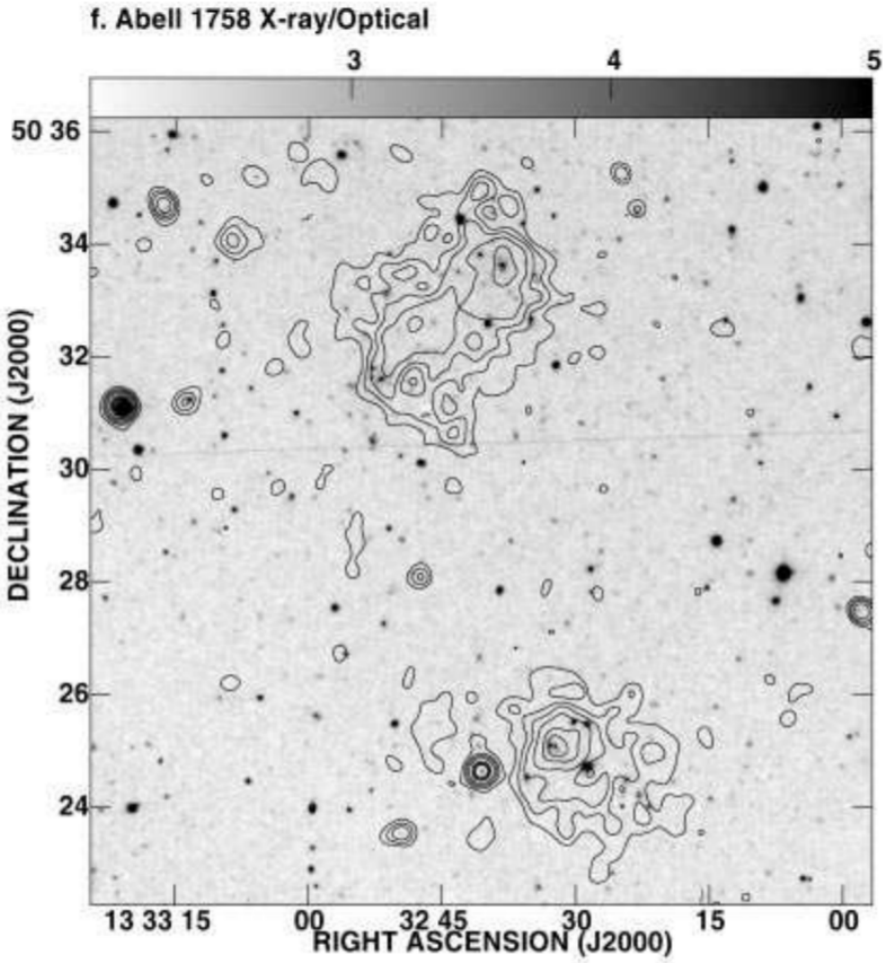

Figure 2.3: The contours of the HRI surface brightness overlaid on to the Digital Sky Survey optical grey-scale. A1758 was smoothed with a 20-arcsec Gaussian (Rizza et al., 1998).

The cluster A1758 contains complex structure in X-ray emission near the cluster (Figure 2.3) as observed by Rizza et al. (1998). Through matching the X-ray peaks with density of galaxy distribution the cluster appears to be bimodal, with the dominant galaxy in the south east sector aligning with a narrow angle tailed radio source (O'Dea & Owen, 1985) and producing approximately 40% of the combined luminosity (Giovannini et al., 1999). Approximately 1 Mpc south of the cluster is an extended clump of X-ray emission correlated with group of galaxies. Rizza et al. (1998) matches the magnitude range of these galaxies to the rest of A1758, suggesting that this group is infalling to A1758. Dahle et al. (2002) suggests that A1758 is a double cluster, potentially in the process of merging into a single massive cluster. They state that each sub-clump is independently, locally relaxed and concentrated

around a bright early type galaxy and that an elongated mass concentration exists between the two clusters ((Dahle et al., 2002), (Jeltema et al., 2005)).

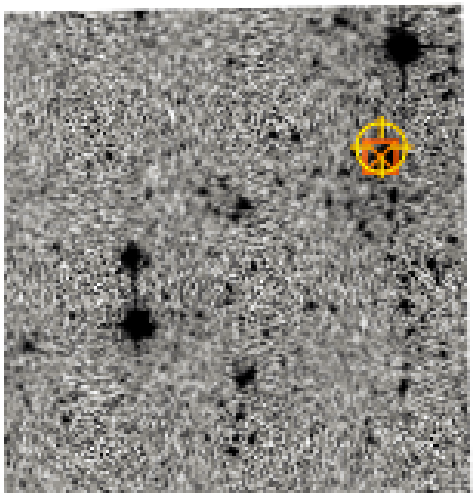

Figure 2.4: An image showing A1835 in r band, from SDSS. Centered on the yellow circle. This shows the distribution of the galaxies in the cluster in the r band.

Analysis of cluster A1835 (Figure 2.4) by Schmidt et al. (2001) shows a drop in X-ray gas temperature at the cluster core of ≈8keV and the presence of a strong cluster cooling flow. Dahle et al. (2002), by studying images in X-ray and the cluster cooling flow, state that the cluster has a regular morphology and is a relaxed system that is in dynamic equilibrium. The mass, light and density distributions align with a central cD type galaxy. Dust emission from this central galaxy has also been detected by Edge et al. (1999) and is associated with the detection of CO emission. Ueda et al. (2017) describes A1835 as a typical cool core cluster with lumpy substructure in the core with spiral patterns extending out to the intracluster medium (ICM), they state that it may also be going through an off axis minor merger.

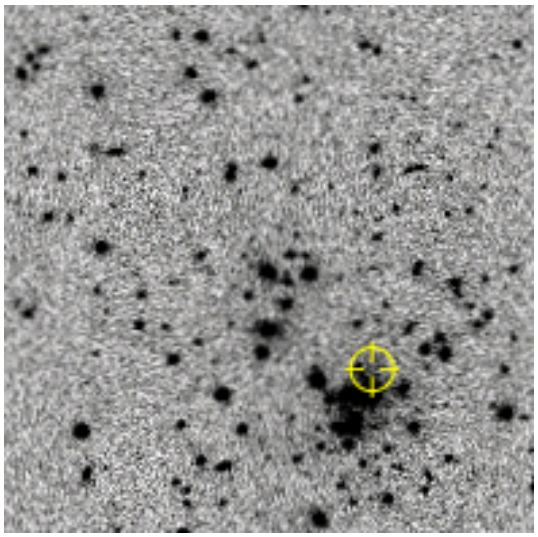

Figure 2.5: An image showing A1689 in r band, from SDSS. Centered on the yellow circle. This shows the distribution of the galaxies in the cluster in the r band.

Work on cluster A1689 (Figure 2.5) from Newell (1979) and Balogh et al. (2002) describe it as centrally concentrated and rich in morphology respectively and Bonamente et al. (2002) reports there is no evidence of soft excess emission. Butcher & Oemler (1984) measure the blue fraction of this galaxy as being 0.09. A1689 is an understudied cluster making it a good candidate for analysis.

3. Data processing

3.1 Chapter overview

In this chapter I will discuss measurements I took from the LoCuSS data set for each galaxy and their importance in understanding the characteristics of these galaxies. All the spectral data and redshift values used for this work is archival data, however, all measurements of equivalent width are my own calculations. In total I measured the equivalent widths for five spectral lines as well as measuring the D4000 break for 5675 galaxies over five separate clusters.

3.2 Equivalent width

We can detect the spectra of distant galaxies, which shows us the luminosity of photons detected at different wavelengths. By finding the integral of the line profile at the continuum level (Fc) we obtain the equivalent width (EW) (Equation 3.1 Pimbblet et al. (2006)). Finding the equivalent width, at wavelengths we know represent certain elements allows us to understand what elements are present in the gas and dust surrounding that galaxy. Depending on what is present in the surrounding gas and dust allows us to make assumptions about the galaxy, such as its SFR (Dijkstra & Westra, 2010) and therefore, we can infer if it has gone through a starburst phase. LoCuSS data came with redshifts, this allowed us to be able to shift the spectral data and take the equivalent width values at specific wavelengths, allowing us to identify certain emission lines.

$$EW = \int_{\lambda_B}^{\lambda_A} (1 - F_\lambda / F_C) \tag{3.1}$$

3.3 Emission line spectra and the Balmer series

The emission line spectra of an element is a set of frequencies of electromagnetic radiation emitted when an atom transitions from a high to a low energy state. Each element has a unique energy gap between states and when the transition occurs it translates to a distinct wavelength that represents the element. Studying the spectra of galaxies shows us the composition of the gas and dust in these galaxies via spikes at wavelengths that correspond to certain elements. The Balmer series in particular tell us alot about a galaxy. The Balmer series is a set of emission lines for the hydrogen atom, finding the equivalent widths of some of the Balmer lines can give insight into properties of a galaxy. The lines I have focused on throughout this research are Hα and Hδ located at 6564.61Å and 4102.89Å respectively, Figure 3.1 shows the location of both of these lines on a spectra.

3.3.1 Hα

In star-forming galaxies, Hα photons are produced by gas ionized by young hot stars. So by measuring the EW of Hα (6583Å) we can determine whether the galaxy has a large number of young stars. Understanding that if a galaxy has a lot of young stars indicates to us that it must also have a high rate of star formation, and so through using equivalent widths we can assign a value to quantify star formation rate. In my thesis I have used a value of Hα EW>-3Å from Wilkinson et al. (2017) to determine a high star formation rate.

3.3.2 Hδ

A deep Hδ absorption line (Hδ EW>3Å) is used as an indicator that a starburst has occured 0.5-1.5 Gyr prior to the moment of observation (Dressler & Gunn (1983)). Poggianti & Barbaro (1997) showed that even metal poor populations can produce strong Hδ, so metalicity does not interfere with using hδ as an indicator for recent enhanced star formation.

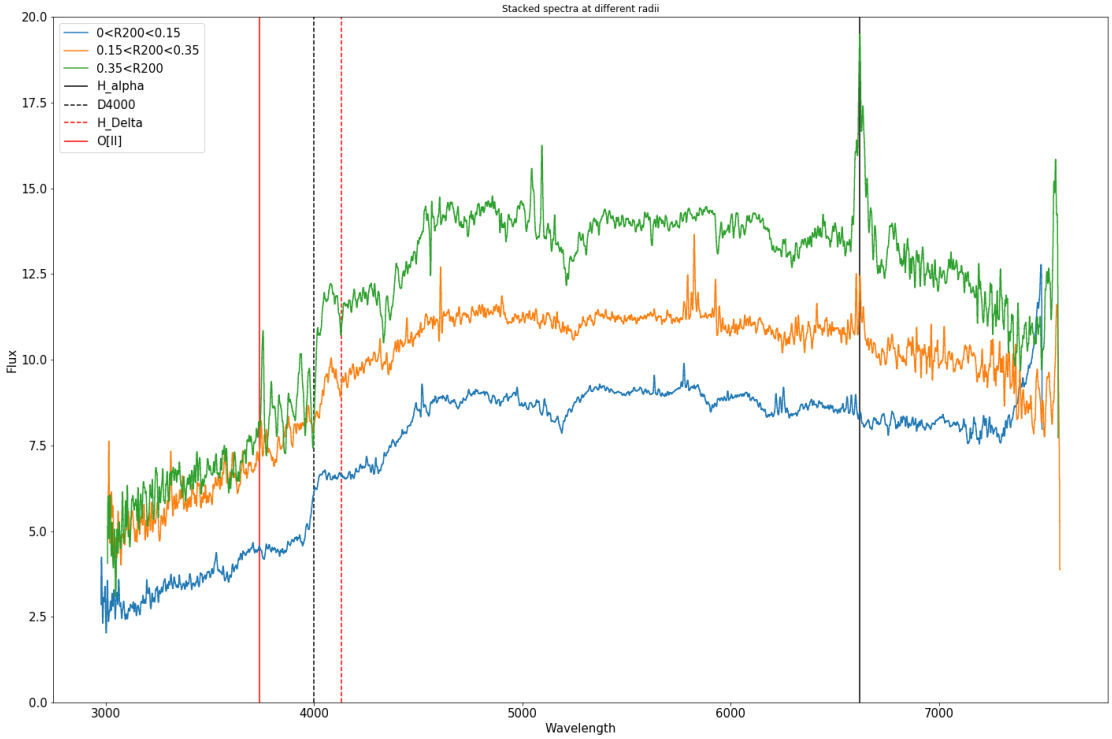

Figure 3.1: Spectral data for 3 galaxies at different radii from the center of A1763. Showing the difference in measured Hα, Hδ, [OII] and D4000 for three different spectra from different cluster centric radii in Abell 1763. The Hα values for example increase as a function of radius from the center.

3.4 [OII](3727Å)

[OII] is another indicator of star formation and is useful at higher redshifts when H-alpha moves out of the optical window (Kennicutt (1992), Rosa-González et al. (2002)). However, [OII] is not just an indicator of star formation, its measured flux can also be as a result of AGN activity so it is important to note that high [OII] flux is not, on its own, a certain measure of star formation rate (Yan et al., 2006). In post starburst galaxies, a lack of [OII] emission line is used, alongside Hδ absorption and Hα emission to define if star formation has stopped.

3.5 The D4000 break

The D4000 break is defined as the ratio of the average flux density between 4050Å and 4250Å to the average flux density between 3750Å and 3950Å (Bruzual A., 1983). D4000 is commonly used as an indicator of age, as it is representative of metalicity in a galaxy (Brinchmann et al., 2004). Figure 3.2 from (Poggianti & Barbaro, 1997) quantify the relationship between age and D4000 value.

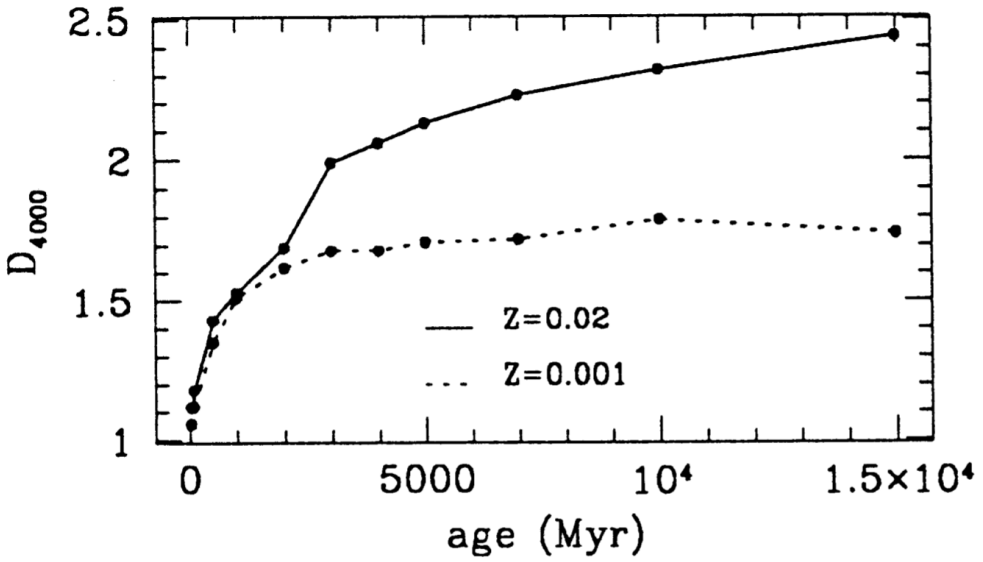

Figure 3.2: D4000 values for single stellar populations from (Poggianti & Barbaro, 1997). The value for D4000 increases as a function of age.

3.6 Sample selection cuts

Once we understand the physical implications of the above mentioned measurable features we can start to apply a filter to remove poorer quality data sets. The first phase of filtering the data sets was to apply a cut in redshift to eliminate all galaxies with a redshift of less than 0.35, any galaxy with a redshift higher than that has its Hα line pushed out the optical range. The sample we used is reduced to only galaxies with a redshift lower than 0.35. We can measure their Hα line of all of these galaxies, we then apply a signal to noise filter to make sure we are picking up primarily strong signals with minimal noise. Work by Mathis

et al. (2006) uses a S/N of 20 to 30 on spectral lines and work by Wild et al. (2007) uses a S/N as low as 8 per pixel. As I was testing a multitude of spectral lines for each spectra as well as measuring the D4000 break I used a different approach by applying the signal to noise cut to the whole spectra. This would ensure that I only allowed a spectra where all the spectral lines for every member in my sample were accurately measurable. I tested different signal to noise ratios, applying them to the whole spectra and finally used a signal to noise ratio of 2. The decision to use a signal to noise ratio of 2 was to make sure we had a balanced number of galaxies that were left in our sample. A higher signal to noise ratio could have been used for example 4 or 8 but both of these left us with very few galaxies overall. I chose to use 2 as it gave us a representative number of galaxies with the downside that some had very large noise. I visually inspected galaxies both above and below the threshold set and found that the detections when using a ratio of 2 were valid.

4. A1763 Results

4.1 Chapter overview

In this chapter I will detail the process I used to analyse the data for Abell 1763, the results I obtained and the conclusions I drew. I have singled out Abell 1763 as the main focus of this study due to early data availability, and use the other four Abell clusters to act as a comparison sample. Using caustic diagrams (section 4.2) I determine that A1763 is comprised of 293 galaxies and is being fed by two star forming filaments that link it to a nearby cluster Abell 1770 (section 4.4.1). I determine that there is a backsplashing population (section 4.4.2). I analyse Hα (section 4.4.3), Hδ and the D4000 break (section 4.4.4) in the galaxies to show that A1763 has a rich morphology with an inward population of young star forming galaxies and a central population of older metal rich galaxies. Using a Dressler style plot I classified the galaxy types (section 4.4.5) and re plotted them in phase space to see how the different galaxy types are distributed. From the plot I determined that 6% of galaxies are post starburst galaxies (section 4.4.6) and plotted how they are situated in phase space. I use cumulative frequency diagrams to show the distribution of galaxies with respect to both cluster centric radius and model magnitude (section 4.4.7). In order to determine how this cluster has evolved I had to compare it to a field sample (section 4.4.8) by using a two tailed Kolmogorov-Smirnov test I analysed the field sample against the cluster sample (section 4.4.9) and found that the cluster contained an increased number of active galaxies and a metalicity that isnt significantly different from the field. I show the significance of a signal to noise ratio of 2 and how passive galaxies are eliminated from the sample if we use a signal to noise ratio greater than 2 (section 4.4.10). Lastly, I round off the analysis (section 4.4.11) of the cluster by determining the number of blue galaxies in the cluster, that is the blue fraction and get a value of 13% ± 0.4%.

4.2 Cluster Selection

Using the data collected by LoCuSS, I started out with the spectral data for 1200 fibers and redshift values for 1038 objects, after matching these I had a set of 1038 objects from both the cluster and the field complete with redshift values. Before performing analysis on the spectra in the sample I made some choices about reductions to the data. For galaxies at a higher redshift Hα is pushed out of the optical range. Since the measurement of the Hα emission line is a focal point of this thesis and my basis for determining the SFR of a galaxy, I decided to cut any galaxy with a redshift measured higher than 0.35 from my sample. This reduced the sample from 1038 objects to 667 where Hα could be measured.

To define which of these belonged to the cluster and which do not, I plotted each of the 667 objects in a phase space diagram (Figure 4.1) with the densest collection of points coloured in yellow and the least dense points in dark blue. In the plot the y-axis represents line of sight velocity and the x-axis represents the cluster centric radius (r/r_{200}). Carlberg et al. (1997) define r200, as the radius at which the mean interior density is 200 times the critical density, this radius is assumed to contain the majority of the cluster mass. By using r_0 as the X-ray centre (Piffaretti et al., 2011) I was able to calculate the (r/r_{200}) value for each object in the sample. This combined with the knowledge of redshift values from ACRES allowed me to plot each point in phase space. The next step was to eliminate non cluster members, to do this I used the Carlberg, Yee and Ellingson (CYE) mass model (Carlberg et al. (1997) CF. Pimbblet et al. (2006)) to place caustics aligning with the 3σ contour defined in the model. This model is accurate to 20-30% in estimating mass to light ratios, the error is mainly down to random substructure differences in clusters. Once these caustics are applied to the phase space diagram all galaxies lying outside of them are removed from the sample and treated as external to the cluster dynamic, this leaves the final cluster sample containing 293 galaxies.

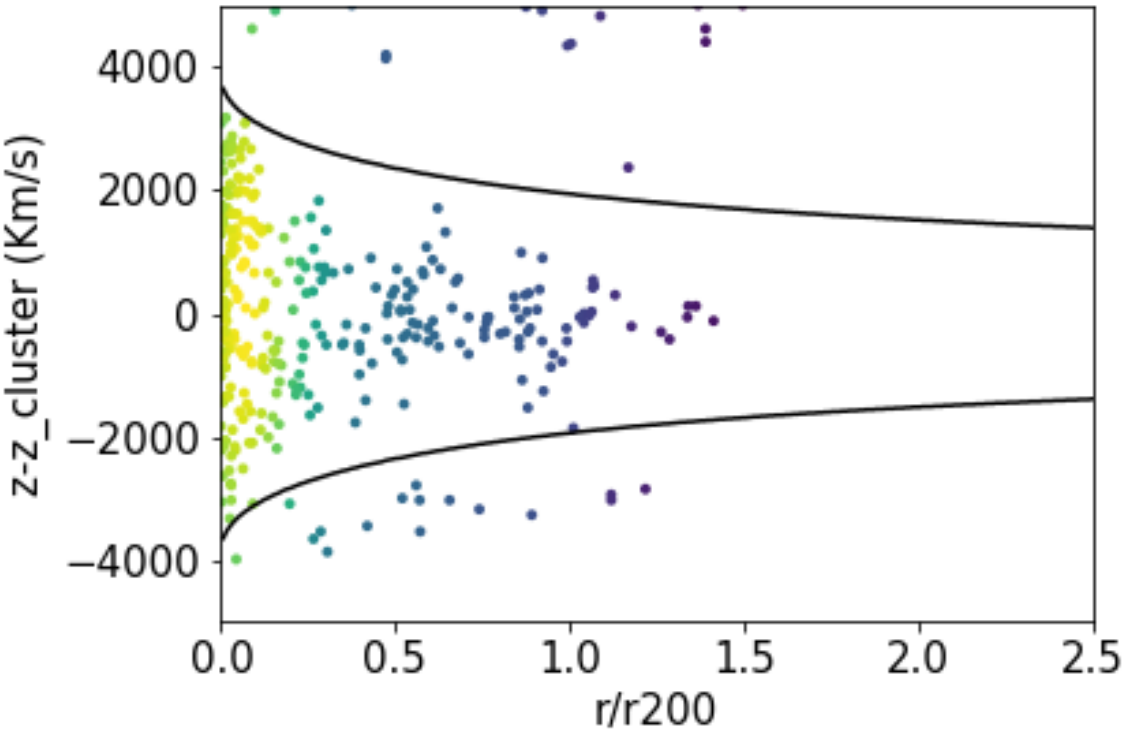

Figure 4.1: Abell 1763 shown in full in with CYE mass model caustics. The caustics define cluster membership, all points outside of them are defined as outside of the cluster.

4.3 Cuts

Plotting the final cluster sample in figure 4.2 shows how the cluster is structured in traditional coordinate space, against the full sample that was captured. This sample, however, contains signals with a range of accompanying noise, to determine what signals were real, I went back to the full sample introduced a signal to noise ratio (SNR) cut. To determine the SNR, I took each galaxy averaging the signal of each galaxy sample then divided it by the average noise in each sample. Applying the signal to noise cut allowed me to split the sample of 667 galaxies into a high signal to noise group of 268 galaxies (figure 4.2) and a low signal to noise group of 399 galaxies (figure 4.3). Throughout this thesis I will be using either just the high signal group or the both groups combined, depending on the analysis being performed.

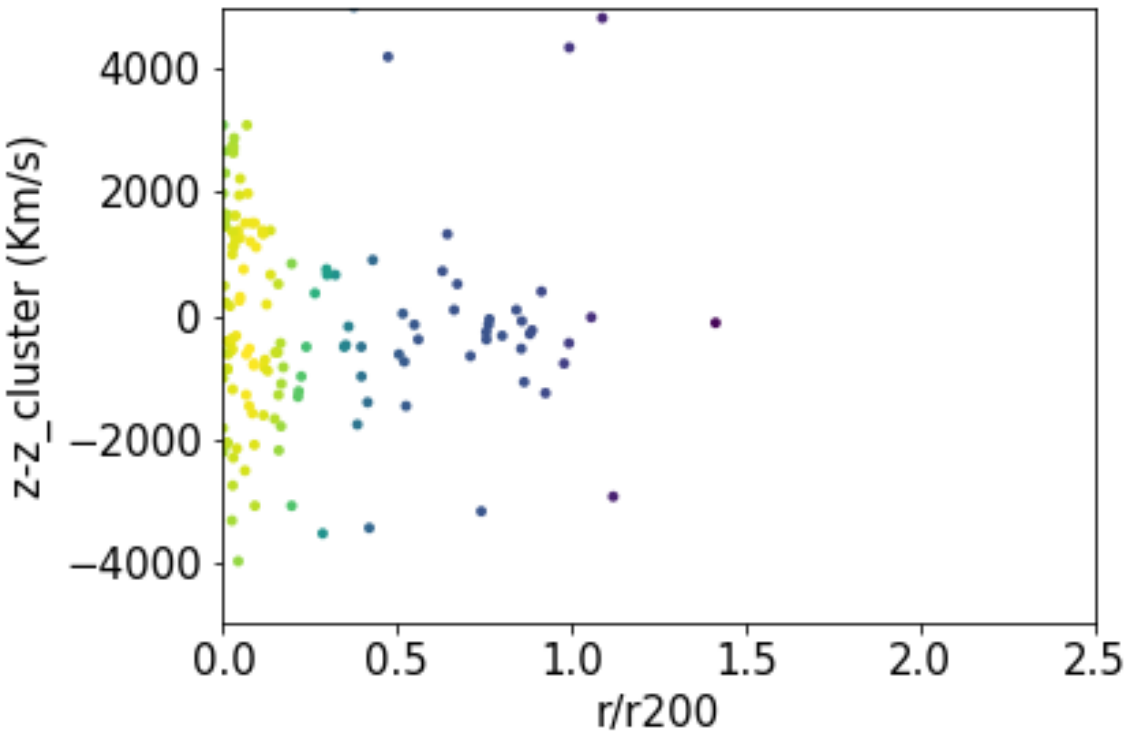

Figure 4.2: Abell 1763 redshift cut sample showing high signal to noise only. This shows the amount of the sample we use when determining equivalent widths of galaxies.

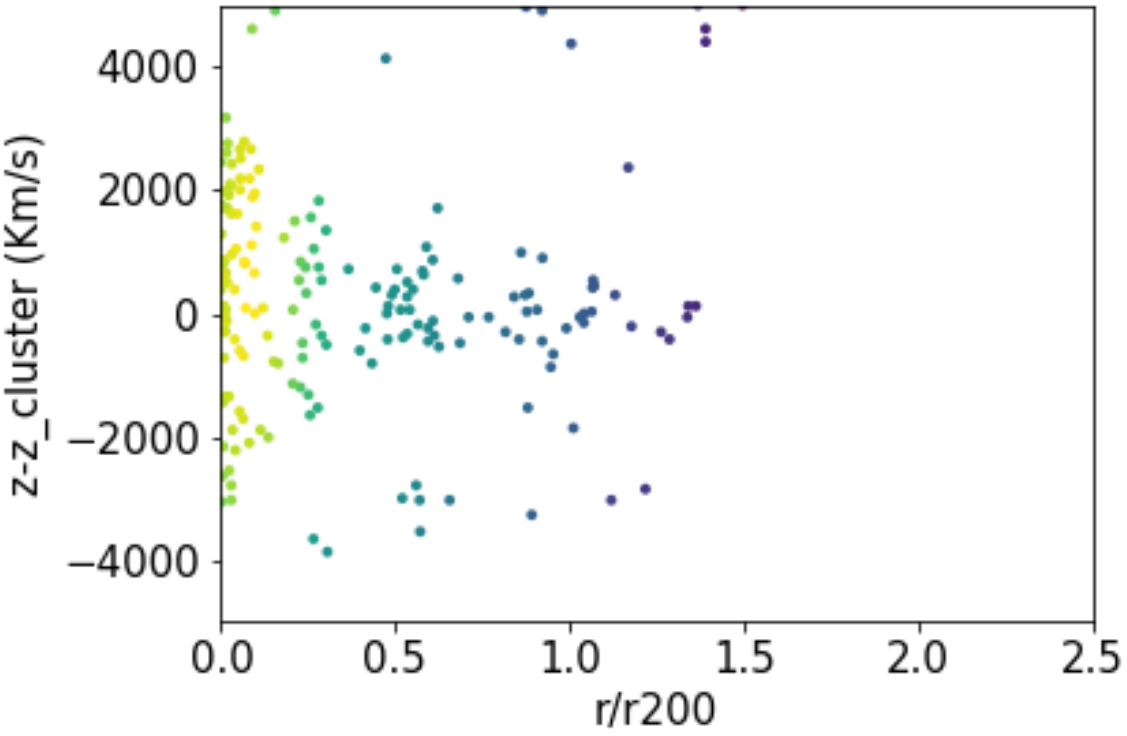

Figure 4.3: Abell 1763 redshift cut sample showing low signal to noise only. This is the distribution of the sample that we cut out when measuring equivalent widths.

4.4 Substructure of A1763

In this section I will discuss the analysis of the substructure; substructure is important in detailing the galaxies history, it is also indicative of star formation rate. This will focus on the filament that feeds the cluster with infalling groups of galaxies and potential back splashing that occurs upon galaxies infalling.

4.4.1 Filaments and Infalling groups

A1763 is fed by two star forming filaments that link it to Abell 1770. Galaxies that travel from the filament to a cluster environment are more likely to have a higher star formation rate than at the cluster centre (Edwards et al., 2010). To further probe at the filament structure that feeds A1763, I used data from Dr Chris Haines, where he had identified infalling groups and the filament. To identify the groups infalling into the cluster, he identified extended X-ray sources in the XMM-Newton image of A1763. Identifying centres of X-ray emission and examining the redshifts of galaxies nearby allowed him to determine if these galaxies existed in a group. In cases where 4 or more galaxies had a redshift within $500 kms^{-1}$ of each other, within the X-ray contours, they were determined to be an X-ray group. Using the Lx-mass calibration from Leauthaud et al. (2010) and the X-ray luminosity from the observed flux for each galaxy, the halo mass and r200 values can be calculated. Members of the group within $1000 kms^{-1}$ of the central group redshift (mean velocity of the group members) are identified as group members. If these groups have redshifts that place them within the caustics of A1763 (Figure 4.1) then they are identified as infalling groups (Haines et al., 2018). Using this data I plotted the infalling groups in both RA/DEC (Figure 4.4) and in phase space (Figure 4.7). These filaments will clearly make the cluster grow and increase the blue fracion.

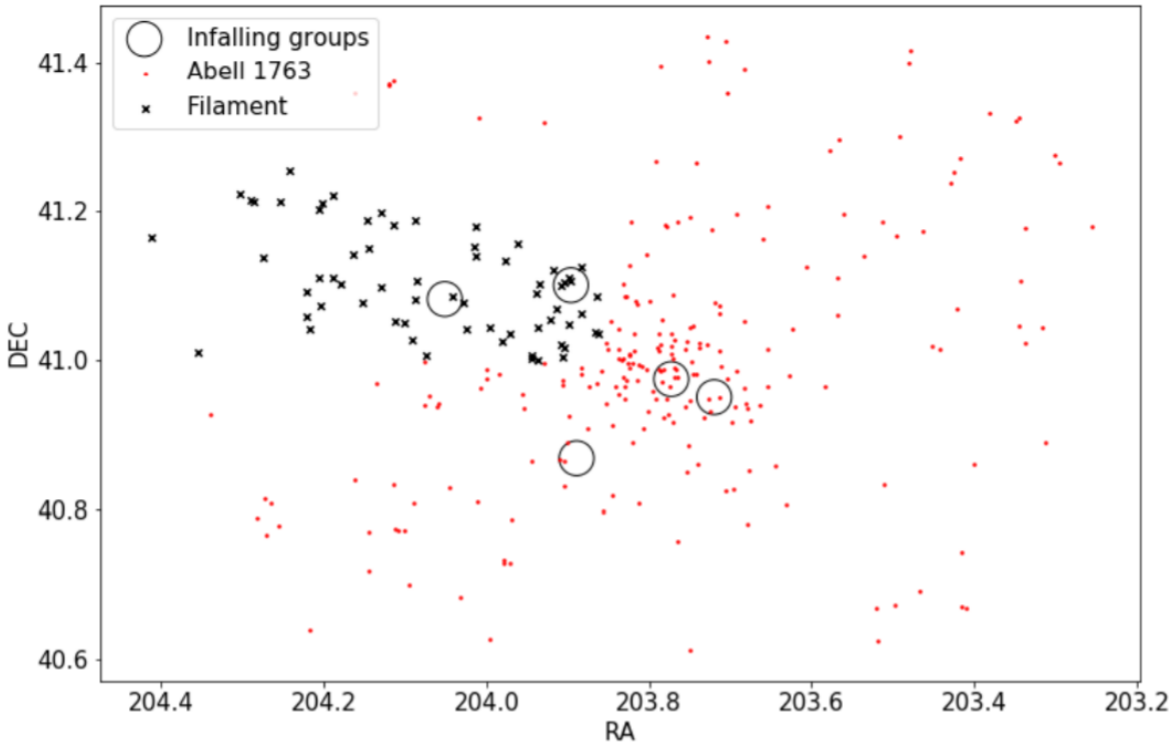

Figure 4.4: Abell 1763 plotted in coordinate space, displaying the position of the infalling groups, the filament and the other cluster members.

4.4.2 Backsplashing

It is important to understand if a cluster has a backsplashing population as it plays a crucial role in understanding cluster dynamics and galaxy evolution. Both Gill et al. (2005) and Pimbblet (2011) refer to the importance of identifying a backsplashing population in a cluster environment. Figure 4.5 from Gill et al. (2005) shows a simulated cluster and the path a backsplashing galaxy takes through the cluster. To test whether the infalling galaxy groups in Abell 1763 are backsplashing, I plotted them in phase space added (Figure 4.7) and removed all galaxies outside of the caustics. All five of the infalling groups detected fall within the caustics and are ,therefore, not backsplashing galaxies. As for the non infalling groups, there is a backsplashing population within Abell 1763 agreeing with the findings of Gill et al. (2005). This can be seen in Figure 4.6, with the higher radial bins containing galaxies with a higher velocity dispersion.

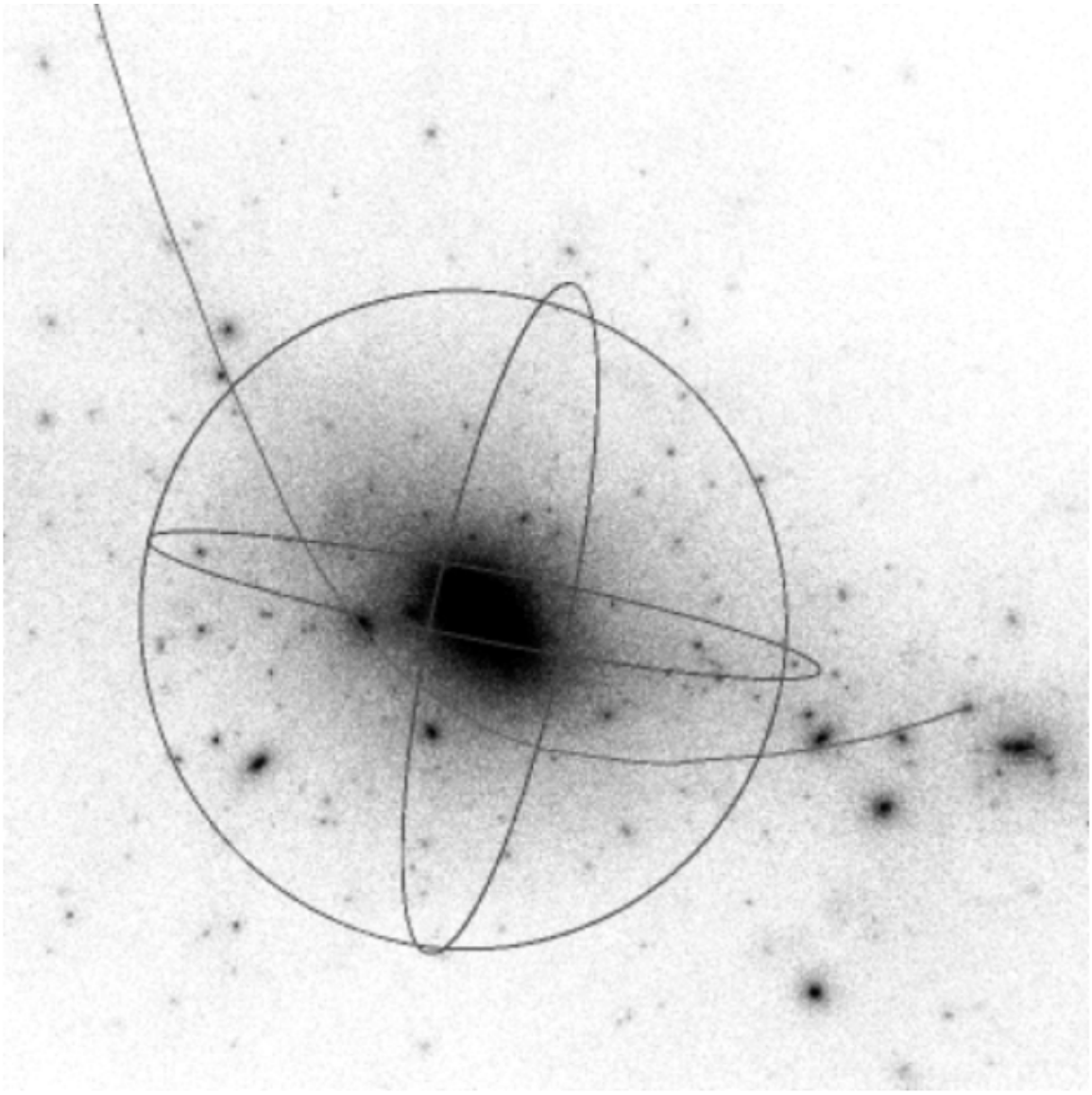

Figure 4.5: A cluster simulation at z=0, the dark sphere indicates virial radius, the line indicates the path of a backsplashing galaxy. The backsplashing galaxy will have undergone changes to its gas profile and SFR as it passed through the cluster (Gill et al., 2005).

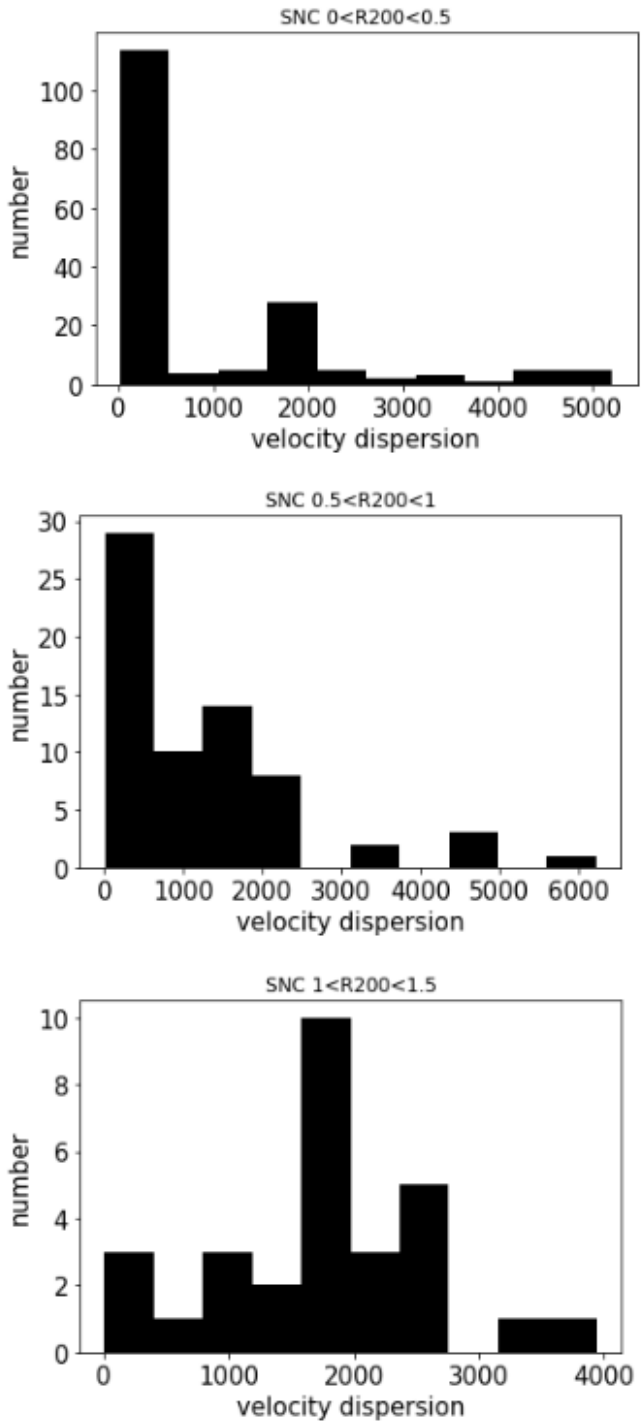

Figure 4.6: A set of histograms showing velocity dispersion with increasing cluster centric radius. The highest radial band contains the backsplashing population in the form of a number of galaxies all with high velocity dispersion.

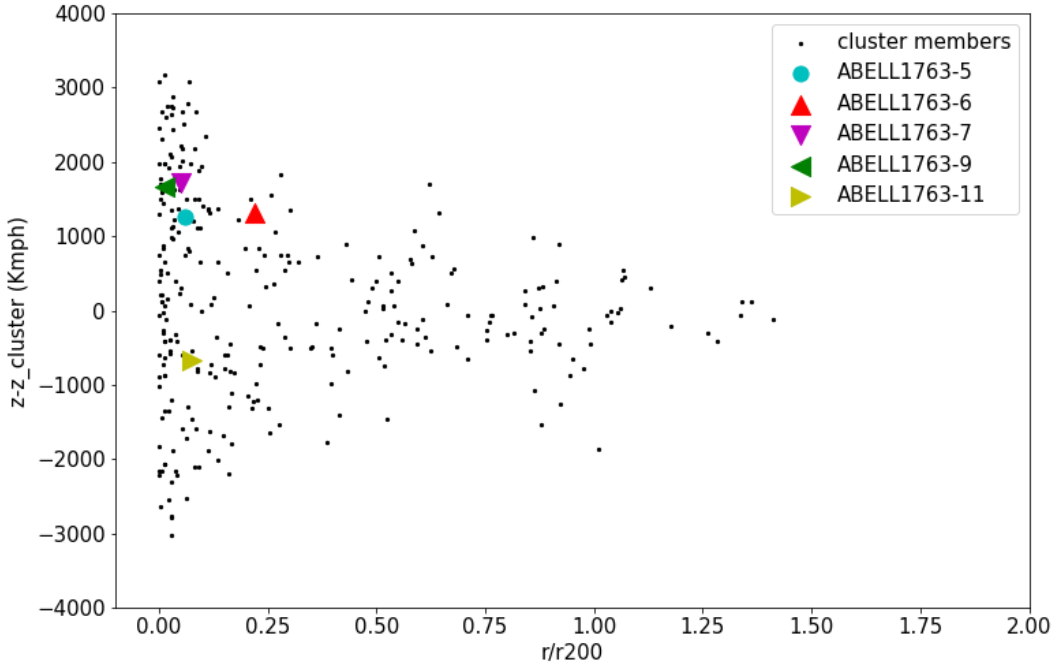

Figure 4.7: Cluster members shown in a phase space diagram with the five infalling groups shown.

4.4.3 Hα emission in Stacked Spectra

Hα (6583Å) emission is one of the primary identifiers for star formation rate in galactic environments, it is a line produced by young hot stars and is a direct indicator of the number of these young hot stars and , therefore, the star formation rate. When analysing the H-alpha emission for the data set, I found that most of the spectra have a lot of noise and getting an accurate measurement for equivalent width was challenging. This is most likely due to the low exposure time attached to the fits file containing the data. To combat this issue I decided to stack the spectra in equal sized groups of 20 galaxies and plot their combined spectra in these groups, with each plot increasing in radius from the cluster centre. I applied a Gaussian to smooth each of the stacked spectra this further reduced the noise and allowed the emission lines to be seen clearly. The Hα emission line can be found at 6583Å and can be seen to increase in the first six (a-f) plots in Figure 4.8, this trend is followed in Figure 4.9 in plots a-c. This relationship of increasing Hα equivalent width with increasing radius can be seen in Figure 4.10, where the mean increase as well as the inter quartile range can be seen for each of

the stacks. This increase in Hα means that at radii far from the cluster center, star formation rate is higher than it is nearer the centre of the cluster due to a decrease in local density at higher radii. This result is in agreement with the findings by Lewis et al. (2002), where they found local density to be the one of the most important factors effecting star formation rates.

4.4.4 Hδ and the D4000 break

Hδ and the D4000 break are both important indicators of star formation and metalicity respectively. Hδ is an indicator of recent enhanced star formation (Dressler & Gunn, 1983) and in Figure 4.8 and 4.10 this can be seen as increasing with cluster centric radius. This is due to star formation rate being closely tied with local density as mentioned in Lewis et al. (2002), as local density increases the probability of a galaxy having gone through a starburst event increases. As a result we see a lower D4000 value at distances further from the cluster center. The D4000 break can clearly be seen to be increase as we move closer to the cluster center, this is representative of the increase of age of galaxies as we move inward. This combined with the Hα lines shows that the cluster isn't static and has a rich morphology with an inward population of young star forming galaxies and a central population of older metal rich galaxies.

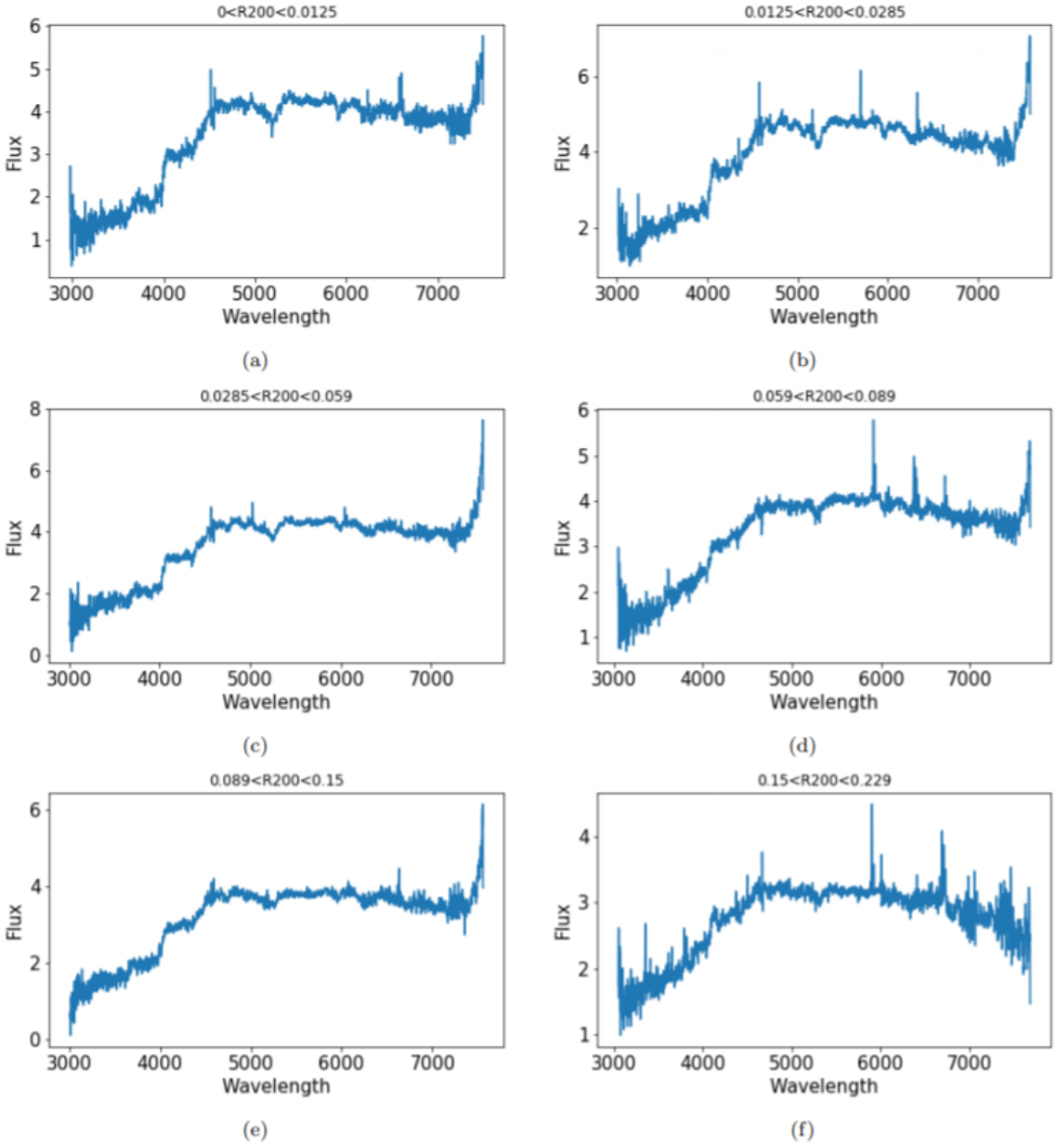

Figure 4.8: Stacked spectra between the cluster centric radius values of 0 and 0.229, each stack is comprised of 20 galaxies. The value of Hα can be seen to increase, and D4000 can be seen to decrease as you move away from the cluster center.

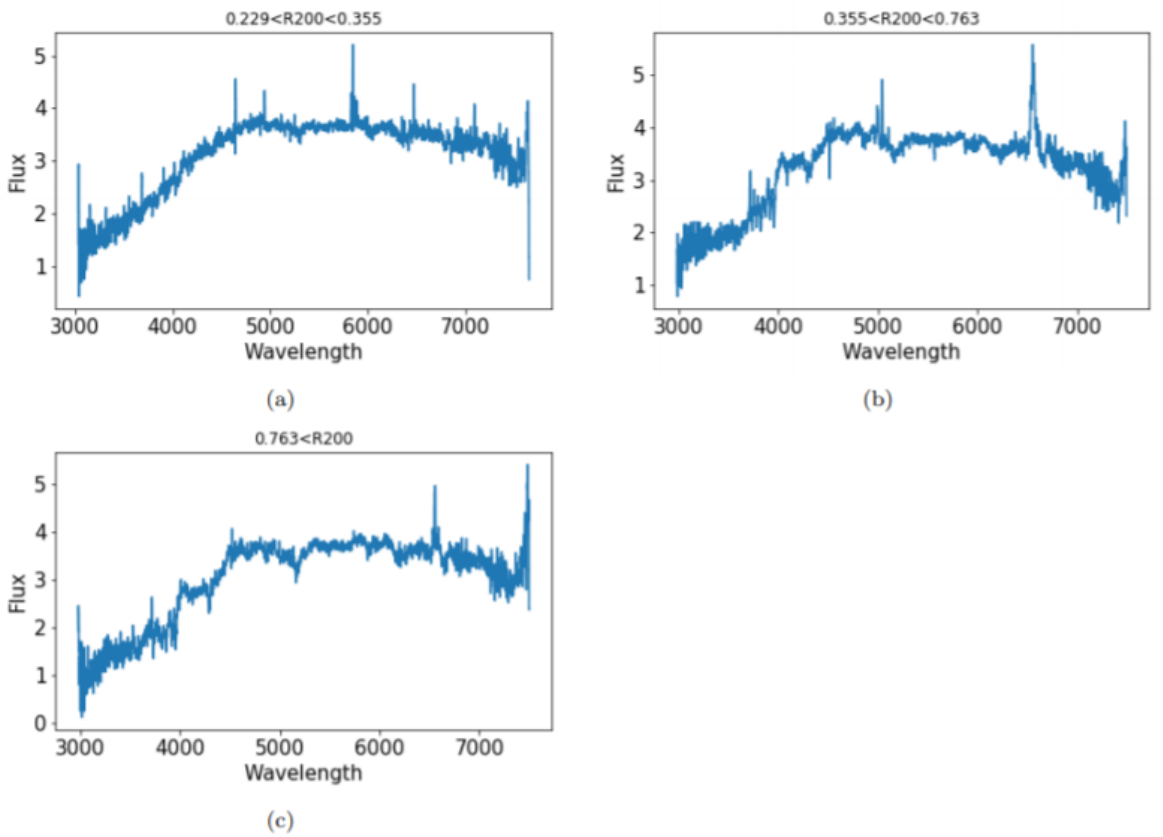

Figure 4.9: Stacked spectra with cluster centric radius values higher than 0.229, each stack is comprised of 20 galaxies. The value of Hα can be seen to increase, and D4000 can be seen to decrease as you move away from the cluster center.

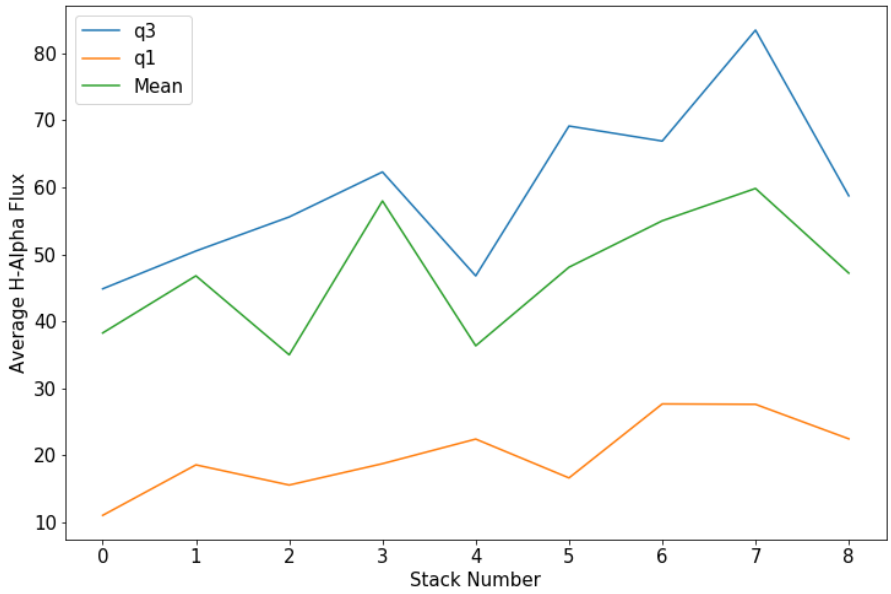

Figure 4.10: The upper and lower quartiles as well as the mean of Hα flux for each stack. The stats show that the average Hα value increases as a function of radius (stack number).

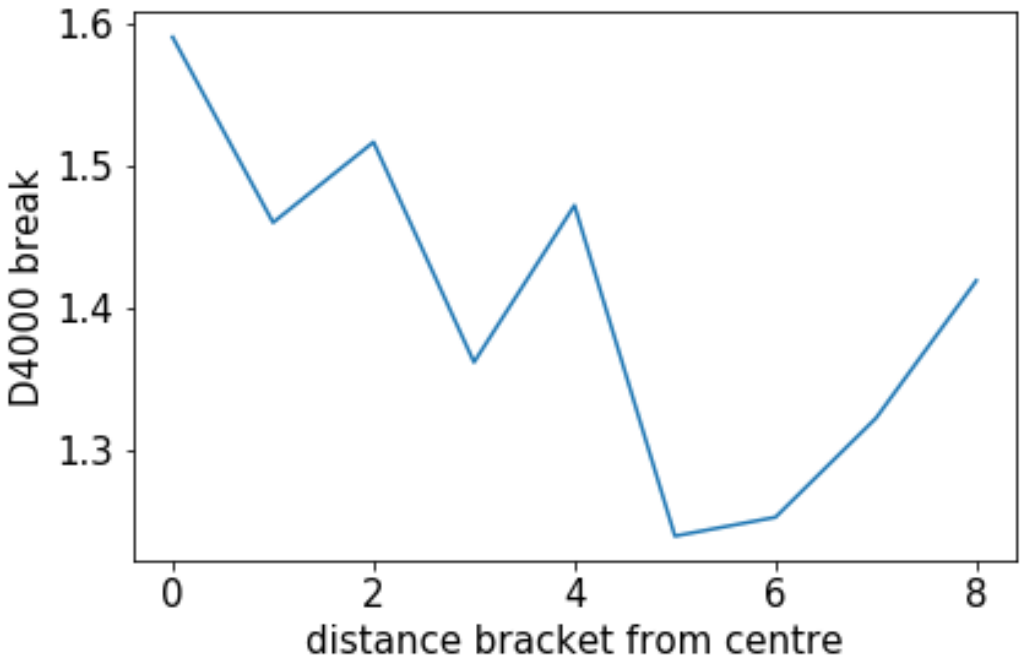

Figure 4.11: The D4000 break for each stack. The stats show that the average D4000 value decreases as a function of radius (stack number).

Galaxy Type	Fraction
k	19%
k+a	17%
a+k	6%
e(a)	46%
e(b)	7%
e(c)	6%

Table 4.1: The fraction of different galaxy types in Abell 1763.

4.4.5 Galaxy Classification

To classify the galaxy types in the Abell 1763 sample, I used a Dressler style plot (Dressler et al., 1999) (Figure 4.12). This plot uses measurements of both the [OII] and Hδ equivalent widths to determine the most likely spectral type of the galaxy. The diagram splits e-type emission line galaxies into 3 types, those with strong Balmer absorption are labelled e(a) types. Those with weak or moderate Balmer absorption are labelled e(c) types, and those with very strong [OII] are labelled e(b). These are reflective of the populations that inhabit each galaxy, with e(a) types containing a population of A-type stars, e(b) types have a spectrum representative of a burst of star formation and e(c) types have a steady SFR. The a+k region and the borderline between a+k and k+a contains the bulk of post starburst galaxies and the k region is representative of the passive type galaxies. By measuring both [OII] and Hδ equivalent widths, I recreated the diagram and placed each galaxy in Abell 1763, this can be seen in Figure 4.13. Using a phase space diagram and the classifications made by Dressler et al. (1999) allow the distribution of galaxy types to be seen in phase space (Figure 4.14), the distribution is complex and contains a rich variation of galaxy types (Table 4.1). Now we know the distribution of galaxy types we need to understand how these fit into place.

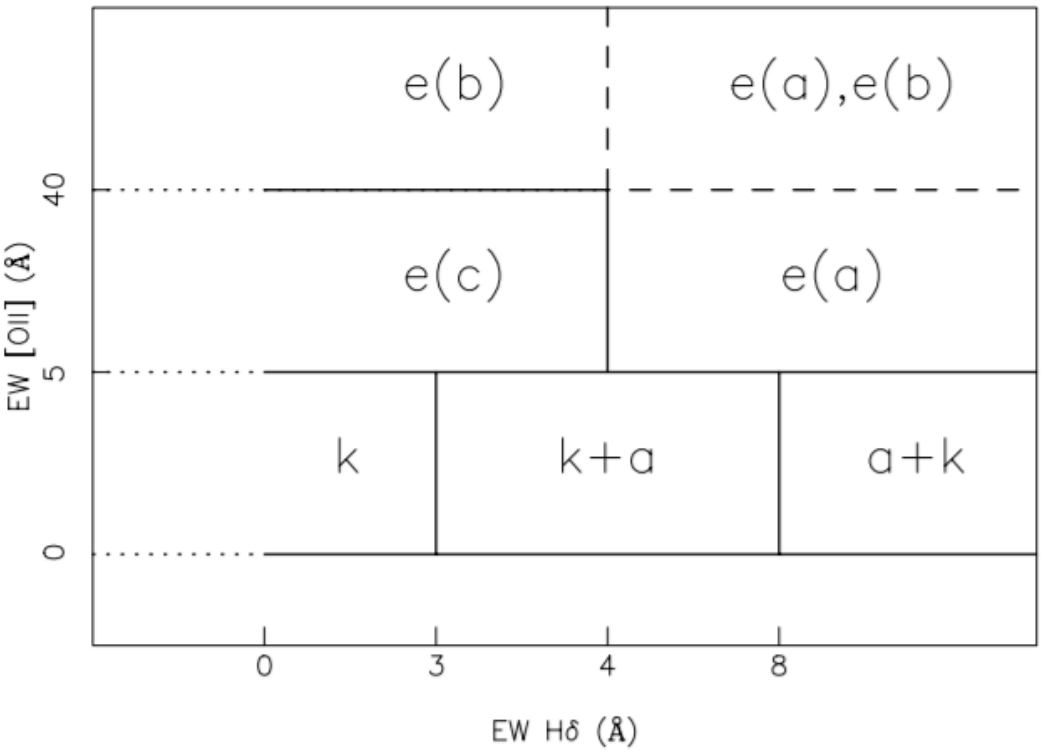

Figure 4.12: A Dressler plot showing the galaxy types that can be seen and how they are defined by EW[OII] and EW Hδ.

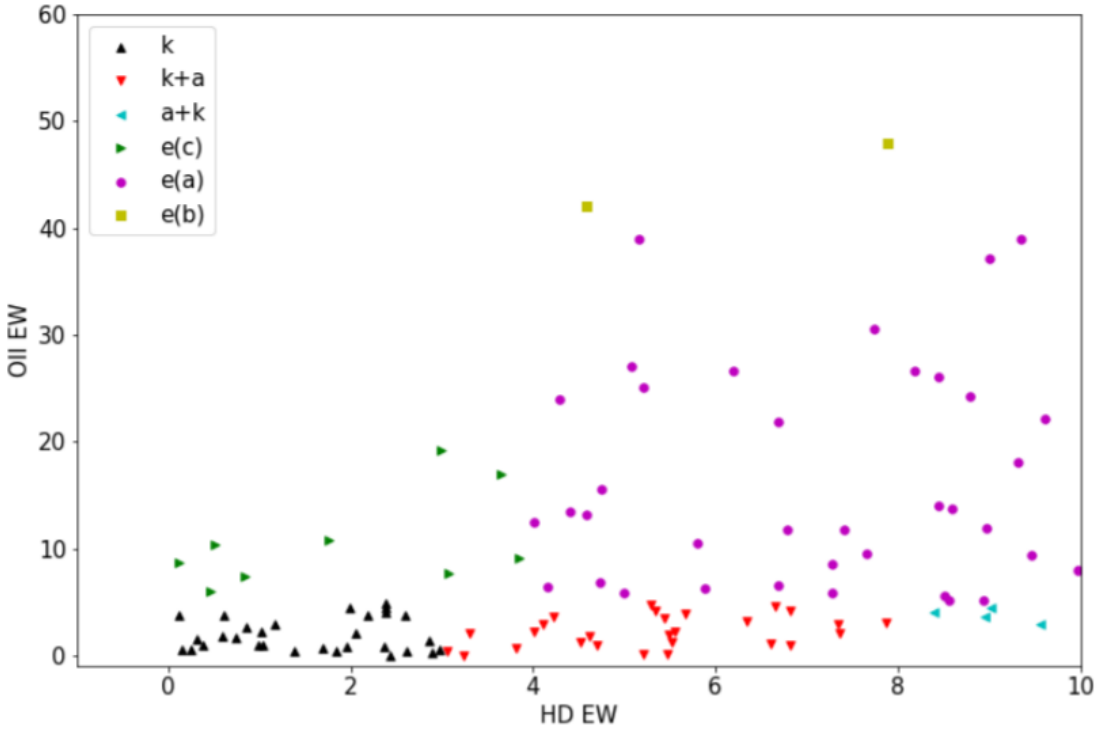

Figure 4.13: A Dressler plot showing the galaxy types in A1763 defined by EW[OII] and EW Hδ.

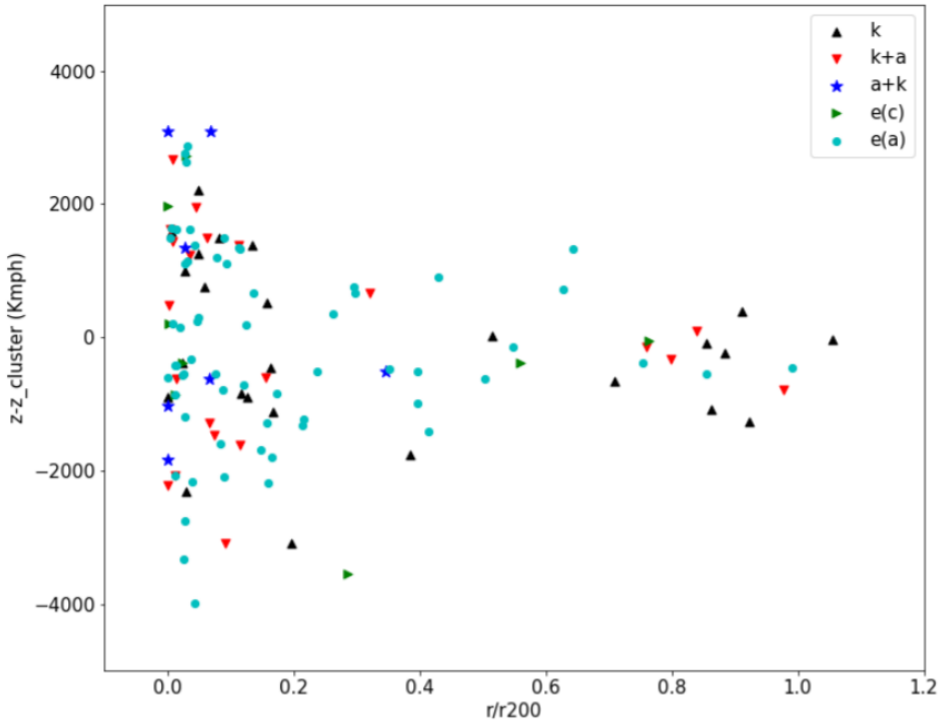

Figure 4.14: A plot of the Dressler defined galaxy types showing their distribution in phase space.

4.4.6 Identifying post starburst galaxies

The location of post starburst galaxies (PSB) is important in understanding the history of a cluster, since a post starburst event normally occurs during in-fall or harassment, they give us a way of understanding, previous galaxy interactions. Using the Dressler et al. (1999) paper to define PSBs as falling in the a+k region, I mapped the distribution of PSBs in phase space (Figure 4.15) and as shown in Table 4.1 the fraction of PSBs is 6%. This distribution of PSBs is concentrated at very low cluster centric radii with a large variation on line of sight velocity, this is evidence that the cluster is complex. Passive galaxies that make up 18.75% of galaxies are situated mainly at small cluster centric radii, but there is a small scattering that extend out to larger radii. Finally the k+a types, that make up 16.88% of galaxies, exist in a similar distribution to the passive types, with a concentration at low cluster centric radii and a scattering at a higher radii, they do, however, exist on average at a higher line of sight velocity to the passive galaxies.

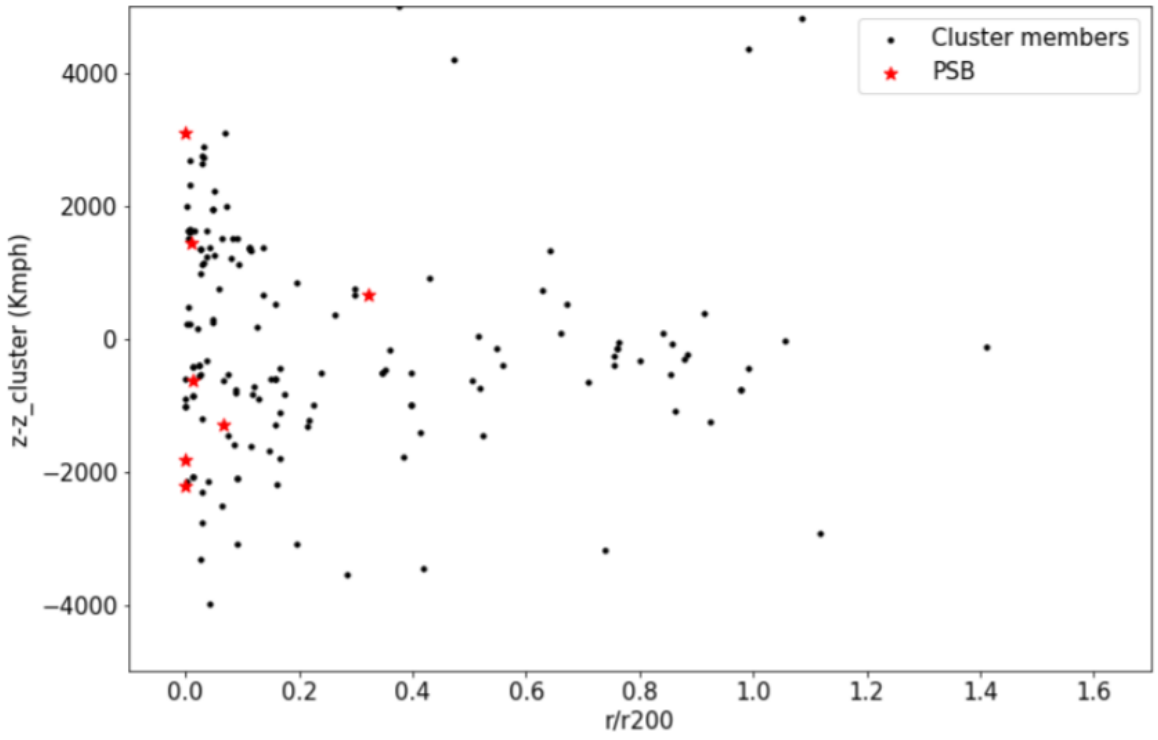

Figure 4.15: Post star burst type galaxies displayed in phase space. Using just the high signal to noise group to ensure accurate measurement of equivalent width values.

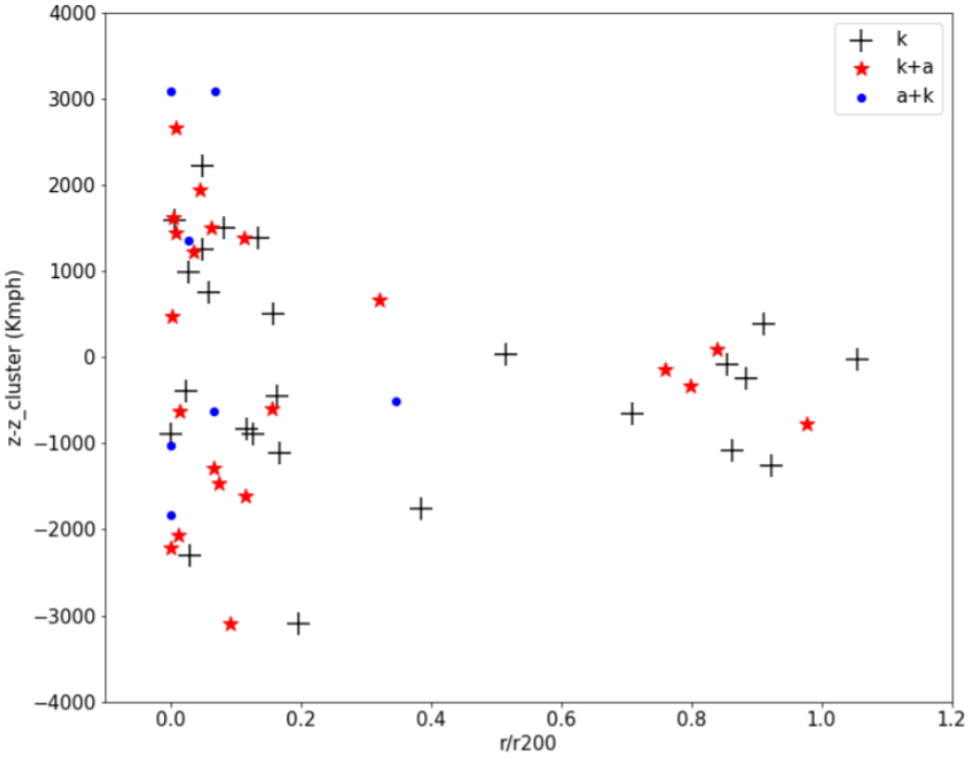

Figure 4.16: k,k+a and a+k type galaxies displayed in phase space. This displays the passive types, the borderline and not borderline starburst and post starburst types

4.4.7 Comparison of galaxy type distribution

Figure 4.17 and 4.18 are both cumulative frequency plots showing the distribution of different galaxy classifications against model magnitude and cluster centric radius respectively. Figure 4.17 shows there exists, for each galaxy type, a wide range of detected magnitudes. With star forming types, such as e(c) types, having a brighter distribution overall and the post starburst population being dimmer than the star forming types but brighter than other types on average. Passive types such as k types or galaxies containing A class stars indicating a previous star forming period, have a fainter distribution than both star forming and post starburst types.

Figure 4.18 shows how the galaxy types are situated in phase space, with the complete post starburst population existing at low cluster centric radii. For the other galaxy types the distribution is not simple. With a large concentration of all other types (k,a+k,e(a),e(c)) near the cluster center, stagnation then occurs in the distribution and we find that there are few galaxies until we reach the outer parts of the cluster.

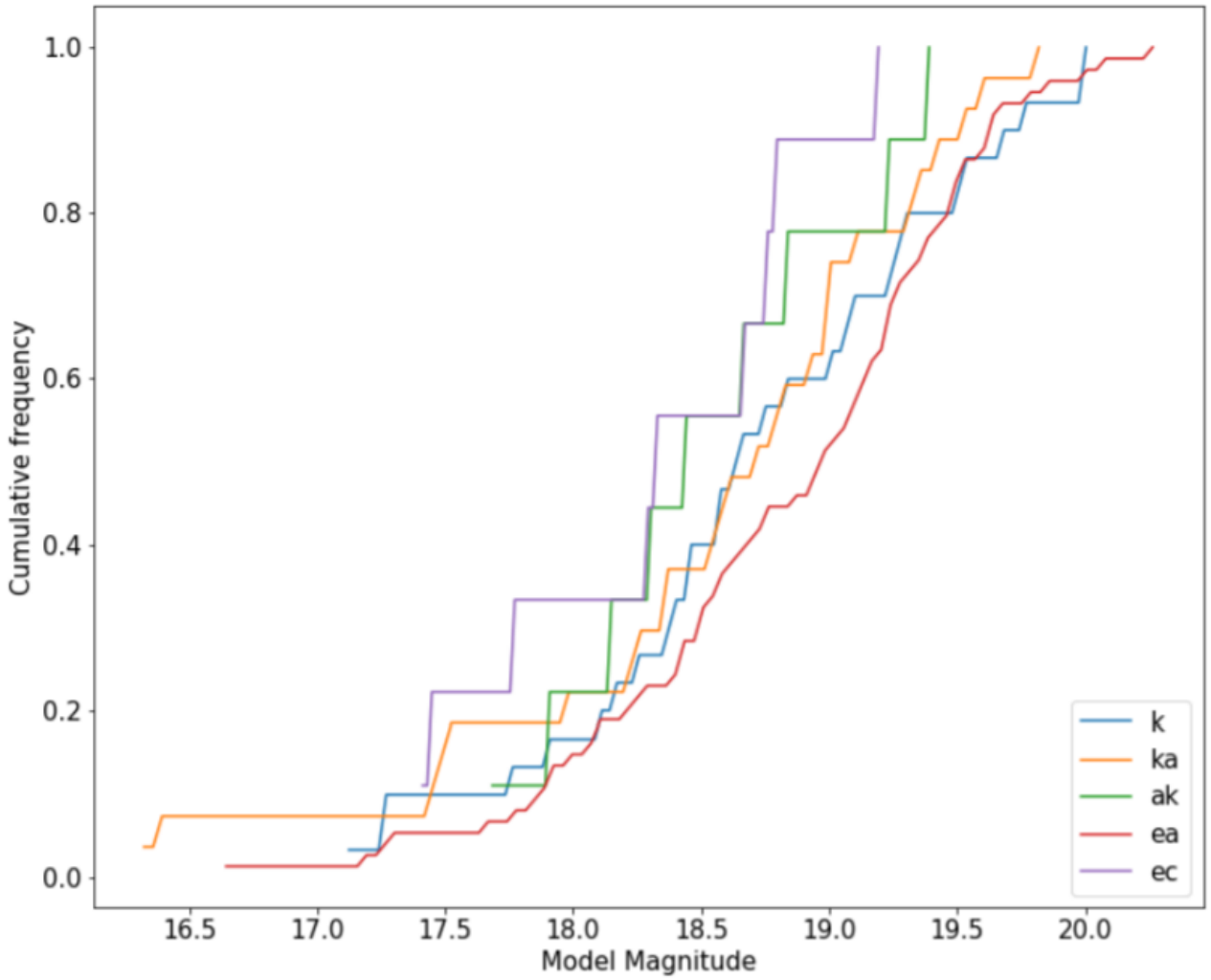

Figure 4.17: A cumulative plot of model magnitude for each galaxy type. This shows the distribution of the magnitude of galaxy types and which distribution of galaxy types are fainter or brighter.

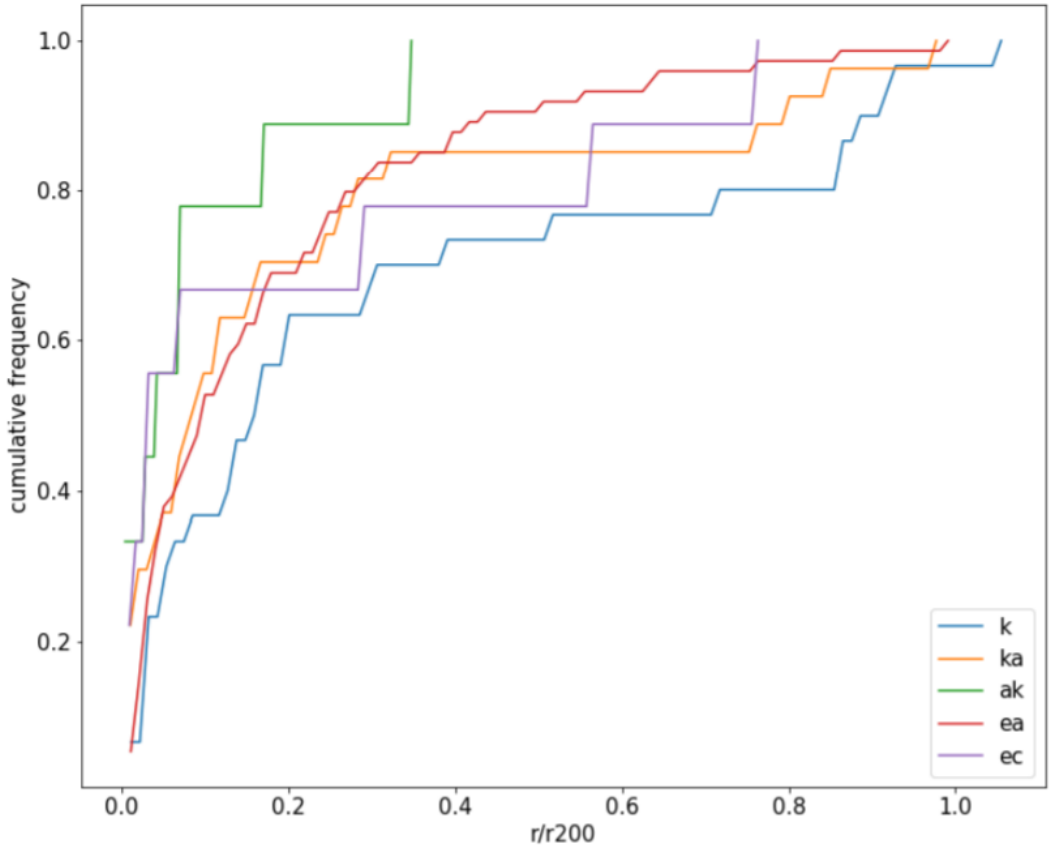

Figure 4.18: A cumulative plot of cluster centric radius for each galaxy type. This shows how galaxy types are distributed in the cluster.

4.4.8 Definition of the field

To be able to infer galaxy evolution within the cluster we need to be able to compare it to a field sample. To define the field sample I first used the objects from the same sample that were defined as outside of the cluster as the field and later instead used other clusters as a field sample. In Figure 4.19 the field can be seen as all galaxies in the sample outside of the redshift peak ≈0.225. I used 4 other Abell clusters to define the later version of the field, and ran a 2 tailed Kolmogorov–Smirnov (KS) test to see if there was a statistical difference between the D4000 values of the two. Figure 4.20 shows the two distributions of D4000 values in each of the field definitions. The results were a p-value of $4.867x10^{-8}$ and a D-statistic of 0.186, this means the results show that there isnt a statistical significance between the two definitions of the field as the p-value is below the significance level.

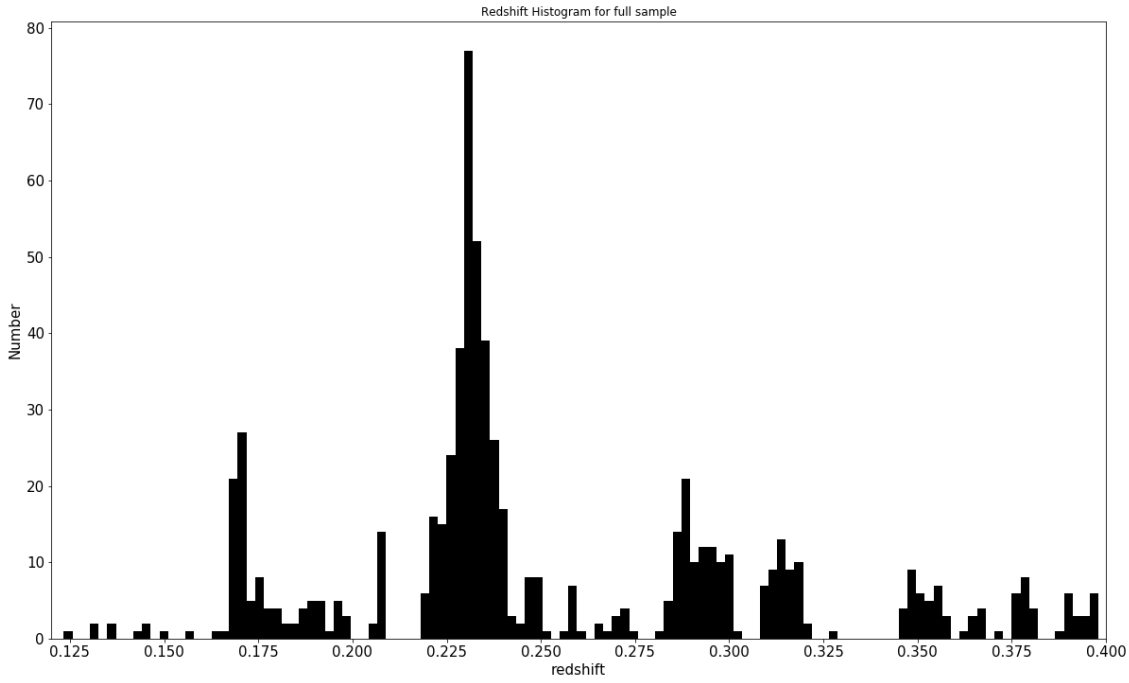

Figure 4.19: A redshift histogram showing the cluster as the peak around 0.225.

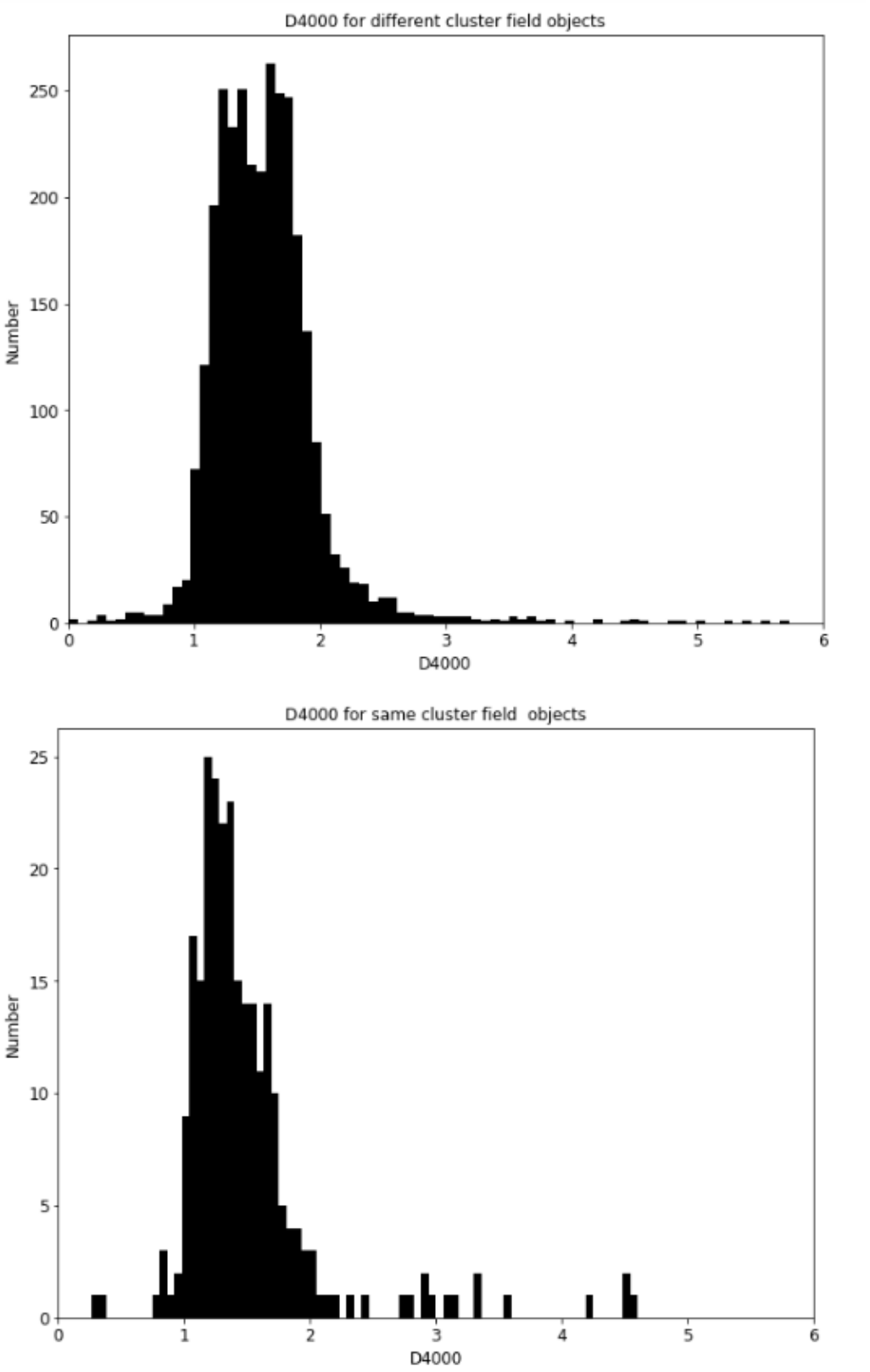

Figure 4.20: A comparison of D4000 for using the other clusters as a field sample against using the non cluster members from the A1763 sample.

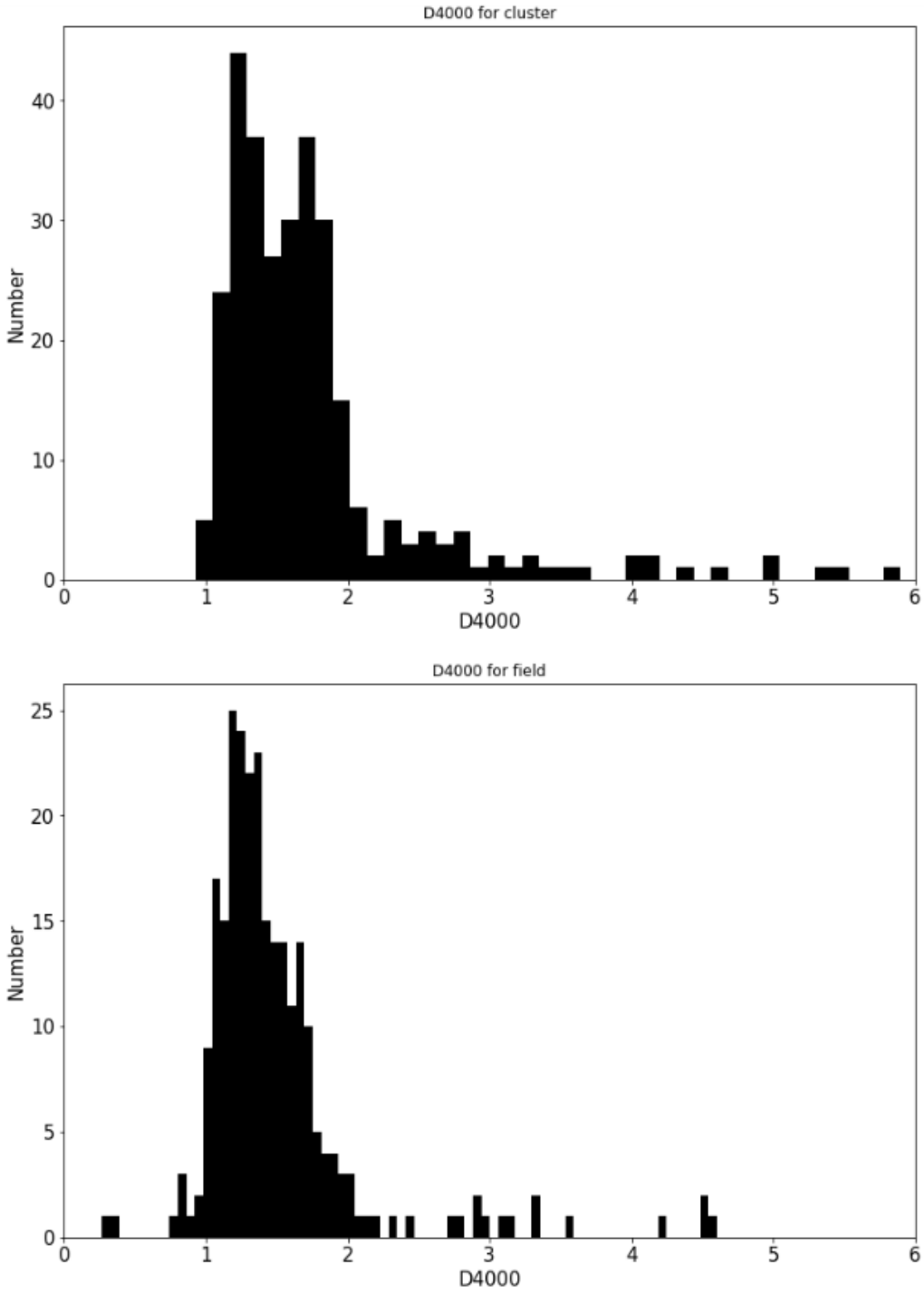

Figure 4.21: A comparison of D4000 for the cluster vs D4000 for the field.

4.4.9 Field analysis

Now that the field had been defined we can start to analyse it and compare it to A1763. The main comparisons made are values of D4000, this allows us to judge the difference in metalicity of the cluster. This comparison can be seen in Figure 4.21, where a 2 tailed ks test

gave a D statistic of 0.217 and a p-value of $1.788x10^{-6}$ this shows the two samples are not significantly different and that the metalicity of A1763 does not vary too far from the field values. The other comparisons I made were that of galaxy type, utilising Dressler style plots (Dressler et al., 1999). Figure 4.22 shows the galaxy distribution of the field in a Dressler style plot and Table 4.2 shows the fractions of galaxy types in the field and the percentage they vary from A1763. The cluster can now be seen to host a lower fraction of passive, e(b) and e(c) galaxies, while having increased fraction of k+a, a+k and e(a) types.

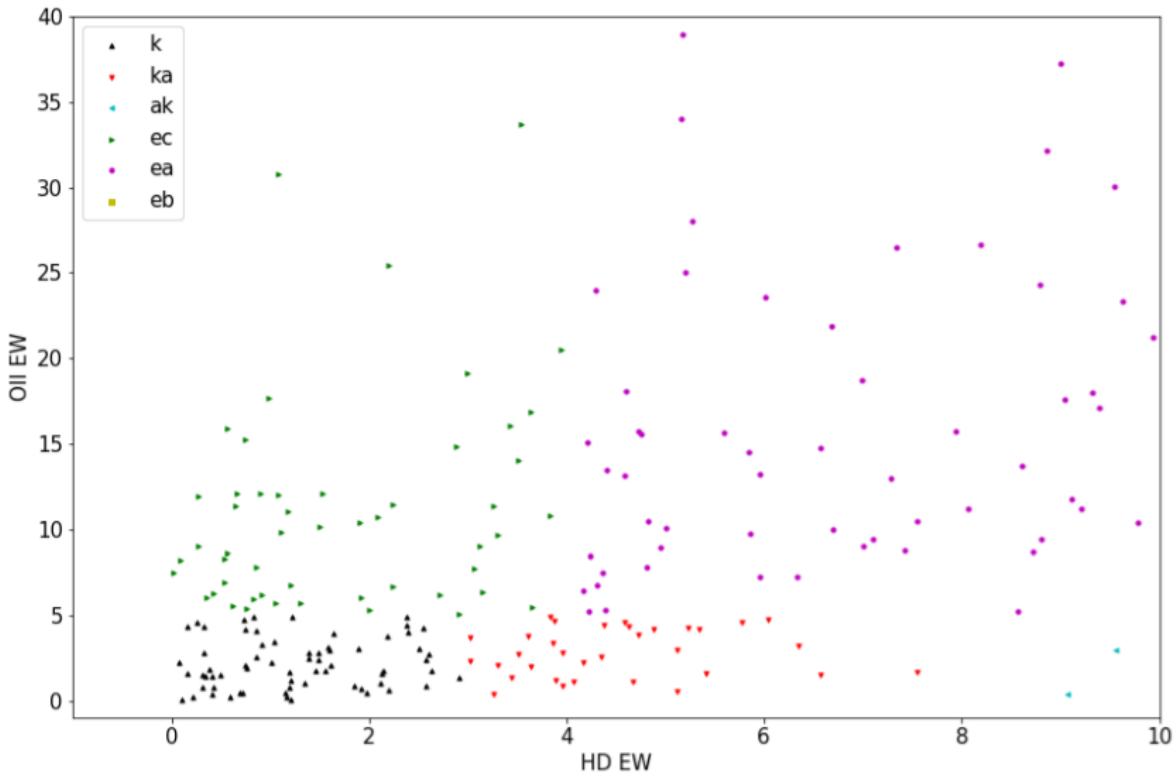

Figure 4.22: Dressler style plot displaying the galaxy types of the same cluster field sample

Galaxy Type	Cluster Fraction ± Uncertainty	Field Fraction ± Uncertainty	Difference
k	19% ± 3%	24% ±3%	+5%
k+a	17% ± 3%	12% ±2%	-5%
a+k	6% ± 2%	3%± 1%	-3%
e(a)	46 % ± 5%	32%± 3%	-14%
e(b)	7% ± 2%	10%± 2%	+3%
e(c)	6% ± 2%	19% ± 3%	+13%

Table 4.2: The fraction of different galaxy types in Abell 1763 compared to the fraction in the field.

4.4.10 Signal to noise in the field

When filtering by signal to noise we see a trend in elimination of certain galaxy types. In Figure 4.23 the low signal to noise group (Figure 4.23 (c)) is dominated by passive type galaxies, unlike their active counterparts the passive types are lacking huge spikes at Hα and [OII] or other noticeable emission lines, this makes it easy for them to be lost in a sea of noise. This loss of primarily passive types, is inevitable when reducing the sample with a signal to noise cut. The cut however is useful for determining galaxies with high values of [OII] EW and Hδ EW that also contain a lot of noise, for example in Figure 4.23(c) you can see a scattering of galaxies that would have been detected as a+k,k+a,e(a) or even e(b) types without the cut in place. I used the same signal to noise cut in both the field and the cluster sample, this way our boundary for using the data of a galaxy was the same in both cases.

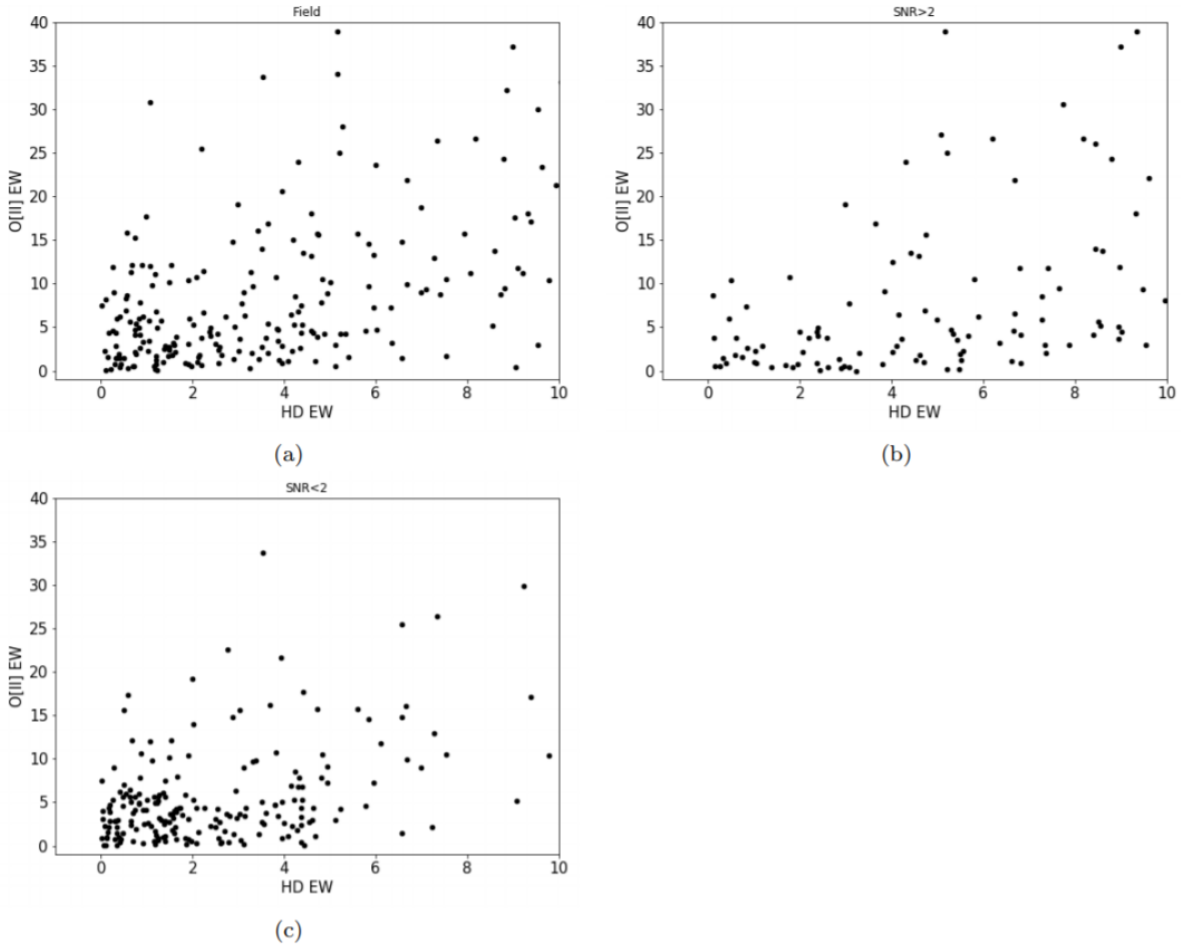

Figure 4.23: A comparison of Dressler style plots for the field (a) , the high signal to noise (b) sample and the low signal to noise sample (c). There is a large number of passive types in the low signal to noise sample compared to the high signal to noise sample.

4.4.11 Determining blue fraction

The blue fraction is important as it gives us and understanding of how many galaxies are younger and more likely to be star forming. A high blue fraction at certain redshift can also be a sign of a cluster cluster merger, as during an event like this blue fraction would rise, it is therefore not only important in understanding age and SFR but also potential mergers. To determine the blue fraction I used the Butcher Oemler method (Butcher & Oemler, 1984), this entailed making a G-R vs absolute R band magnitude plot for the cluster members with no signal to noise cut (Figure 4.24) taken from the central mass region. Figure 4.25 shows the next step which is to eliminate all objects at a magnitude >19.5 as well as all objects where G-R>1.1, then placing a line of best fit through the remaining objects. Finally Figure

4.26 adds a line 0.61 below the line of best fit plotted in Figure 4.24 and defines all objects under that line as blue. The difference between the blue and red line was computed using the method in Fukugita et al. (1995), where we consider how the gap evolves with different redshift values. Using this method I get a value of blue fraction for the cluster as being 13% ± 0.4%.

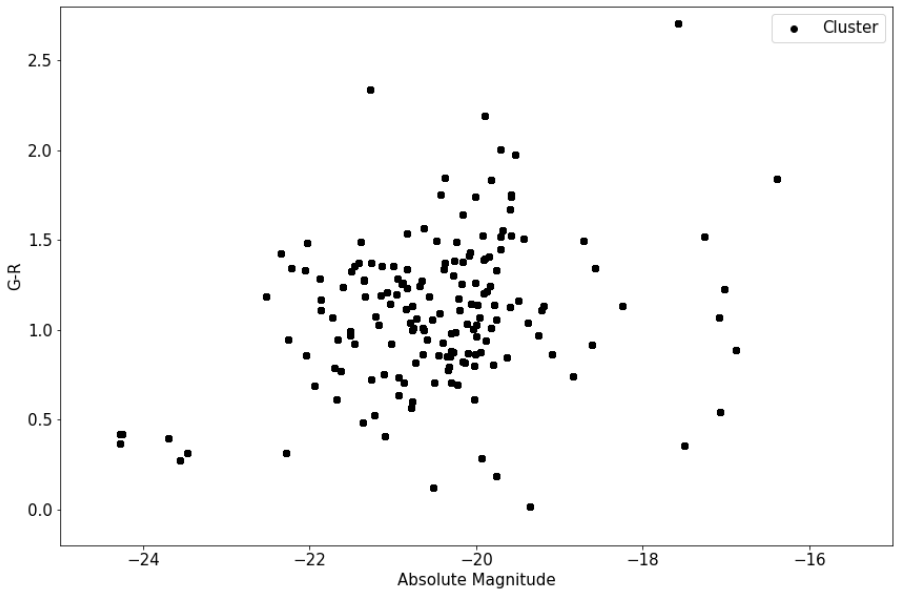

Figure 4.24: The first plot in determining blue fraction, a G-R vs R band magnitude plot, with a line of best fit plotted.

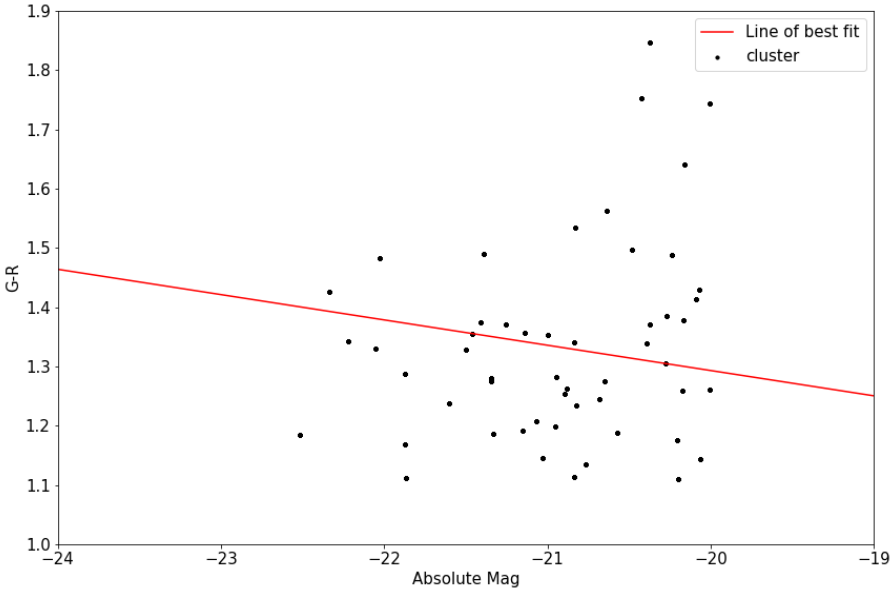

Figure 4.25: The second plot, Eliminating faint objects at a magnitude >19.5 and placing a line of best fit through objects G-R>1.1.

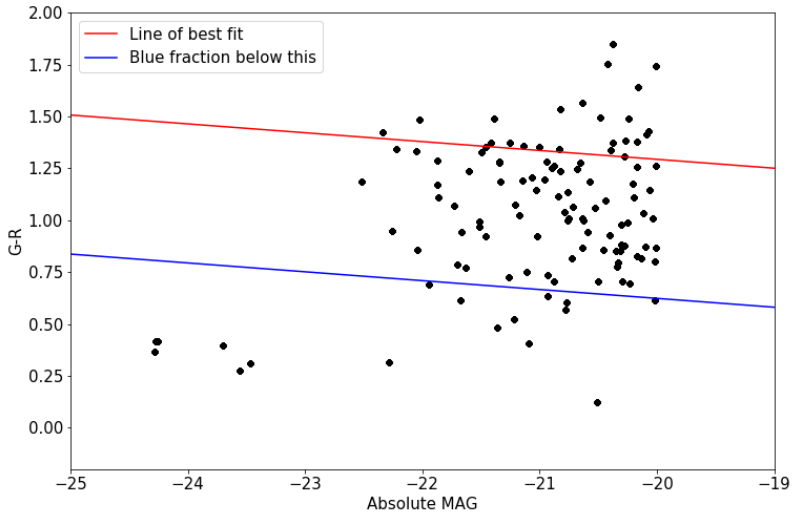

Figure 4.26: The final plot, places a line 0.61 below the line of best fit, with any galaxy under this line being defined as blue.

5. Results for other Abell Clusters

5.1 Chapter overview

In this chapter I analyse the other four aforementioned Abell clusters to act as a comparison sample for A1763, these clusters are A1689,A1758,A1835 and A963. Due to time constraints of the thesis and data availability, analysis of these clusters is not as deep as A1763 however it is enough to give us a good comparison to work with to analyse galaxy evolution in these clusters with the main cluster of this study.

5.1.1 Cluster Selection and signal to noise cuts

The process of defining members belonging to the cluster is identical to the process used in Chapter 4 for A1763, where I used the CYE mass model caustics to eliminate any non-member galaxies for each cluster (Figures 5.1, 7.1, 7.2 and 7.3). I then made the cut in redshift at 0.35 to avoid losing the H-alpha measurement from being pushed out the optical range. Finally I make the signal to noise cut using a ratio of 2 the same as I did for A1763 which reduces each of the 4 Abell clusters to a sample size shown in Table 5.1.

Cluster name	Starting Sample size	Size after reduction	Percentage left
A1689	1511	600	40%
A1758	1274	197	16%
A1835	1281	282	22%
A963	545	178	33%
A1763	1038	293	28%

Table 5.1: Table showing the reduction in sample size for all clusters after the signal to noise cut.

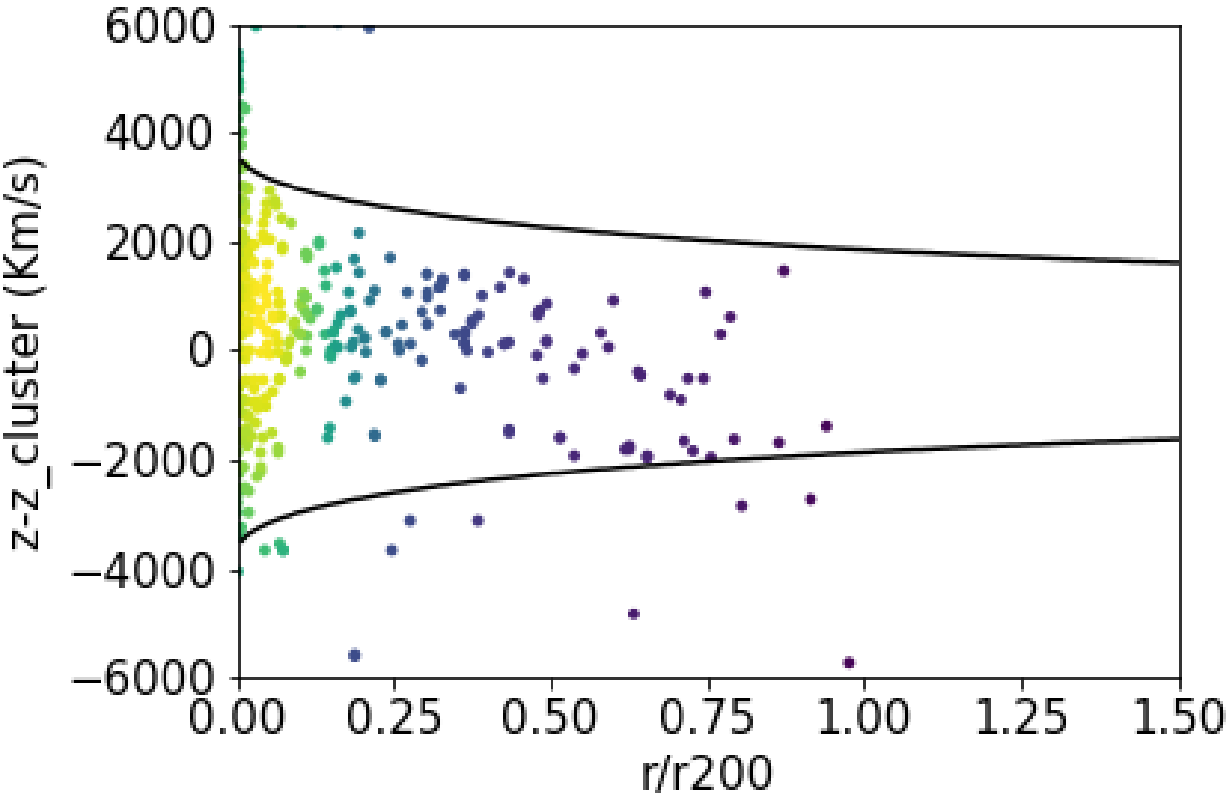

Figure 5.1: Abell 1689 shown in full in with CYE mass model caustics. The caustics define cluster membership, all points outside of them are defined as outside of the cluster.

The signal to noise cuts can be seen in Figure 5.2, they show both the low and high signal noise ratio samples alongside one another. The low signal to noise is once again dominated by passive and k+a types as well as a scattering of a+k, e(a),e(b),e(c) types. On the other hand the high signal to noise group contains almost no passive types across every cluster, but does contain scatterings of every other galaxy type. Using a signal to noise ratio like this is a trade off, it allows us to be more certain that the data points we operate on are real and as long as we are aware that in these cases we have lost a portion of galaxy types, primarily k types. Moving forward when comparing the clusters to the field I will be using more complete samples, with the mindset that sheer sample size will be more useful as a comparative tool than a noise reduced set. However, when analysing line spectra I will be using the signal to noise reduced set, as the measurements made are highly sensitive to noise.

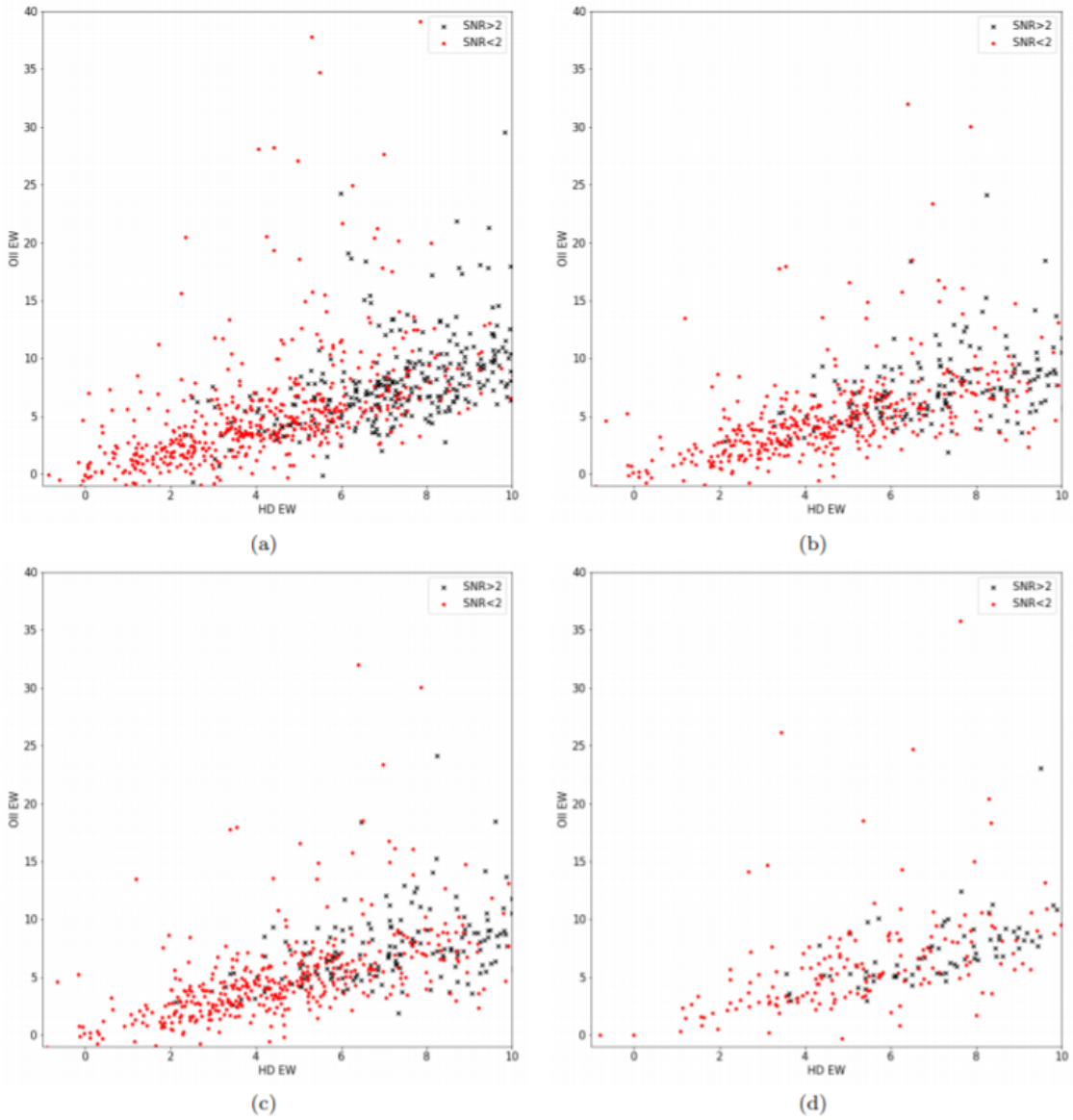

Figure 5.2: A comparison plot of A1689(a),A1758(b),A1835(c),A963(d) showing the distribution of both a low SNR and a high SNR on a Dressler style plot. The difference in the number of passive galaxies in the low and high signal to noise group can be seen.

Cluster name	D statistic	P-Value	Relevant Figures
A1689	0.0706	0.0014	Figures 5.6,5.7
A1758	0.0334	0.5229	Figures 7.4,7.5
A1835	0.0688	0.0072	Figures 7.6,7.7
A963	0.0829	0.0205	Figures 7.8,7.9

Table 5.2: Table showing the results of the KS tests on each cluster.

5.1.2 D4000

In this section I will be using the complete sample for each galaxy cluster to compare the D4000 values to the values of the field. The field in this section is defined as the combination of the other galaxy clusters, not including the target cluster. To quantify the difference between the two D4000 histograms in each set, I ran a 2 tailed KS test, the results of which can be seen in table 5.2.

The KS tests show us two things, firstly the D statistic which shows the cumulative difference between the two samples. Secondly we receive a p-value, if the p-value is below the significance level (0.05) then we reject the null hypothesis and state there is a difference between the values in the sample. We can see from Table 5.2 that A1689,A1835 and A963 have P-values far below the significance level, so we can reject the null hypothesis and state there is a statistical difference between the field sample and the cluster sample, when looking at D4000 values. A1758 is an outlier we can see its p-value is far above the significance level so we cannot reject the null hypothesis and must state that the D4000 values in A1758 are not significantly different from the field. This is further reflected in the D-statistic, as A1758 has the lowest value for a D-statistic and therefore the lowest cumulative difference between the samples.

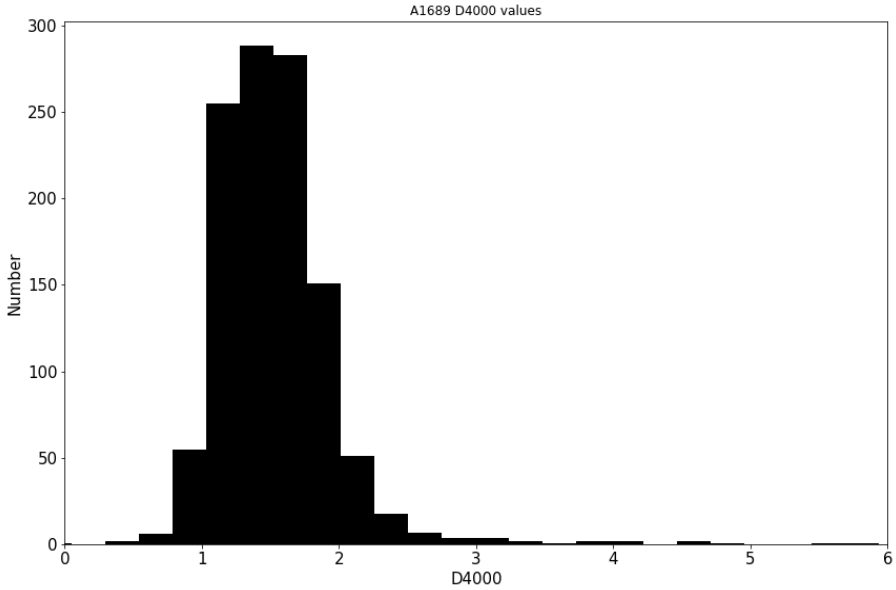

Figure 5.3: D4000 values in A1689.

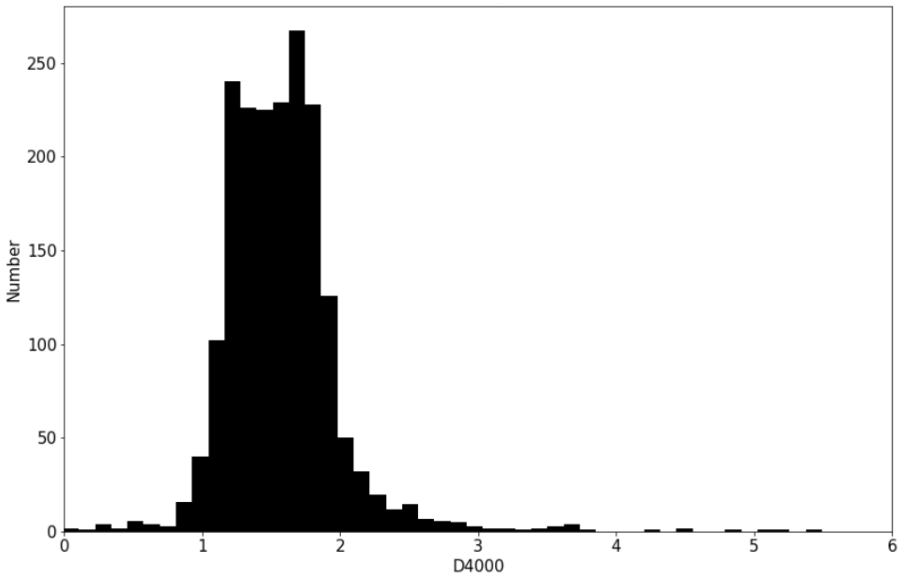

Figure 5.4: D4000 values for the field, where the field is A1758, A1835 and A963.

Cluster name	Percentage of D4000 strong	Relevant Figures
A1689	11% ± 2%	Figure 5.5
A1758	9% ± 3%	Figure 7.10
A1835	10% ± 3%	Figure 7.11
A963	9% ± 3%	Figure 7.12

Table 5.3: Table showing the percentage of D4000 strong galaxies within each cluster.

5.1.3 D4000 in phase space

D4000 is indicative of a drop of intensity on the blue end of the spectrum, this drop comes from a lack of blue stars in older stellar populations and increased metal rich population in this populations. Therefore, we use D4000 as a measure of metalicity and age of a galaxy. To analyse the population age and the distribution of older galaxies I plotted each of the 4 Abell clusters in phase space and plotted D4000 strong galaxies for each cluster as well. I define strong D4000 as any galaxy where the D4000 value is greater than 2, this gives me percentage of D4000 strong (Table 5.3) and plotting this in phase space gives us Figures 5.5, 7.10, 7.11 and 7.12. In A1689 (Figure 5.5) D4000 strong galaxies are located mainly at low cluster centric radii with a range of line of sight velocities, there exists also a scattering of a few at higher cluster centric radii but this isn't common. In A1758 (Figure 7.10) there is a similar trend, with the majority being located at low cluster centric radii and a scattering found on the boundary of the cluster. In A1835 (Figure 7.11) there is little trend connecting the strength of D4000 with position in the cluster as there is an even scattering of D4000 strong through the cluster. In A963 (Figure 7.12) there again is no trend to the position of D4000 strong.

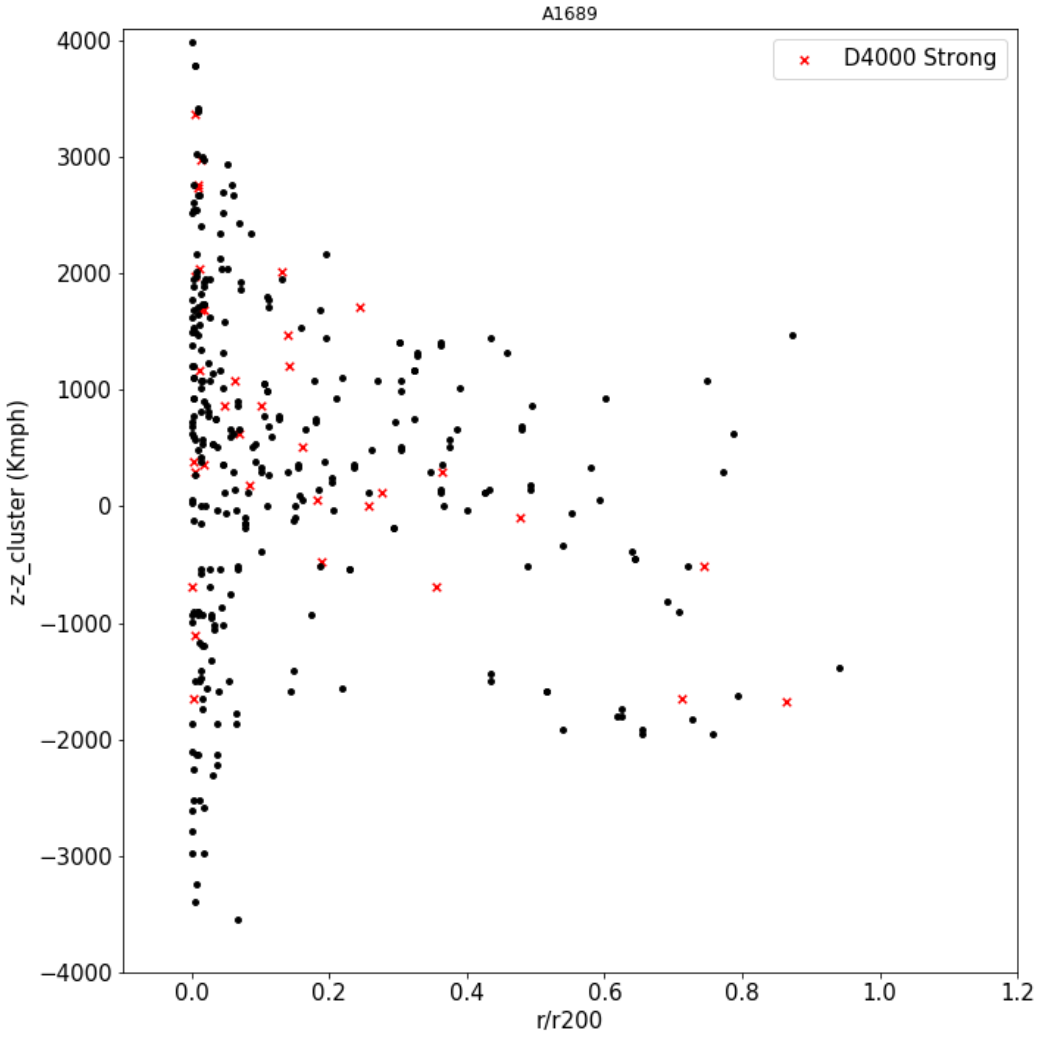

Figure 5.5: D4000 strong galaxies in phase space in A1689.

5.1.4 Blue fraction

To determine the blue fraction I used the same method as for A1763, the Butcher Oemler method Butcher & Oemler (1984) in combination with the method in Fukugita et al. (1995). The Figures 5.6, 7.13, 7.14 and 7.15 show the final step of this method with the resulting blue fraction for each galaxy being shown in Table 5.4. A1689 contains a blue fraction similar to our main cluster, A1763, where as A1758 and A963 both have significantly smaller blue fraction and A1835 is between the two ends of the blue fraction values. This result for blue fraction is a good indicator of activity and age in the cluster dynamic, our two oldest clusters are likely to be A1758 and A963 as they both contain such a low fraction of blue galaxies. A1835 and A1689 on the other hand are younger, similar to A1763 as they contain a much

Cluster name	Blue fraction ± Uncertainty	Relevant Figures
A1763	13% ± .4%	Figures 4.25,4.26,4.27
A1689	12% ± 3%	Figure 5.6
A1758	3% ± 2%	Figure 7.13
A1835	6% ± 4%	Figure 7.14
A963	3% ± 3%	Figure 7.15

Table 5.4: Table showing the blue fraction of galaxies within each cluster.

greater fraction of blue galaxies. The results for blue fraction are close somewhat to previous literature, Rizza et al. (2003) and (Andreon & Ettori, 1999) cite values for A1758 as 12% and 9% respectively and Butcher & Oemler (1984) state the blue fraction for A1689 is 9%. Using Butcher & Oemler (1984) also allows us to see that the blue fraction should be between 9% to 19% for Abell clusters at similar redshifts to the clusters studied for this thesis which falls withing 3σ of my values.

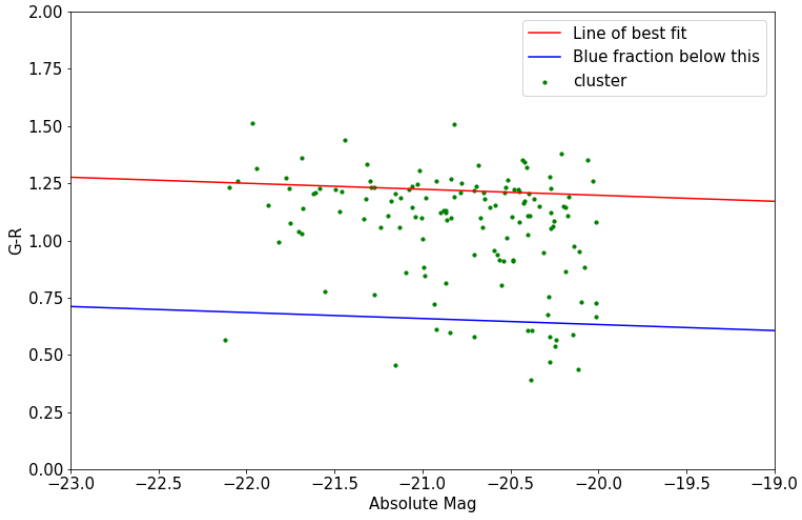

Figure 5.6: Blue fraction diagram for A1689.

6. Final considerations and conclusions

In this chapter I conclude the results for each of the 5 clusters by using stacked plots, representative of each cluster. The stacked plots show us 3 separate trends in the galaxies and how the variables that create those trends effect each other. I discuss the limitations of my research and what, given more time, I would do for future work into this field.

I present these stacks to show, for each cluster, the relationship between measured quantities. The reason I stack is to improve the signal to noise ratio. Each stack is broken into 3 sections, section (a) shows the the G-R colour index vs the measured value for D4000 break. Section (b) shows the value for Hα equivalent width vs G-R colour index. Section (c) shows Hα vs D4000 break. I will discuss for each of the 5 clusters what can be seen from the stacked diagrams.

Section (a) in Figure 6.1 represents the relationship between age or metalicity with G-R colour index for A1763. As G-R colour index is a magnitude, higher values of G-R represent a more red population and higher values of D4000 are representative of an older or more metal rich population. A trend heading from the bottom left to top right can be seen, with a large range of G-R values. This is indicative that the cluster population is made up of a rich mixture of blue and red galaxies of varying ages and the blue galaxies are moving towards the red end of the spectrum.

Section (b) in Figure 6.1 shows the relationship between Hδ and G-R colour index, Hδ acts as an indicator of recent starburst events and plotting it against colour gives an idea about motion and interaction between cluster members. The concentration of members is in the bottom right corner, this is representative of the red population that have not exhibited recent star formation as they are probably passive now. The scattering of galaxies towards the top left are indicative of blue galaxies that have recently interacted and gone through a star burst phase, leaving them with increased Hδ. This is also seen by Pimbblet (2003) shown in Figure 6.2 and Poggianti et al. (1999), where the bottom right section is dominated by the passive

types and [OII] emission line galaxies are scattered but primarily focused towards the left (bluer) side.

Section (c) in Figure 6.1 shows the relationship between star formation rates and age of a galaxy, the younger galaxies are shown at lower D4000 values and a trend towards high Hα exists for these younger galaxies as star formation rates are less likely to have been shut down by interaction with the cluster.

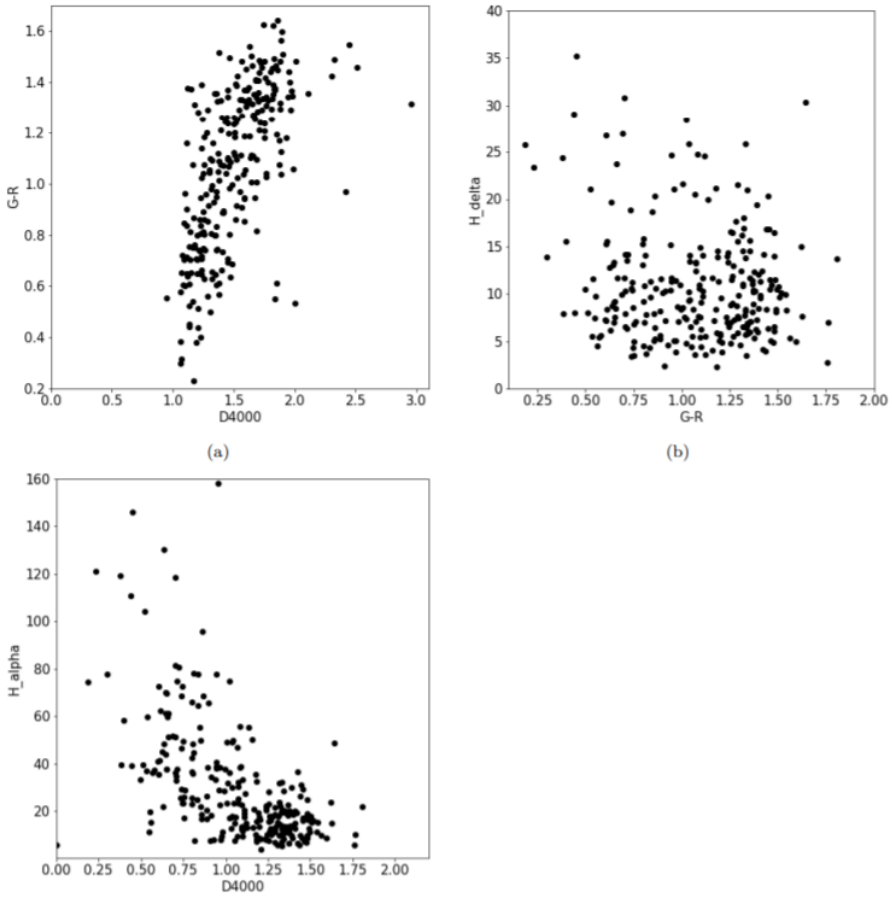

Figure 6.1: Plot for A1763 showing D4000 vs G-R colour index in section (a), H-delta vs G-R colour index for section (b) and H-alpha vs D4000 for section (c).

Section (a) of Figure 6.3 representing A1689 shows comparatively less of a trend than in A1763, however there is still a concentration of galaxies at intermediate D4000 and towards the redder end of the G-R colour index. This may be due to a difference in selection functions that has lead to a difference in sample completeness. Section (b) of Figure 6.3 shows an extreme concentration of points towards the red end of the colour index with a small scattering of Hδ strong representative of galaxies having gone through recent starburst similarly to A1763.

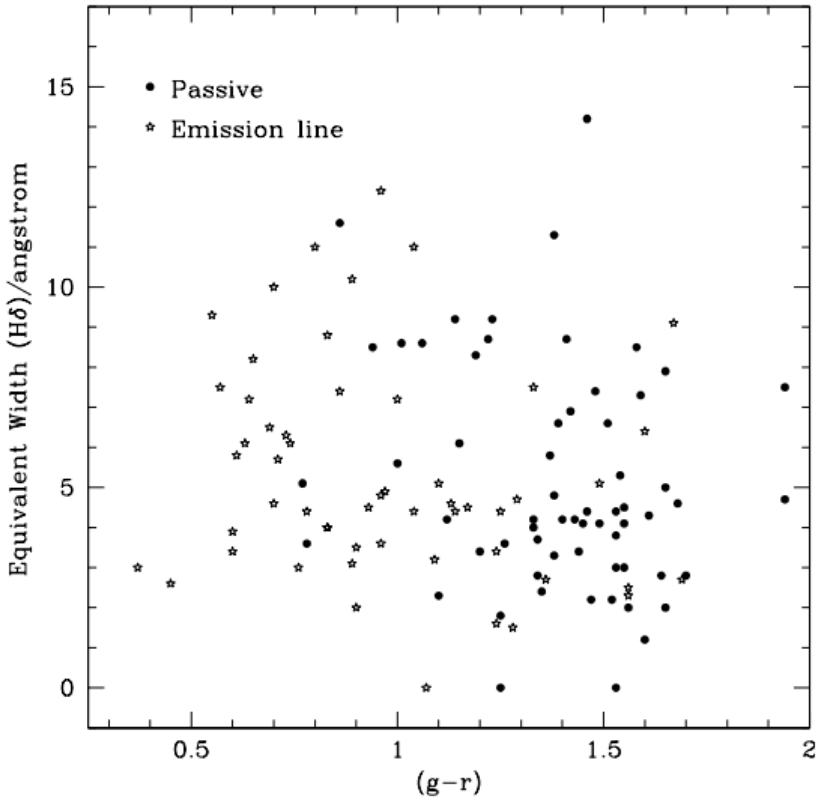

Figure 6.2: Distribution of cluster galaxies (mean redshift z 0.44). Passive galaxies are marked with filled circles and [OII] emission line galaxies with open stars (Pimbblet, 2003).

Section (c) of Figure 6.3 shows a similar upwards trend to Abell 1763 but at a much bigger range of D4000 values. This shows that for this cluster there are a range of ages of galaxies that are going through a phase of star formation.

For A1758 Section (a) of Figure 6.4 shows the end of the branch of blue galaxies moving towards the red end of the spectrum to join the rest population, this cluster is older than others looked at. Section (b) of Figure 6.4 shows a concentration of cluster members exhibiting low Hδ, with a scattering of galaxies with higher Hδ that have gone through recent star formation phase. Section (c) of Figure 6.4 has little trend but contains a scattering of high D4000 galaxies exhibiting low star formation rate, this is indicative of the older passive part of the population, which when comparing with section (a) can be seen to be noticeably more red.

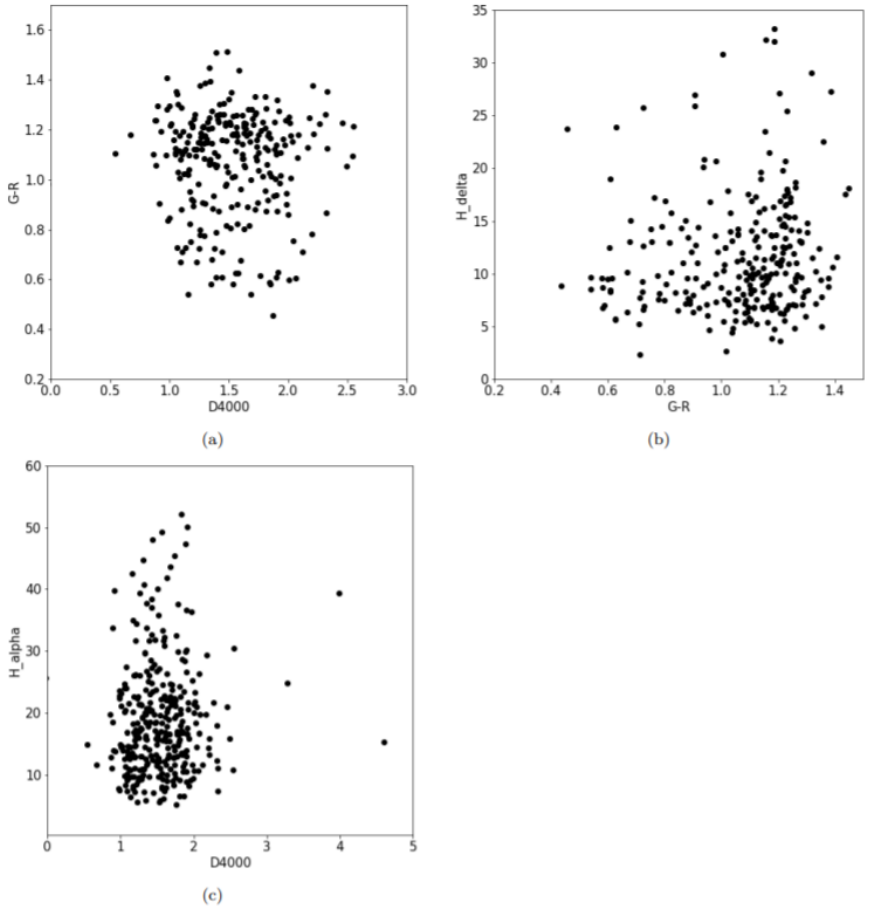

Figure 6.3: Plot for A1689 showing D4000 vs G-R colour index in section (a), H-delta vs G-R colour index for section (b) and H-alpha vs D4000 for section (c).

A1835 shows the biggest spread of D4000 values as seen in Section (a) of Figure 6.5, this is indicative of a rich population of many varying ages. There is a branch upwards similar to A1758 showing the population moving towards the redder end. Section (b) of Figure 6.5 shows a similar shape to A1689 where a small scattering of starbursted galaxies can be seen towards higher values of Hδ but the main bulk is towards the bottom right with no recent enhanced star formation rate. Section (c) of Figure 6.5 shows a slight trend towards younger galaxies having stronger Hα values, representative of the younger star forming galaxies. Also containing scattering of older galaxies lacking in H-alpha.

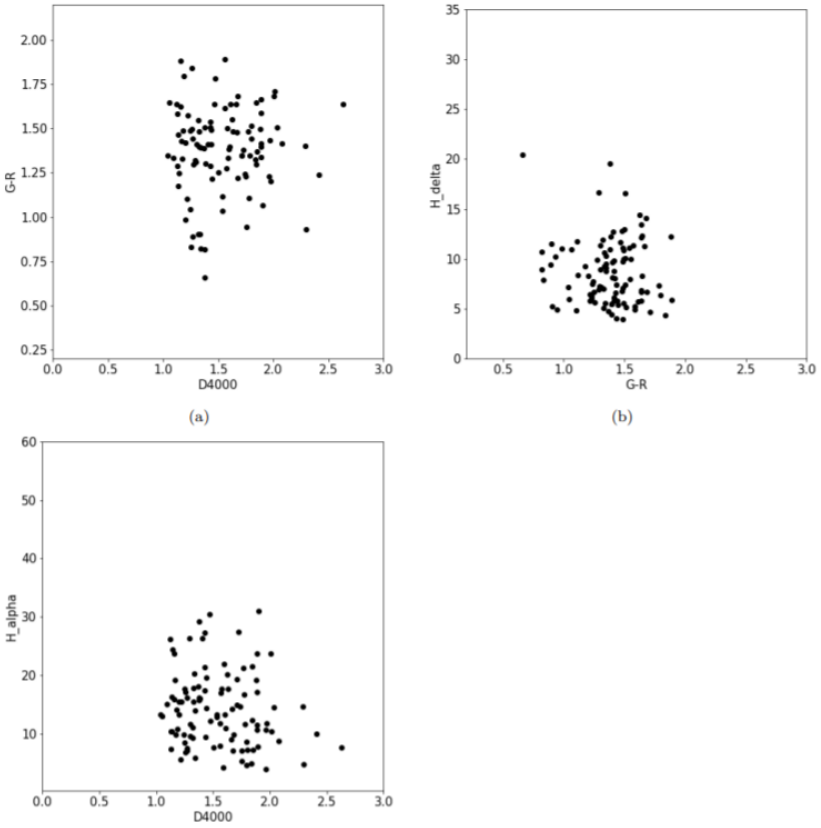

Figure 6.4: Plot for A1758 showing D4000 vs G-R colour index in section (a), H-delta vs G-R colour index for section (b) and H-alpha vs D4000 for section (c).

A963 has a fairly similar trend to A1758 seen in section (a) of Figure 6.6, looking at the blue fractions for these two 3%±3% and 3%±2% respectively they both contain much older populations. The lack of blue galaxies may be explained from the scattering in section (b) of Figure 6.6, where the large range of Hδ values at varying colour may be indicative of a complex history of interactions between cluster members, that have led to these recently enhanced periods of star formation. In section C of figure 6.6 is a similar relationship as seen previously with the bulk of high Hα values existing in high density towards the lower end of D4000 values.

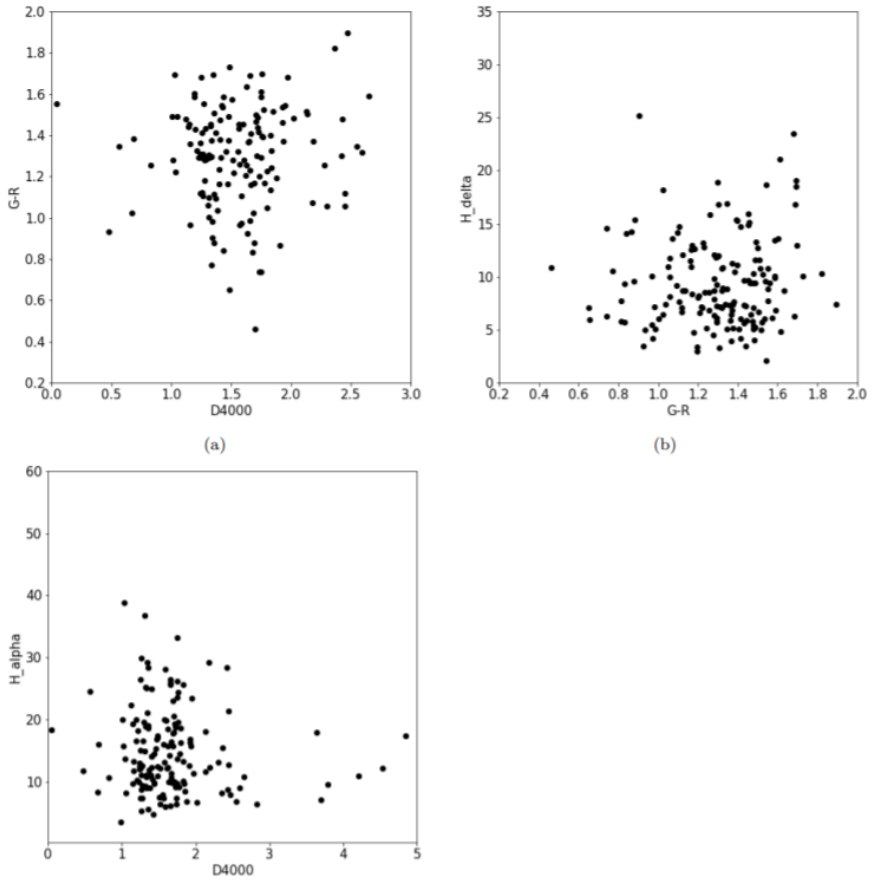

Figure 6.5: Plot for A1835 showing D4000 vs G-R colour index in section (a), H-delta vs G-R colour index for section (b) and H-alpha vs D4000 for section (c).

Throughout this last chapter it is important to note that each of the clusters have all gone through the same process of cuts, the difference in shape may occur due to an unseen bias created through the selection tools used. Figure 6.7 shows us the overall pattern as well as the spread of values for each cluster. As all of the clusters exist at similar values for redshift and the measured values for both blue fraction and D4000 strong fall closely to one another, we expect to see similar patterns for the three plots made for each cluster. I think although there are some differences, to be expected, the breakdown of population within each cluster can be seen through these diagrams.

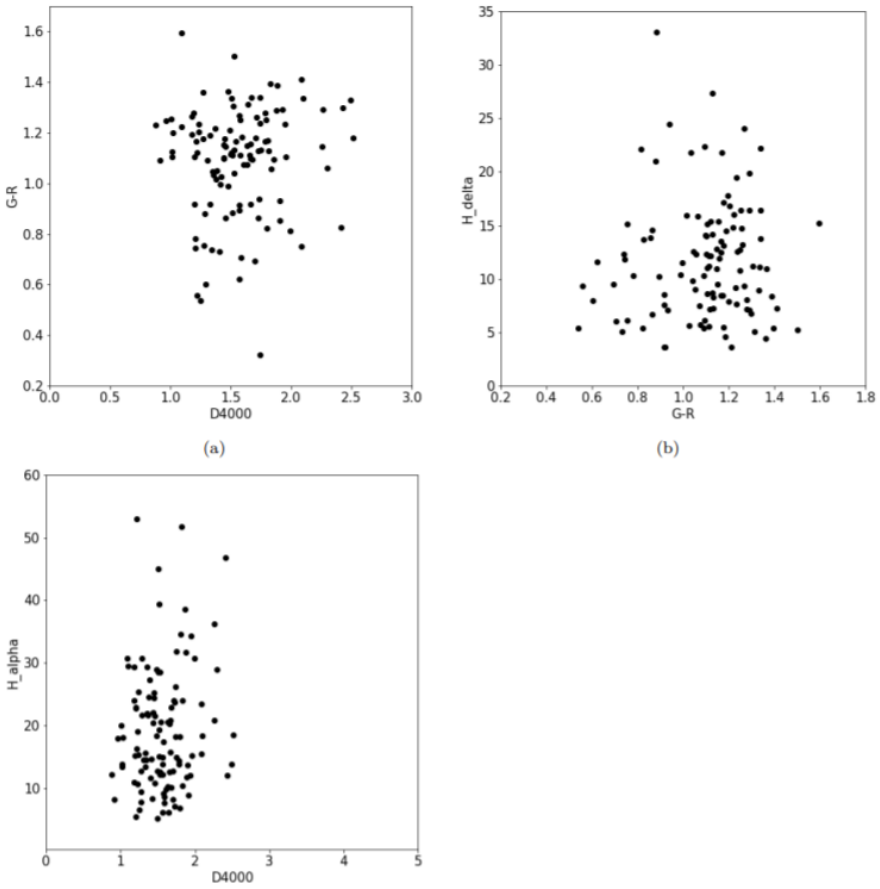

Figure 6.6: Plot for A963 showing D4000 vs G-R colour index in section (a), H-delta vs G-R colour index for section (b) and H-alpha vs D4000 for section (c).

To conclude, the work done during this research is a start to successfully understanding the evolution and structure of these 5 Abell clusters. Without the time constraints there are a few main extensions I would have prioritised for this work. Firstly I would connect the phase space plots in Chapter 4 and 5 with the stacked plots in Chapter 6, I would propose connecting these two sections of my work would be key to start to understand the complex cluster dynamics. The next objective of most importance would be a deeper look at the four supplementary clusters, that I used as a comparison for A1763. I think the data sets have more to offer, with greater time I would have liked to analyse them to the depth I did A1763. However, I processed a lot of data and have presented an analysis of this data as a legacy study that will be able to assist in furthering research in this field. Superior morphological data would from the LSST would provide more photometric depth which to the imaging, which would complement that analysis of this work.

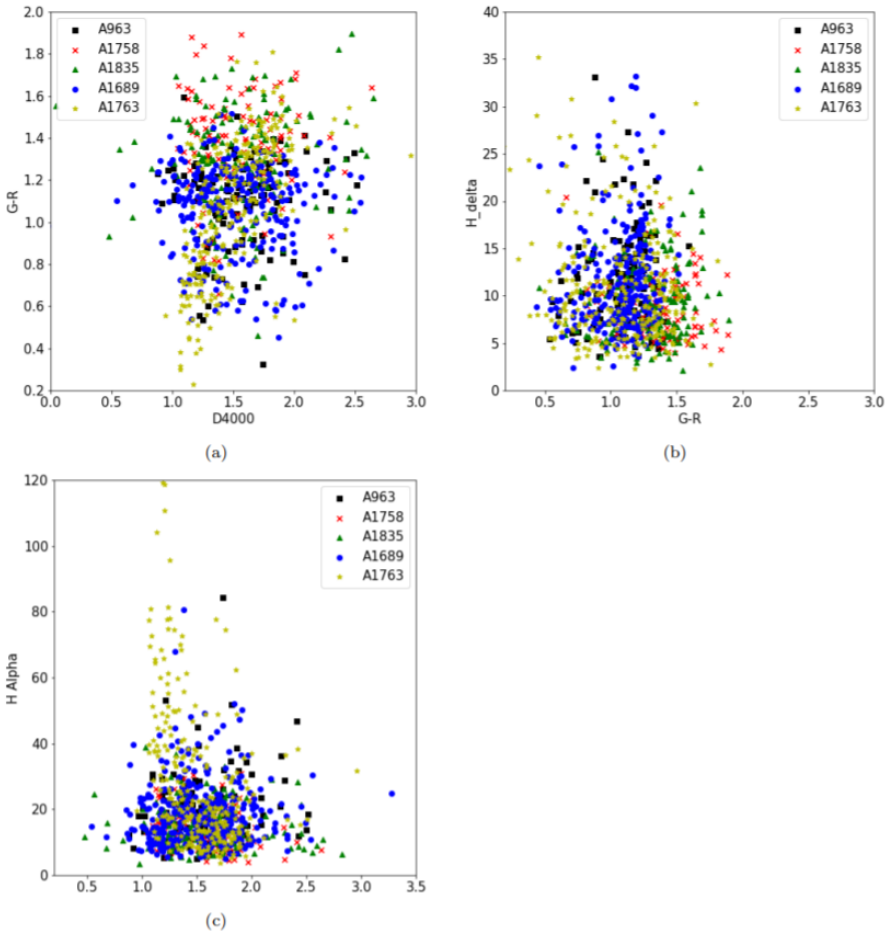

Figure 6.7: Plot for all five clusters showing D4000 vs G-R colour index in section (a), H-delta vs G-R colour index for section (b) and H-alpha vs D4000 for section (c). A963 is represented by black squares, A1758 by red crosses, A1835 by green triangles, A1689 by blue circles and A1763 by yellow stars.

7. Appendix

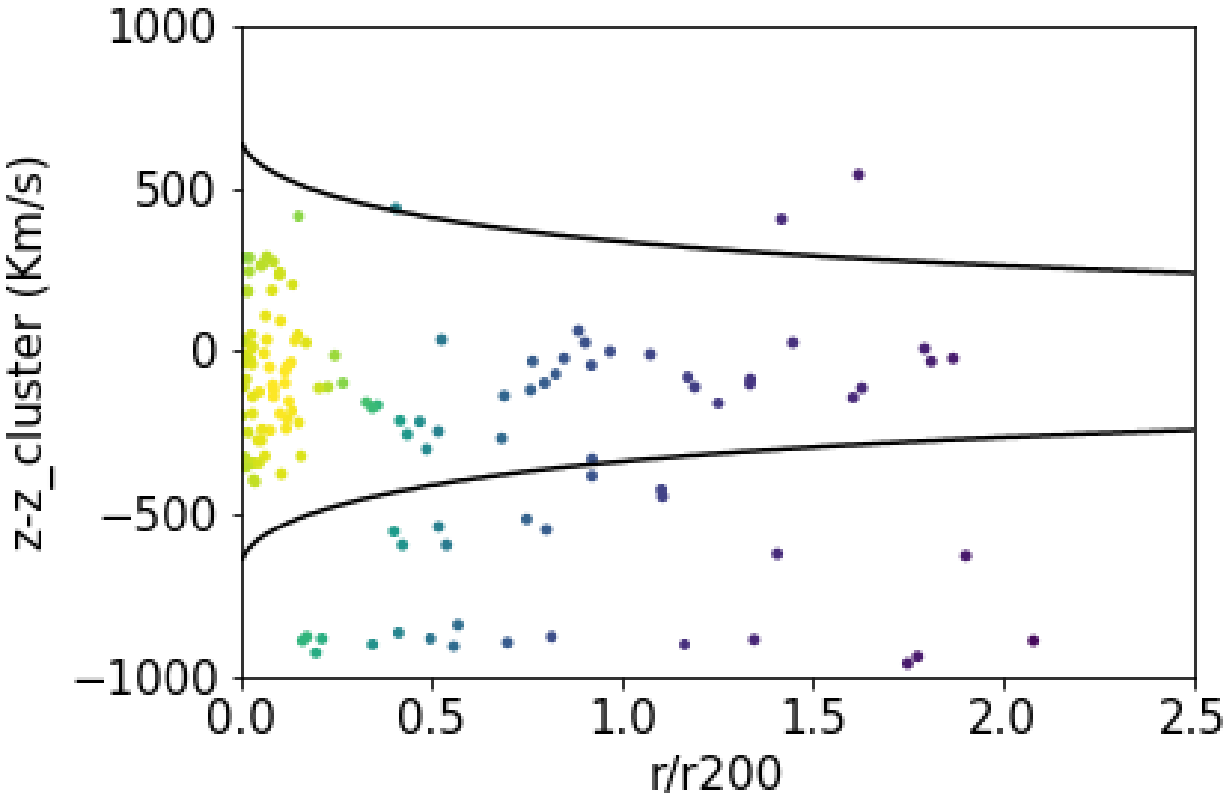

Figure 7.1: Abell 1758 shown in full in with CYE mass model caustics. The caustics define cluster membership, all points outside of them are defined as outside of the cluster.

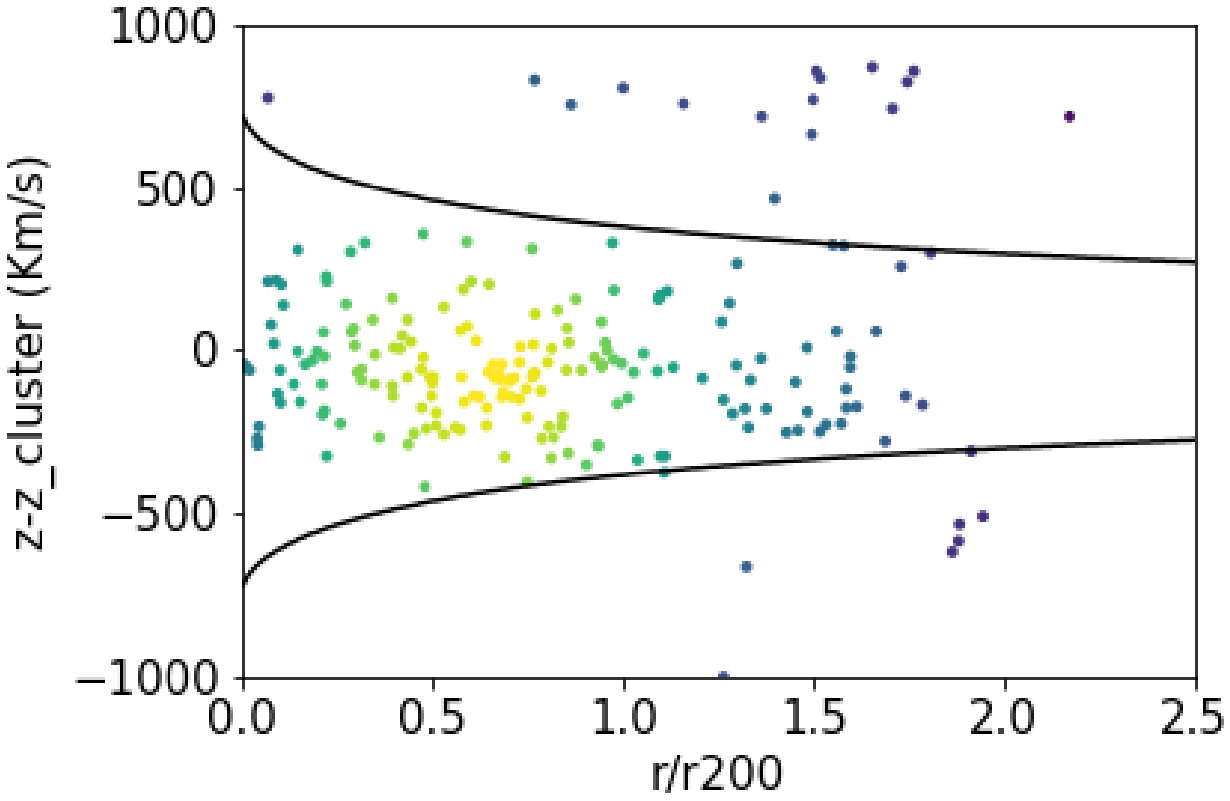

Figure 7.2: Abell 1835 shown in full in with CYE mass model caustics. The caustics define cluster membership, all points outside of them are defined as outside of the cluster.

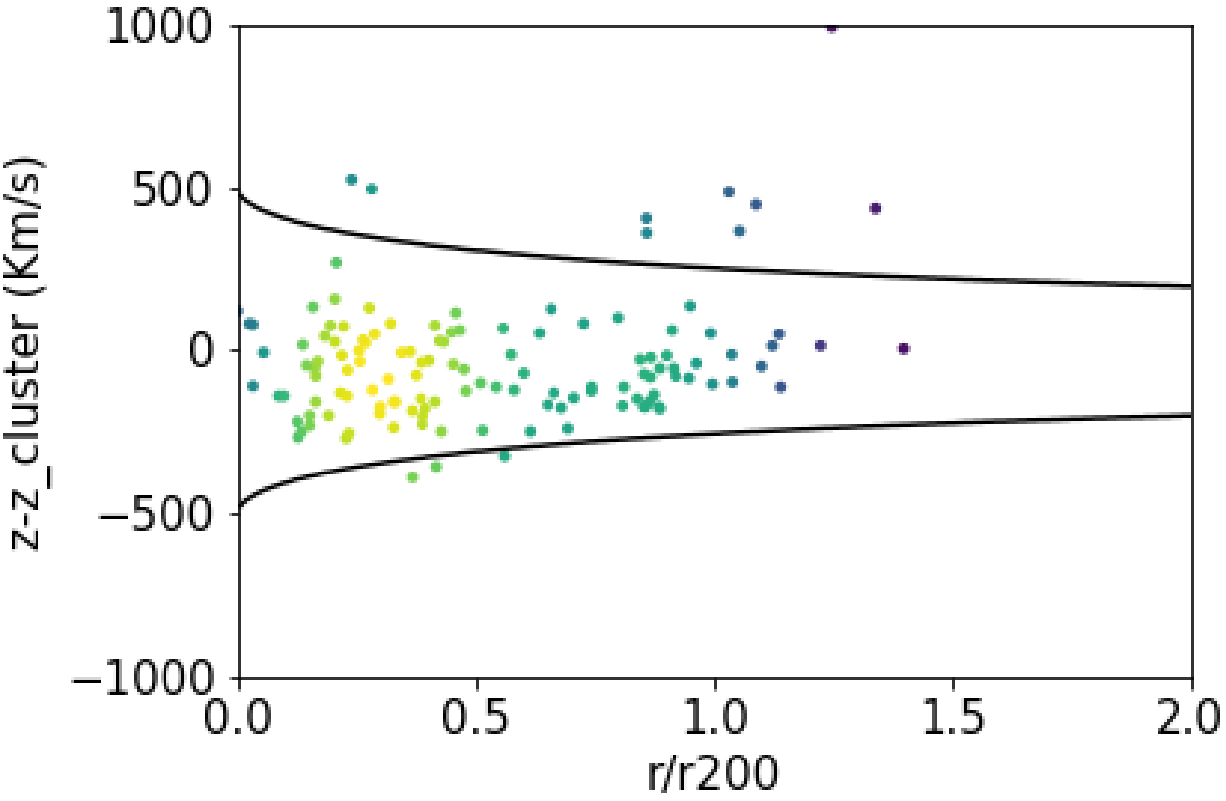

Figure 7.3: Abell 963 shown in full in with CYE mass model caustics. The caustics define cluster membership, all points outside of them are defined as outside of the cluster.

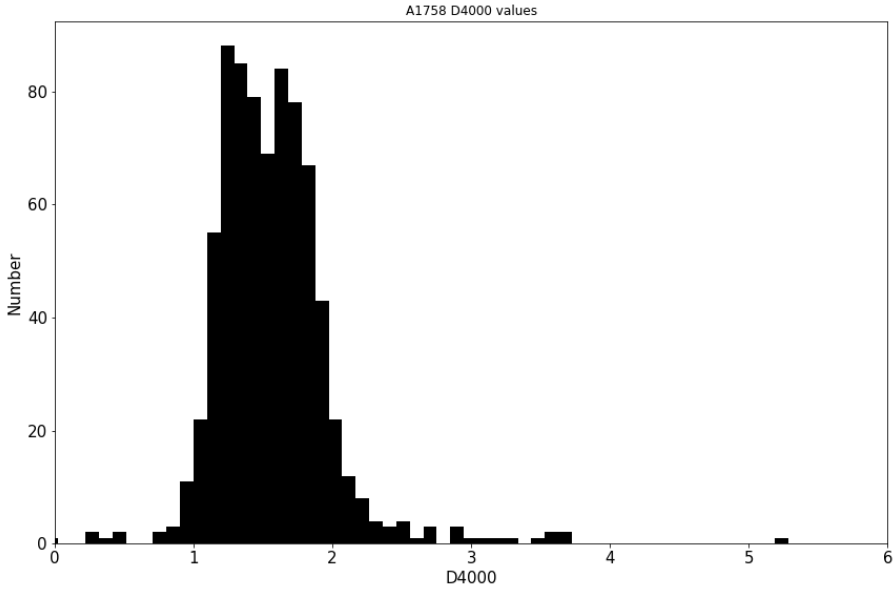

Figure 7.4: D4000 values in A1758.

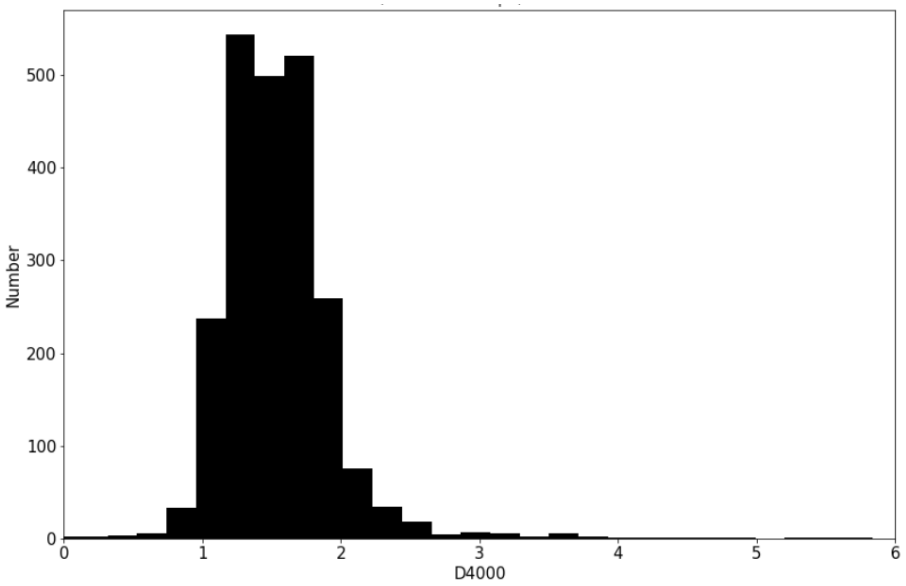

Figure 7.5: D4000 values for the field, where the field is A1689, A1835 and A963.

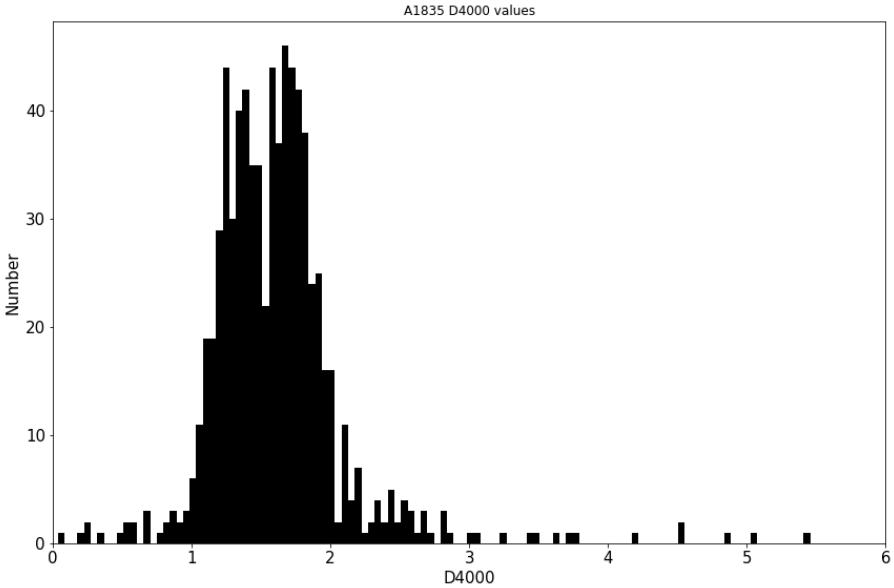

Figure 7.6: D4000 values in A1835.

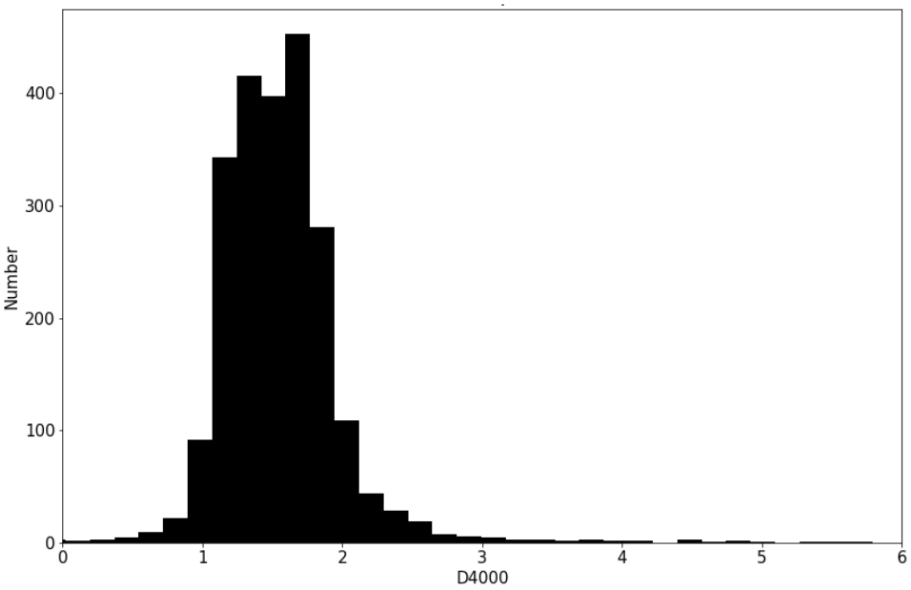

Figure 7.7: D4000 values for the field, where the field is A1758, A1689 and A963.

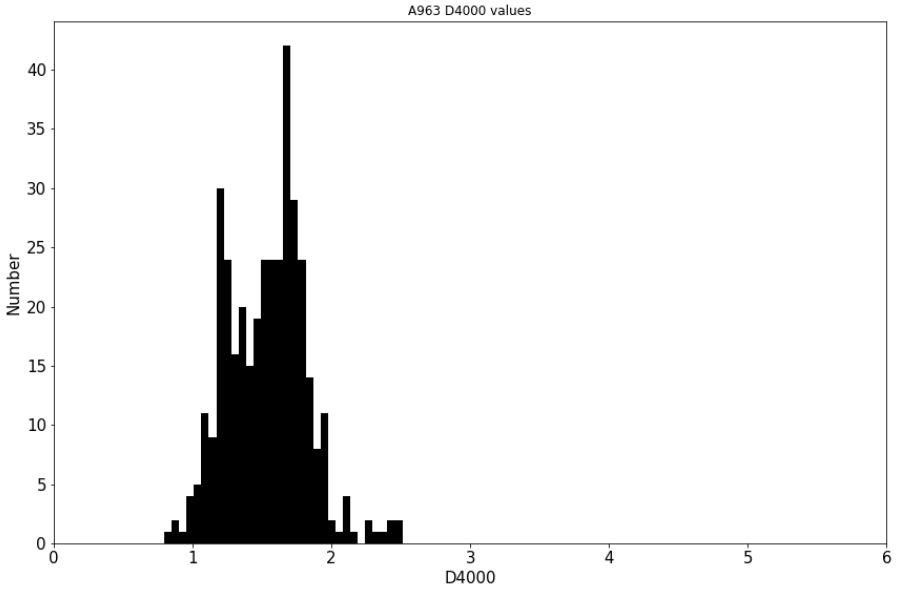

Figure 7.8: D4000 values in A963.

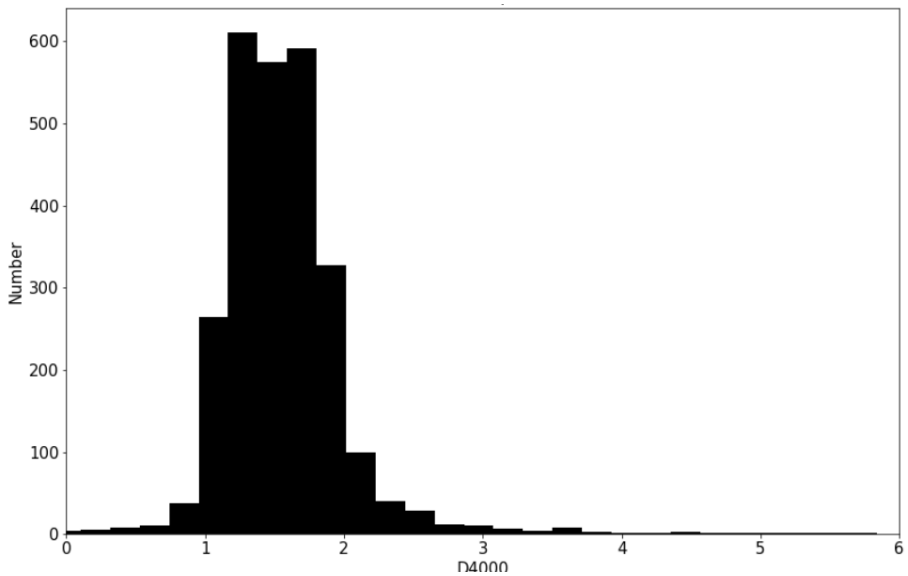

Figure 7.9: D4000 values for the field, where the field is A1758, A1835 and A1689.

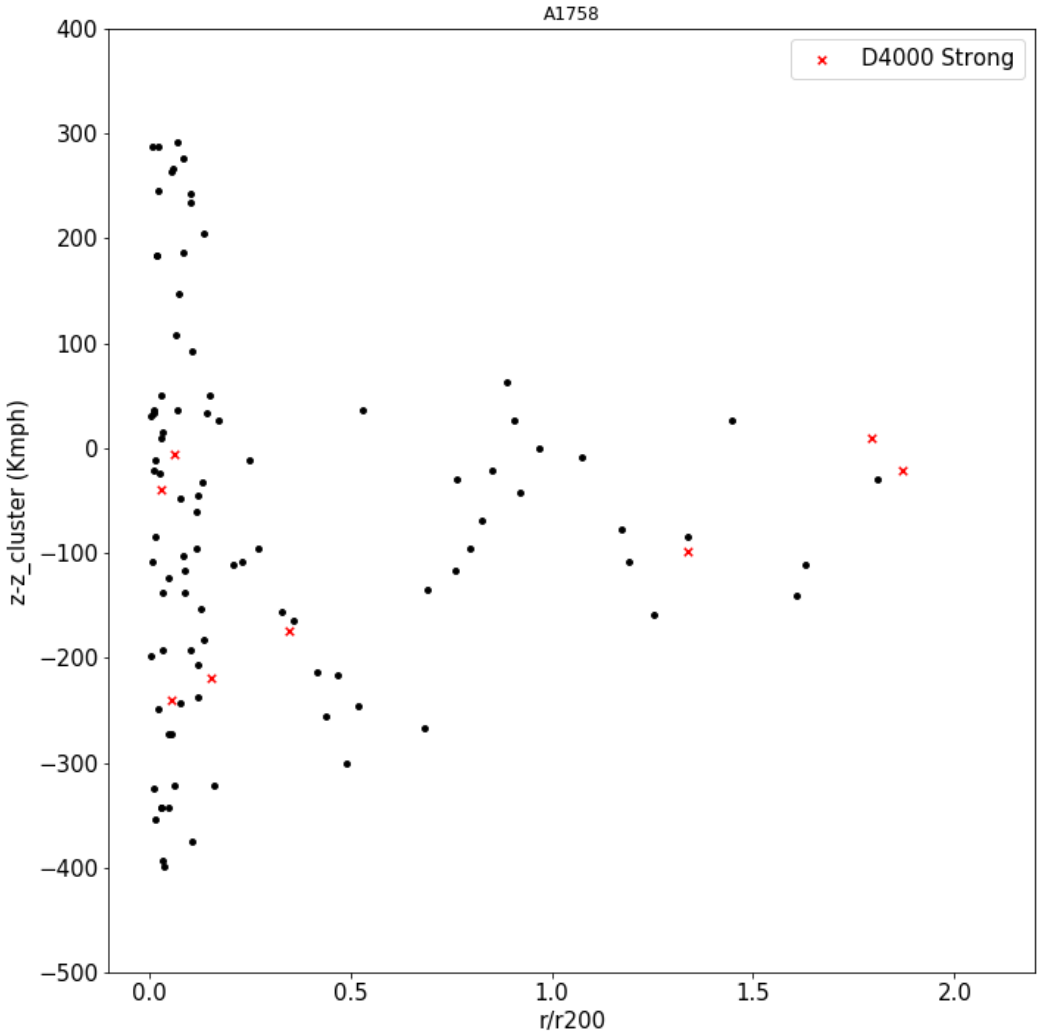

Figure 7.10: D4000 strong galaxies in phase space in A1758.

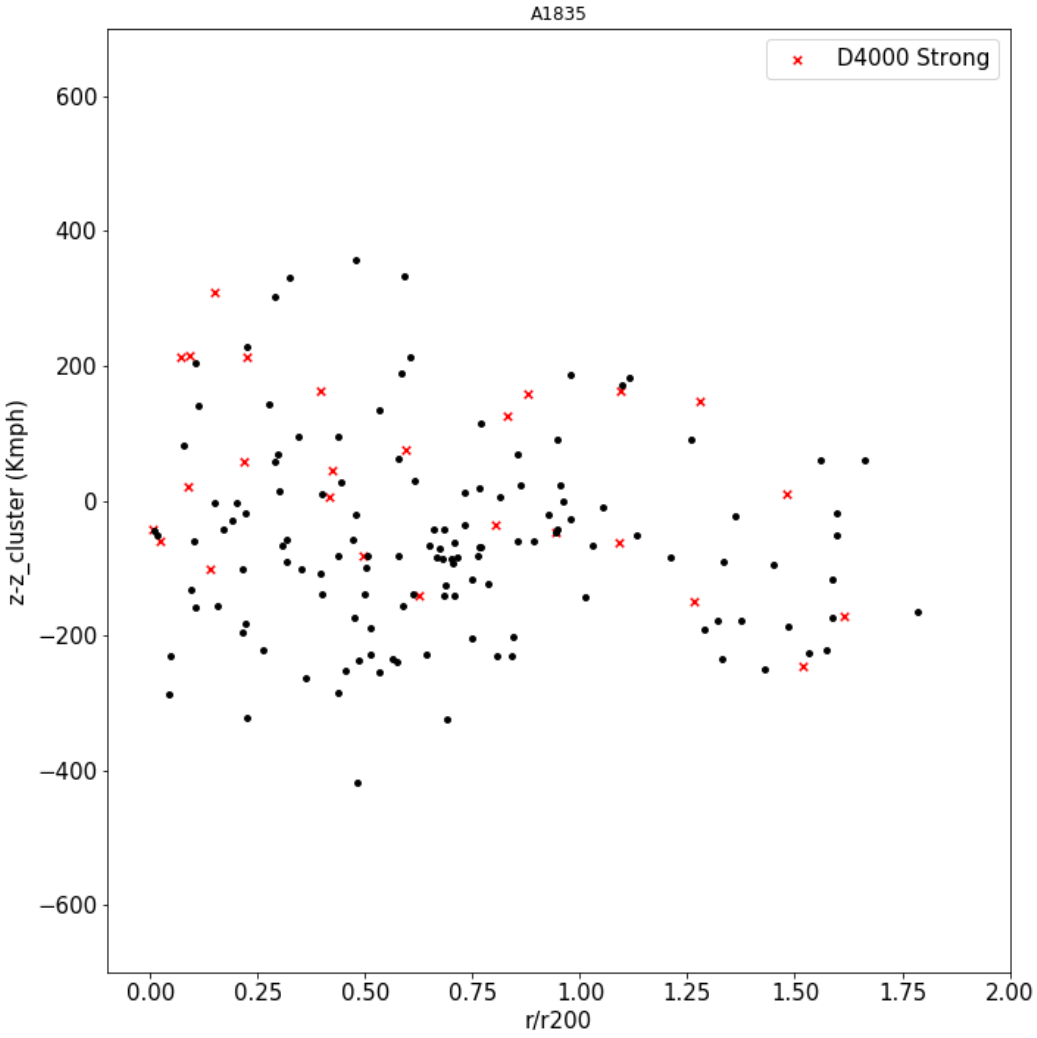

Figure 7.11: D4000 strong galaxies in phase space in A1835.

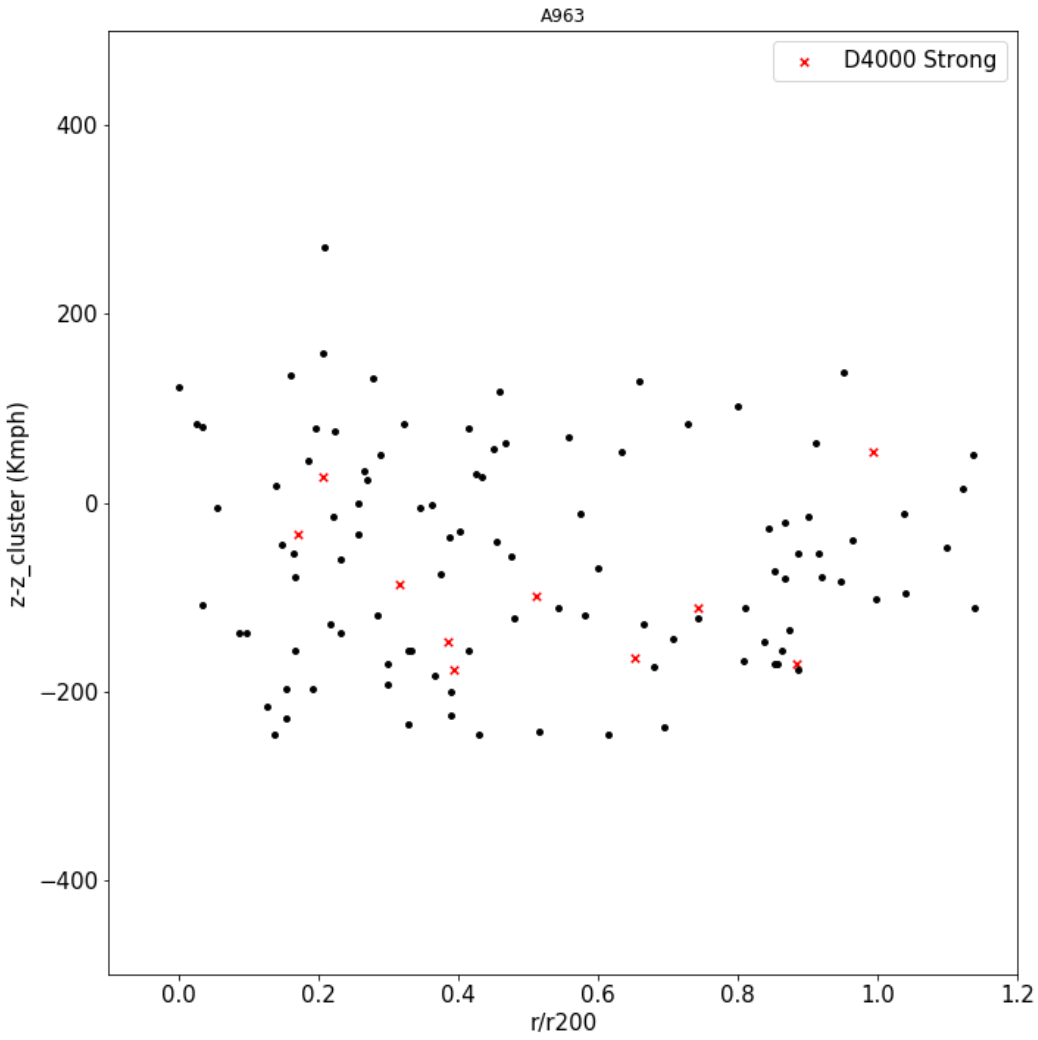

Figure 7.12: D4000 strong galaxies in phase space in A963.

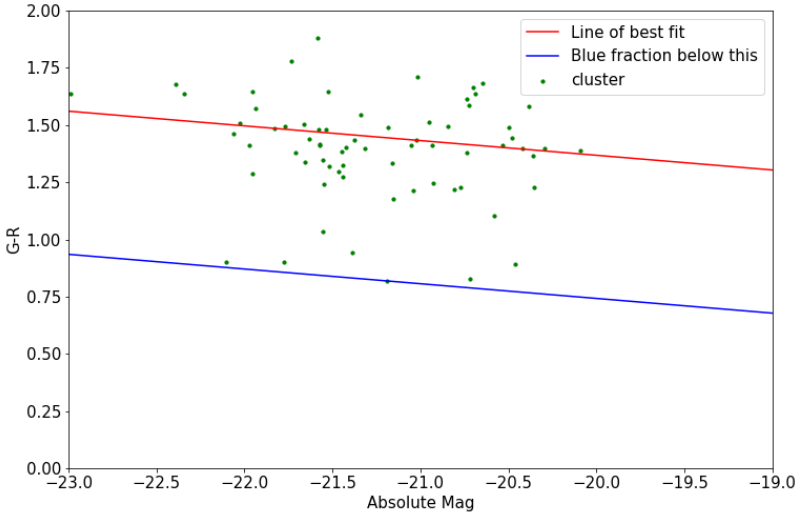

Figure 7.13: Blue fraction diagram for A1758.

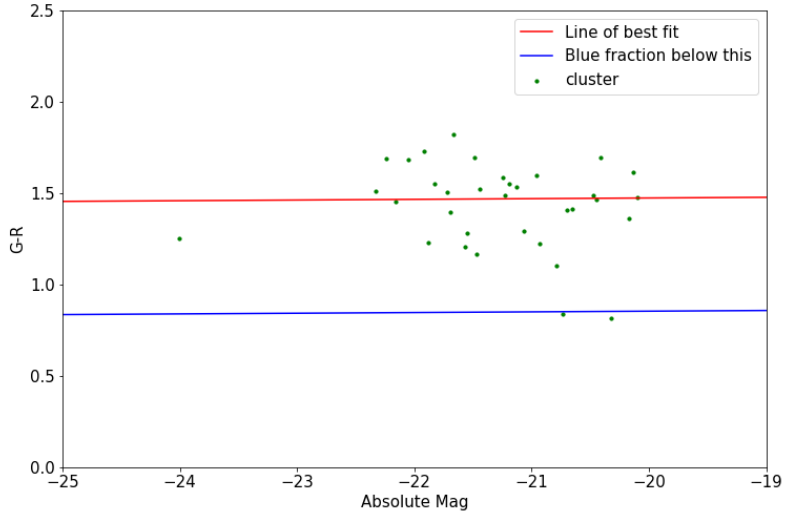

Figure 7.14: Blue fraction diagram for A1835.

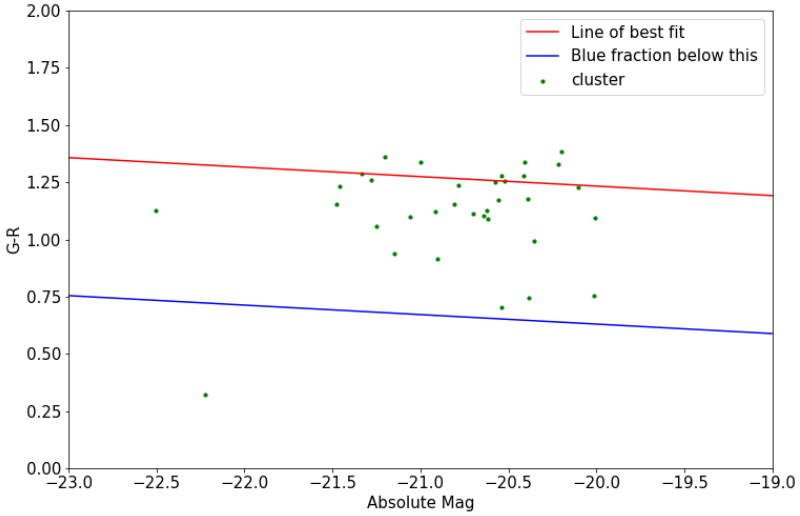

Figure 7.15: Blue fraction diagram for A963.

Bibliography

Andreon S., Ettori S., 1999, ApJ, 516, 647

Balogh M. L., Couch W. J., Smail I., Bower R. G., Glazebrook K., 2002, MNRAS, 335, 10

Bonamente M., Lieu R., Joy M. K., Nevalainen J. H., 2002, ApJ, 576, 688

Bond J. R., Kofman L., Pogosyan D., 1996, Nature, 380, 603

Brinchmann J., Charlot S., White S. D. M., Tremonti C., Kauffmann G., Heckman T., Brinkmann J., 2004, MNRAS, 351, 1151

Bruzual G., Charlot S., 2003, MNRAS, 344, 1000

Bruzual A. G., 1983, ApJ, 273, 105

Butcher H., Oemler A. J., 1984, ApJ, 285, 426

Carlberg R. G., 1986, ApJ, 310, 593

Carlberg R. G., Yee H. K. C., Ellingson E., 1997, ApJ, 478, 462

Dahle H., Kaiser N., Irgens R. J., Lilje P. B., Maddox S. J., 2002, ApJS, 139, 313

Dijkstra M., Westra E., 2010, MNRAS, 401, 2343

Dressler A., 1980, ApJ, 236, 351

Dressler A., Gunn J. E., 1983, ApJ, 270, 7

Dressler A., Smail I., Poggianti B. M., Butcher H., Couch W. J., Ellis R. S., Oemler Augustus J., 1999, ApJS, 122, 51

Ebeling H., Edge A. C., Bohringer H., Allen S. W., Crawford C. S., Fabian A. C., Voges W., Huchra J. P., 1998, MNRAS, 301, 881

Ebeling H., Stephenson L. N., Edge A. C., 2014, ApJL, 781, L40

Edge A. C., Ivison R. J., Smail I., Blain A. W., Kneib J. P., 1999, MNRAS, 306, 599

Edwards L. O. V., Fadda D., Biviano A., Marleau F. R., 2010, AJ, 139, 434

Eisenstein D. J., et al., 2011, AJ, 142, 72

Fadda D., Biviano A., Marleau F. R., Storrie-Lombardi L. J., Durret F., 2008, ApJL, 672, L9

Falgarone E., et al., 2017, Nature, 548, 430

Fukugita M., Shimasaku K., Ichikawa T., 1995, PASP, 107, 945

Gill S. P. D., Knebe A., Gibson B. K., 2005, MNRAS, 356, 1327

Giovannini G., Tordi M., Feretti L., 1999, , 4, 141

Gómez P. L., et al., 2003, ApJ, 584, 210

Gunn J. E., Gott J. Richard I., 1972, ApJ, 176, 1

Haines C. P., et al., 2009, ApJ, 704, 126

Haines C. P., et al., 2012, ApJ, 754, 97

Haines C. P., et al., 2013, ApJ, 775, 126

Haines C. P., et al., 2015, ApJ, 806, 101

Haines C. P., et al., 2018, MNRAS, 477, 4931

Hashimoto T., Goto T., Momose R., Ho C.-C., Makiya R., Chiang C.-Y., Kim S. J., 2019, MNRAS, 489, 2014

Heiles C., Troland T. H., 2005, ApJ, 624, 773

Hirata C. M., Mandelbaum R., Ishak M., Seljak U., Nichol R., Pimbblet K. A., Ross N. P., Wake D., 2007, MNRAS, 381, 1197

Jeltema T. E., Canizares C. R., Bautz M. W., Buote D. A., 2005, ApJ, 624, 606

Kennicutt Robert C. J., 1992, ApJ, 388, 310

Kennicutt Robert C. J., 1998, ARA&A, 36, 189

Landolt A. U., 1992, AJ, 104, 340

Lavery R. J., Henry J. P., 1988, ApJL, 329, L21

Leauthaud A., et al., 2010, ApJ, 709, 97

Lewis I., et al., 2002, MNRAS, 334, 673

Licquia T. C., Newman J. A., 2015, ApJ, 806, 96

Lilly S. J., Carollo C. M., Pipino A., Renzini A., Peng Y., 2013, ApJ, 772, 119

Maier C., Ziegler B. L., Haines C. P., Smith G. P., 2019, A&A, 621, A131

Mathis H., Charlot S., Brinchmann J., 2006, MNRAS, 365, 385

McDonald M., Gaspari M., McNamara B. R., Tremblay G. R., 2018, ApJ, 858, 45

McPartland C., Ebeling H., Roediger E., Blumenthal K., 2016, MNRAS, 455, 2994

Merrifield M. R., 2010, A&A, 523, A12

Miyazaki S., et al., 2002, PASJ, 54, 833

Moore B., Katz N., Lake G., Dressler A., Oemler A., 1996, Nature, 379, 613

Newell B., 1979, New Zealand Journal of Science, 22, 373

Nilsson K. K., Fynbo J. P. U., Møller P., Sommer-Larsen J., Ledoux C., 2006, A&A, 452, L23

O'Dea C. P., Owen F. N., 1985, AJ, 90, 954

Piffaretti R., Arnaud M., Pratt G. W., Pointecouteau E., Melin J. B., 2011, A&A, 534, A109

Pimbblet K. A., 2003, , 20, 294

Pimbblet K. A., 2011, MNRAS, 411, 2637

Pimbblet K. A., Smail I., Edge A. C., O'Hely E., Couch W. J., Zabludoff A. I., 2006, MNRAS, 366, 645

Poggianti B. M., Barbaro G., 1997, A&A, 325, 1025

Poggianti B. M., Smail I., Dressler A., Couch W. J., Barger A. J., Butcher H., Ellis R. S., Oemler Augustus J., 1999, ApJ, 518, 576

Poggianti B. M., et al., 2016, AJ, 151, 78

Refregier A., 2003, ARA&A, 41, 645

Rieke G. H., et al., 2004, ApJS, 154, 25

Rizza E., Burns J. O., Ledlow M. J., Owen F. N., Voges W., Bliton M., 1998, MNRAS, 301, 328

Rizza E., Morrison G. E., Owen F. N., Ledlow M. J., Burns J. O., Hill J., 2003, AJ, 126, 119

Rosa-González D., Terlevich E., Terlevich R., 2002, MNRAS, 332, 283

Sanders D. B., Soifer B. T., Elias J. H., Madore B. F., Matthews K., Neugebauer G., Scoville N. Z., 1988, ApJ, 325, 74

Schmidt R. W., Allen S. W., Fabian A. C., 2001, MNRAS, 327, 1057

Schneider P., 2010, Extragalactic astronomy and cosmology: an introduction. Springer

Sholukhova O., Bizyaev D., Fabrika S., Sarkisyan A., Malanushenko V., Valeev A., 2015, MNRAS, 447, 2459

Smith G., 2006, The Local Cluster Substructure Survey {LoCuSS}: Deep Strong Lensing Observations with WFPC2, HST Proposal

Smith G. P., Kneib J.-P., Smail I., Mazzotta P., Ebeling H., Czoske O., 2005, MNRAS, 359, 417

Sobral D., Best P. N., Geach J. E., Smail I., Cirasuolo M., Garn T., Dalton G. B., Kurk J., 2010, MNRAS, 404, 1551

Ueda S., Kitayama T., Dotani T., 2017, ApJ, 837, 34

Voges W., et al., 1999, A&A, 349, 389

Werner M. W., et al., 2004, ApJS, 154, 1

Wild V., Kauffmann G., Heckman T., Charlot S., Lemson G., Brinchmann J., Reichard T., Pasquali A., 2007, MNRAS, 381, 543

Wilkinson C. L., Pimbblet K. A., Stott J. P., 2017, MNRAS, 472, 1447

Yamasawa D., Habe A., Kozasa T., Nozawa T., Hirashita H., Umeda H., Nomoto K., 2011, ApJ, 735, 44

Yan R., Newman J. A., Faber S. M., Konidaris N., Koo D., Davis M., 2006, ApJ, 648, 281